

**DEVELOPMENT OF A CONTINUOUS METAL RECOVERY CONTACTOR
USING ION-EXCHANGE FIBRES**

Rhulani Nicolas Ntimbani

A dissertation submitted to the Faculty of Engineering and the Built Environment, University of the Witwatersrand, Johannesburg, in fulfilment of the requirements for the degree of Master of Science in Engineering.

Johannesburg, 2015

DECLARATION

I declare that this dissertation is my own unaided work. It is being submitted to the degree of Master of Science in Engineering to the University of the Witwatersrand, Johannesburg. It has not been submitted before for any other degree or examination in any other University.

R Ntimbani

Rhulani Nicolas Ntimbani

30th day of September 2015

ABSTRACT

Wastewater from industrial processes usually contain heavy metals such as copper (Cu^{2+} ions) which are harmful to the environment and human health. Therefore, it is imperative that these effluent streams are treated prior to being discharged. In recent past, ion exchange fibres (IEFs) have been suggested for the treatment of such waste streams because they have higher adsorption/desorption rate due to their larger surface areas and shorter diffusion paths compared to granular ion exchangers. In this study, the development of an IEF contactor for the removal of Cu^{2+} ions from synthetic dilute solutions was carried out. The table pan filter model was proposed for a contactor for continuous and simultaneous Cu^{2+} ions loading, elution and rinsing of Cu^{2+} ions.

In order to generate the equilibrium and kinetic data required for the design of a contactor, IEFs were contacted with dilute synthetic solutions of Cu^{2+} ions in batch systems. The Temkin and pseudo-second order model were found to best describe the equilibrium and kinetics of the system, respectively. The batch tests conducted for multi-component system showed that the selected IEFs have a higher selectivity for Cu^{2+} ions.

The effects of bed packing density and flow rate on loading and elution of Cu^{2+} ions were investigated using columns at lab scale. The results showed that effective loading of Cu^{2+} ions can be conducted at low IEFs bed packing density and low feed flow rate that allowed sufficient residence time for the ion exchange to occur. The results also showed that the elution rate of Cu^{2+} ions can be increased by increasing acid flow rate provided the acid is sufficiently concentrated for elution purposes. In this study, the Yoon-Nelson model was the most suitable model for predicting how effluent concentration during loading varies with time. Other models fitted were the bed depth service time (BDST) model and the Thomas model. However, the Yoon-Nelson model had parameters which were comparable to those obtained experimentally for all tests.

Following the column test results, a segment of a rotating contactor utilising IEFs was proposed, designed and fabricated from clear polyvinyl chloride (PVC). The contactor was

then tested for loading and elution duties. The study showed that the contactor was able to remove 45 mg of Cu^{2+} ions /g of fibre from the feed solution as compared to 54 mg Cu^{2+} ions /g of fibre obtained in column tests. Loading of Cu^{2+} ions onto the designed contactor pan was found to be low due to the higher cross sectional area which consequently resulted in uneven distribution of feed solution. The IEFs loaded with Cu^{2+} ions were successfully regenerated with 3 bed volumes of 2 M HCl which removed 99.84% of the loaded Cu^{2+} ions as compared to the 7 bed volumes which was required to elute the entire loaded Cu^{2+} ions. Although the loading of Cu^{2+} ions was low, the designed contactor is promising as it was able to remove Cu^{2+} ions from feed solution and the IEFs could be completely eluted for reuse. In contrast to column Cu^{2+} ions breakthrough tests, the Yoon-Nelson model was unable to predict the breakthrough of Cu^{2+} ions in the designed IEF contactor pan. It is recommended that mathematical and/or linear driving force models be fitted into the breakthrough profile of the contactor for further development. This will allow simulations of breakthrough profile and consequently optimization of the IEFs contactor.

LIST OF PUBLICATIONS AND WORKSHOPS ATTENDED

1. Ntimbani, R., N., Simate, G., S., Ndlovu, S., 2015. Removal of copper ions from dilute synthetic solution using staple ion exchange fibres: Equilibrium and kinetic studies. *Journal of Environmental Chemical Engineering* 3 (2), 1258-1266.
2. R. N. Ntimbani, G. S. Simate, S. Ndlovu, 2015. Removal of copper ions from dilute synthetic solution using staple ion exchange fibres: Dynamic studies. *Brazilian Journal of Chemical Engineering* (Submitted).
3. R. N. Ntimbani, G. S. Simate, S. Ndlovu, 2014. Development of a continuous metal removal contactor using ion exchange fibres. South African Minerals to Metals Research Institute Workshop, Vineyard Hotel, South Africa.
4. R. N. Ntimbani, G. S. Simate, T. Thulare, S. Ndlovu, 2013. The effect of pH on the extraction of heavy metals from dilute synthetic solutions using ion exchange fibres. South African Minerals to Metals Research Institute Workshop, Vineyard Hotel, South Africa.

DEDICATION

I dedicate this dissertation to all my siblings and parents (Tsakani Irene Shingange and Marikunyi Thompson Timbane).

Ni khensa ku hlohloteriwa no seketeriwa.

ACKNOWLEDGEMENTS

I am grateful to my supervisor Dr. Geoffrey S. Simate and co-supervisor Prof. Sehliselo Ndlovu for their supervision of this study. I appreciate their guidance, mentorship, patience and support provided throughout the study.

I am also thankful to Marthie Kotze, Tresha Udayar, Dr. Leon Kruger, and Peter Craven of the Council of Mineral Technology of South Africa (Mintek). I also appreciate their guidance, mentorship, patience and support provided to the study. I also would like to thank all Mintek staff members who assisted me in conducting this study.

The research would have not been possible without the resources and financial support provided by Mintek and South African Minerals to Metals Research Institute (SAMMRI). I acknowledge and greatly appreciate their financial support in making this study a success. I am also thankful to the University of Witwatersrand for giving me the opportunity to enrol for the Master of Science degree in Engineering.

I also appreciate the words of encouragement from my high school teachers (Mathematics and Physical Sciences) and friends before and during the course of this study.

Lastly, but not least, I am grateful for the support, love and the belief that my family has in me. I acknowledge their understanding as I remained financially depended upon them.

TABLE OF CONTENTS

ABSTRACT	iii
ACKNOWLEDGEMENTS	vii
LIST OF FIGURES	xii
LIST OF TABLES	xv
Chapter 1: Introduction	1
1.1 Introduction	1
1.2 Research problem	2
1.3 Objectives	3
1.4 Research methodology	4
1.5 Report layout	4
1.6 Summary	5
Chapter 2: Literature review	6
2.1 Introduction	6
2.2 Ion exchange in general	7
2.2.1 Ion exchange mechanism	8
2.2.2 Structure and properties of ion exchangers	8
2.2.3 Selectivity and ion exchange materials	9
2.2.4 Capacity of ion exchange materials	10
2.3 Fibrous ion exchangers	11
2.3.1 Fabrication of ion exchange fibres from special polymers	12
2.3.2 Composite fibres	12
2.3.3 Grafting techniques for ion exchange fibre synthesis	13
2.4 Ion exchange operations	13
2.4.1 Batch	14
2.4.2 Fixed packed bed column	14
2.4.3 Recoflo technology	15
2.4.4 Fluidised bed column	16
2.4.5 Moving beds	16
2.4.6 Cascade columns	17
2.4.7 Ion exchange membranes	18
2.5 Other ion exchange compatible systems	21

2.5.1	Diatomaceous earth filter	21
2.5.2	Cartridge filters	22
2.5.3	Filter presses and belt filters	22
2.6	Adsorption isotherms and kinetic models	22
2.6.1	Adsorption equilibrium isotherms	22
2.6.2	Adsorption kinetic models	26
Chapter 3: Materials and Methods		28
3.1	Introduction	28
3.2	Material acquisition.....	28
3.3	Fibre preparation	29
3.4	Reagent and solution preparations	29
3.5	Effect of pH on extraction (s-curves).....	30
3.6	Maximum loading capacity of copper.....	31
3.7	Generation of equilibrium adsorption isotherms.....	31
3.8	Elution test work	32
3.9	Kinetic tests	33
3.10	Sample analysis	33
Chapter 4: Results and discussions		35
4.1	Introduction	35
4.2	Effects of pH on metal loading	36
4.3	Maximum metal loading	38
4.4	Equilibrium Isotherm	38
4.5	Elution tests	43
4.6	Kinetics test	45
4.7	Summary	48
Chapter 5: Column tests.....		50
5.1	Introduction	50
5.2	Materials and Methods	51
5.2.1	Material acquisition, fibre and reagent preparation	51
5.2.2	Experimental set up.....	51
5.2.3	Effect of bed packing density on Cu ²⁺ ions removal and elution	52
5.2.4	Effects of feed and eluent flow rate on Cu ²⁺ ions removal and elution	52
5.3	Results and discussions	53
5.3.1	Effect of packing density on Cu ²⁺ ions removal	53

5.3.2	Effect of feed flow rate on Cu ²⁺ ions removal	55
5.3.3	Effect of bed packing density on elution	56
5.3.4	Effect of eluent flow rate on elution	57
5.3.5	Computation of u and τ	58
5.4	Model fitting.....	59
5.4.1	Thomas model.....	59
5.4.2	The Yoon-Nelson model.....	61
5.4.3	The Adam's-Bohart model	63
5.4.4	Comparison of models	65
5.5	Summary	70
Chapter 6: Fibre contactor design		71
6.1	Introduction	71
6.2	Choice of contactor(s)	71
6.3	Adsorption stages	74
6.4	Design of IEF sorption pan	77
6.5	Mechanical design of IEF pan.....	78
6.6	Summary	80
Chapter 7: Contactor testing		81
7.1	Introduction	81
7.2	Materials and Methods	81
7.2.1	Material acquisition, fibre and reagent preparation	81
7.2.2	Experimental set up.....	81
7.2.3	Experimental procedure	82
7.3	Results and discussions	83
7.3.1	Breakthrough profile of the IEFs table pan contactor.....	83
7.3.2	Comparison of contactor and column packing density profile	84
7.3.3	Elution profile of the contactor	86
7.3.4	Model fitting into the IEFs contactor pan	87
7.4	Summary	89
Chapter 8: Conclusions and recommendations.....		90
8.1	Conclusions	90
8.1.1.	Introduction.....	90
8.1.2.	Batch tests	91
8.1.3.	Choice of contactor type and column tests	92

8.1.4	Design of the table pan contactor.....	93
8.1.5	Contacting testing	93
8.2	Recommendations	94
	References	95
	Appendix A	107
	Appendix B	111
	Appendix C	127
	Appendix D	175
	Appendix E	183

LIST OF FIGURES

Figure 2. 1: Forms of IEF: (a) Staple fibre of anion exchanger FIBAN A-6. (b) Nonwoven fabrics of different FIBAN materials (Kosandrovich and Soldatov, 2012).....	12
Figure 2. 2: Higgins contactor in water deionization process (Zagorodni, 2007).	17
Figure 2. 3: Cascade technology employing cyclic columns.....	18
Figure 3. 1: Chemical structure of Fiban X-1 (Yahorova et al., 2013).....	28
Figure 3. 2: Schematic experimental set up for loading tests.	31
Figure 4. 1: Mass percentage of metal extracted (based on metal adsorbed) versus pH.	36
Figure 4. 2: Experimental equilibrium data points.	39
Figure 4. 3: Linearized Freundlich isotherm model fit into experimental data.	40
Figure 4. 4: Linearized Langmuir isotherm model fit into experimental data.	40
Figure 4. 5: Linearized Temkin isotherm model fit into experimental data.	40
Figure 4.6: Linearized Dubinin and Radushkevich isotherm model fit into experimental data.	41
Figure 4. 7: Linearised Redlich-Peterson isotherm fit into experimental data.	41
Figure 4. 8: Mass percentage eluted from IEFs versus hydrochloric acid concentration in molar units.	44
Figure 4. 9: Experimental loading of Cu^{2+} on IEF as a function of time.....	45
Figure 4. 10: Pseudo-first-order model fit on the kinetics experimental results.....	46
Figure 4. 11: Pseudo-second-order model fit on the kinetics experimental results.....	46
Figure 4. 12: Elovich model fit on the kinetics experimental results.	47
Figure 5. 1: Experimental set up.	51
Figure 5. 2: Effluent concentration versus feed volume passed through various bed packing densities (IEFs mass 2.56 g) at constant flow rate of 8 mL/min.....	54
Figure 5. 3: Effluent concentration versus feed volume passed at various flow rates through a bed of 2.56 g IEFs adjusted to packing density of 0.16 g/cm ³	55
Figure 5. 4: Effect of bed packing density on elution of IEFs at constant flow rate and IEFs mass (8 mL/min and 2.56 g).	57

Figure 5. 5: Effect of flow rate on elution of IEFs at constant bed packing density and IEFs mass (0.16 g/cm ³ and 2.56 g).	58
Figure 5. 6: Plot of Cu concentration from experiments and those predicted by the Thomas, Yoon-Nelson and Adam's Bohart model versus time at bed depth and flow rate of 10.5 cm and 8 mL/min.	67
Figure 5. 7: Plot of Cu concentration from experiments and those predicted by the Thomas, Yoon-Nelson and Adam's Bohart model versus time at bed depth and flow rate of 8.5 cm and 8 mL/min.	67
Figure 5. 8: Plot of Cu concentration from experiments and those predicted by the Thomas, Yoon-Nelson and Adam's Bohart model versus time at bed depth and flow rate of 6.0 cm and 8 mL/min.	68
Figure 5. 9: Plot of Cu concentration from experiments and those predicted by the Thomas, Yoon-Nelson and Adam's Bohart model versus time at bed depth and flow rate of 4.5 cm and 8 mL/min.	68
Figure 5. 10: Plot of Cu concentration from experiments and those predicted by the Thomas, Yoon-Nelson and Adam's Bohart model versus time at bed depth and flow rate of 10.5 cm and 12 mL/min.	69
Figure 5. 11: Plot of Cu concentration from experiments and those predicted by the Thomas, Yoon-Nelson and Adam's Bohart model versus time at bed depth and flow rate of 10.5 cm and 17 mL/min.	69
Figure 5. 12: Plot of Cu concentration from experiments and those predicted by the Thomas, Yoon-Nelson and Adam's Bohart model versus time at bed depth and flow rate of 10.5 cm and 28 mL/min.	70
Figure 6. 1: Semi-batch belt contactor.	72
Figure 6. 2: Horizontal moving belt fibre contactor.	72
Figure 6. 3: Improved horizontal moving belt fibre contactor.	73
Figure 6. 4: Table pan fibre contactor.	74
Figure 6. 5: Graphical representation of the number of theoretical adsorption stages required to produce a barren solution.	75
Figure 6. 6: Schematic top view diagram of the IEF contactor sections.	76

Figure 7. 1: Schematic presentation of the experimental set up for contactor testing.	82
Figure 7. 2: Breakthrough profile of the IEFs contactor and column at 0.16g/cm^3	84
Figure 7. 3: Breakthrough profiles of the contactor and the column at 0.28g/cm^3	85
Figure 7. 4: Breakthrough profile of the contactor and column at 0.37g/cm^3	86
Figure 7. 5: Regeneration profile of the IEFs contactor.	87
Figure 7. 6: Plot of experimental Cu concentration and that predicted by the Thomas, Yoon-Nelson and Adam's Bohart model versus time for the IEFs contactor.	88

LIST OF TABLES

Table 2. 1: Comparison of various ion exchange systems (Nasef and Ujang, 2012)	20
Table 2. 2: Characteristics of pressure and vacuum filters (Bhardwaj and Mirliss, 2001).	21
Table 3. 1: Characteristics of Fiban X-1 cationic ion-exchange fibres (Soldatov et al., 1999; Kosandrovich and Soldatov et al., 2012; Institute Of Physical Organic Chemistry of NASB, 2009).	29
Table 3. 2: Mass of sulphate salts used to prepare the equimolar multicomponent solution.	30
Table 3. 3: Solution to fibre mass ratio for the equilibrium isotherm experiment and the mass of copper in the solutions used.....	32
Table 4. 1: Experimental equilibrium loading and the predicted loading using Redlich-Peterson, Freundlich, Langmuir model, Dubinin & Radushkevich and Temkin model.....	43
Table 4. 2: Mass percentage of Cu loaded from experimental data and that predicted using the pseudo-first-order, pseudo-second-order and the Elovich model.	48
Table 5. 1: Effect of bed packing density on Thomas model parameters.....	60
Table 5. 2: Effect of flow rate on Thomas model parameters.	61
Table 5. 3: Effect of bed depth on parameters of the Yoon-Nelson model.	63
Table 5. 4: Effect of flow rate on parameters of the Yoon-Nelson model.....	63
Table 5. 5: Effect of bed depth on parameters of the BDST model.....	65
Table 5. 6: Effect of bed depth on parameters of the BDST model.....	65
Table 5. 7: Sum of absolute errors between experimental concentrations at various times and those predicted by the Thomas, Yoon-Nelson and Adam's Bohart model at various bed packing densities.	66
Table 5. 8: Sum of absolute errors between experimental concentrations at various times and those predicted by the Thomas, Yoon-Nelson and Adam's Bohart model at various feed flow rates.	66
Table 6. 1: IEF contactor specifications*	77

Table 7. 1: Thomas model parameters for the IEFs contactor pan.	88
Table 7. 2: Yoon-Nelson model parameters for the IEFs contactor pan.....	88
Table 7. 3: Adam's Bohart model parameters for the IEFs contactor pan.	88

Chapter 1: Introduction

1.1 Introduction

An ion exchanger is an insoluble material which traps ions and simultaneously releases ions of the same charge (Park, 2012). This process is known as ion exchange reactions. Thompson and Way were the first to establish the mechanism of the ion exchange reaction in the 1900s (Economy et al., 2002; Nasef and Ujang, 2012). Carbonaceous zeolites were the first organic ion exchangers and were produced by treating soft coals with fuming sulphuric acid (Economy et al, 2002). However, Economy et al. (2002) also states that the first completely organic ion exchanger was prepared in 1935 by Adams and Holmes. It was synthesized through a condensation polymerization reaction, producing a phenol-formaldehyde cation exchange resin. Economy et al. (2002) further states that later, in 1944, D'Alelio patented the now well-known and more stable styrene-based cation exchanger which can be used to generate both cationic and anionic exchange resins.

Over the past 70 years, a number of important advances have been made in the area of ion-exchange systems of various types, such as inorganic clays, zeolites, and specialized polymeric systems designed for the selective removal of unwanted ions (Economy et al, 2002). Today, ion exchange has a wide variety of important applications in industries such as pharmaceutical, food processing, chemical synthesis, biomedical, hydrometallurgy, water treatment, synthetic fibre production, and chromatography (Economy et al, 2002; van Deventer, 2011). In fact, ion exchange is one of the most effective and common method employed in metal recovery systems. Ion exchange is more economical when used to recover valuable metals (Lopes et al., 2012). Furthermore, ion exchange methods have a real potential to achieve complete recovery or removal of metals from solutions without posing other environmental risks and resulting in unreasonable costs (Lopes et al., 2012; Lee et al., 2007; Galan et al., 2005).

Ion exchange materials exist mainly in granular and fibrous form commonly referred to as ion exchange resins and ion exchange fibres (IEFs), respectively. IEFs are preferred due to

their higher reaction rates as well as high selectivity and loading capacities when compared with conventional granular ion exchangers (Soldatov et al., 2004; Kosandrovich and Soldatov, 2012). Furthermore, IEFs can be fabricated in different textures such as fibre, thread, felts, nonwoven cloth, etc., and have higher adsorption/desorption rate due to their larger surface areas and shorter diffusion paths (Huang et al., 2011; Zhang et al., 2008).

However, IEFs require specific technology for efficient application (Kosandrovich and Soldatov, 2012). Since IEFs can exist in the form of felts or fabric, it is technically feasible to design a horizontal moving belt (or drum) system in which ion exchange can occur. In fact as early as 1955, it was demonstrated only on laboratory scale that ion-exchange fabric, in the form of an endless belt could be used for adsorption and continuous concentration of copper (Kotze, 1992). For more extensive and economical applications of IEFs, the development of a continuous loading and elution system is necessary. Therefore, the main aim of this study was to develop an IEFs contactor for continuous removal of Cu^{2+} ions from dilute synthetic solutions. This was done by investigating the feasibility of using an IEF contactor characterized by continuous and simultaneous continuous loading and elution ion exchange system.

1.2 Research problem

Industrial effluent streams contain heavy metals such as Cu^{2+} ions which are harmful to the environment and human health when above certain threshold levels (Ko et al., 2011; Huang et al., 2012; Galan et al., 2005; Ji et al., 2011). It is, therefore, necessary to treat industrial effluent streams prior to their release into the environment. However, techniques like chemical precipitation, reverse osmosis, electrolysis and coagulation that are normally used for heavy metal removal have been found to be inefficient as they result in incomplete metal removal, high reagent and energy requirements, and generate toxic sludge (Alluri et al., 2007; Rodelo et al, 2002). From the literature reviewed, it was found that IEFs are normally used in batch processes and also in columns operated in counter current manner. However, in conventional fixed bed, ion exchange process is not efficient when two or more components are concentrated. Furthermore, fixed beds pressure drops can be significantly increased

thereby reducing ion exchange rate. Therefore, IEFs require specific technology for efficient application (Kosandrovich and Soldatov, 2012). Nevertheless, as early as 1955, a laboratory scale ion-exchange fabric, in the form of an endless belt or drum was used for adsorption and continuous concentration of Cu^{2+} ions. Therefore, this research aims to address the following key questions:

Key Questions:-

- ❖ Can IEFs be fabricated in the form of a “horizontal moving belt” or drum for continuous loading and elution of metals?
- ❖ Can IEFs be fabricated in the form of any other “contactor” for continuous loading and elution of metals?
- ❖ How much loading rates are achievable with IEFs?
- ❖ How much elution rates are achievable with IEFs?
- ❖ Would the process technology be scaled-up from the laboratory to plant?

1.3 Objectives

The objectives of this research project were to develop a continuous ion exchange system utilizing a contactor fabricated from ion exchange fibres that would continuously recover metals in a metallurgical industry set-up.

The specific objectives of the study were:-

- ❖ Determine whether the selected IEFs have a higher selectivity for Cu^{2+} ions.
- ❖ Establish equilibrium and kinetics of the selected IEFs.

- ❖ Determine the required superficial velocity and contact time using columns for the contactor design.
- ❖ Theoretically evaluate various designs of the horizontal ion exchange belts and other compatible systems and select the most suitable one for this application.
- ❖ Investigate the Cu^{2+} ions loading and elution capacity on IEFs packed in a column.
- ❖ Design a segment of the IEFs contactor and test its sorption capacity.

1.4 Research methodology

The research methodology used for this study included the following activities: literature review; batch tests; contactor selection, column tests, contactor design and fabrication and, lastly testing of the fabricated contactor.

1.5 Report layout

This report consists of eight chapters. Chapter 1 entails some back ground information of ion exchange processes, the research problem, as well as the objectives of the study and the research methodology. Chapter 2 contains literature review regarding ion exchange materials mainly fibrous ion exchangers and ion exchange beads. Chapter 3 consists of materials and methods used for batch system studies. Chapter 4 is composed of the results obtained from the batch experiments and discussions of the results. Chapter 5 consists of materials and methods used for column tests as well as the column tests results. The methods used for contactor design are outlined in Chapter 6. The results from testing the designed contactor are contained in Chapter 7. Lastly, Chapter 8 consists of the conclusions and the suggested recommendations.

1.6 Summary

A brief history of ion exchangers was stated as well as advantages of using ion exchange processes over conventional methods of recovering metals from solutions. Furthermore, it was stated that fibrous ion exchangers have several advantages over conventional ion exchange granular beads due to their higher adsorption/desorption rate and ability to exist in the form of felts, cloth and fabric. The problem statement and the objectives of the study and the major tasks that were undertaken have also been outlined in this chapter. Lastly, the report layout was described together with what the report chapters are about.

Chapter 2: Literature review

2.1 Introduction

Demand for copper (Cu) is increasing mainly due to industrialization in the developing countries (RioTinto, 2011). The metal, Cu, is selected for use in a number of households, industrial and technological applications because of its chemical, physical and aesthetic properties. It is also used to produce coins and jewellery. On the other hand, Cu is classified as one of the heavy metals. High consumption of Cu by humans through either contamination or any form of intake may lead to severe mucosal irritation, widespread capillary damage, hepatic and renal damage, central nervous problems followed by depression, gastrointestinal irritation, and possible necrotic changes in the liver and kidney (Rengaraj et al., 2011). The World Health Organization (WHO) has recommended a maximum acceptable concentration of Cu^{2+} ions in portable water of 1.5 mg/L (Rengaraj et al., 2007). Therefore, heavy metals in waste effluent streams need to be reduced to minimal levels. Furthermore, because of its industrial, household and technological importance, it is worthwhile to recover as much Cu^{2+} ions as possible even that found in waste effluent streams so that it can sustain the lives of peoples and ensure economic growth. However, to achieve these more cost effective methods for copper recovery are required.

At present, concentrated solutions of Cu^{2+} ions have been successfully recovered and separated by effective techniques like solvent extraction and ion exchange with resins, but the efficiency of some of these methods decrease when treating less concentrated solutions (Parodi et al., 2008). Furthermore, most of these methods are costly, require extensive labour and time (Rodelo et al., 2002; Alluri et al., 2007). Amongst emerging technologies for the recovery of Cu^{2+} ions, ion exchange fibres (IEF) have been the focus of considerable studies (Ntimbani et al., 2015; Kosandrovich and Soldatov, 2012).

Compared with the conventional ion-exchange beads (IEB), IEFs have several advantages which include the ability to exist in the form of a felt or fabric, leading to improved contact efficiency with the media, thus enhancing both the rates of reaction and regeneration (Dominguez et al., 2001). For example, the half life time of sorption on the chelate IEF is usually less than 1 min compared with several hours for the conventional chelate ion exchangers (Soldatov et al., 2011). From the study conducted by Soldatov et al. (2011), one of the advantage of fibres compared to the microspheric resins is a low hydrodynamic resistance which allows the usage of shallow filtering beds (2 – 5 cm) with a fast linear eluent velocity (5–15 cm/min) and pressure drop less than 20 kPa.

The fast rate of ion exchange on IEF is due to the shorter diffusion path within IEF compared with IEB, which in turn result in an increased overall internal diffusion rate (Kosandrovich and Soldatov, 2012). Furthermore, with respect to ion-exchange membranes (IEM), the IEF have better mechanical properties and are also characterized by a high hydrophilicity (Souilah et al., 2012).

2.2 Ion exchange in general

The ion exchange principle is mainly used in hydrometallurgy for separating ions dissolved in solutions. Depending on the application, the aims and objectives of ion exchange can be categorized as follows (Zagarodni, 2007):

- ❖ *Purification of a solvent* is conducted if the final main product is the solvent, and the entire dissolved ions are seen as impurities.

- ❖ *Purification of solution* is done when the desired product is a solution composed of components suitable for downstream process. The same or similar solution is used as the feed; however, it contains an unwanted solute.

- ❖ *Extraction* is conducted in the case whereby the dissolved ions have to be removed from a solution and the barren solution is valueless.

2.2.1 Ion exchange mechanism

The exchange of metallic ions onto ion exchangers is a heterogeneous complex reaction characterized with the following phenomena:

- ❖ diffusion of metal ions through the solution up to solid ion exchangers (liquid-film diffusion) (Abdelwahab et al, 2013);
- ❖ diffusion of metal ions through the conduits of ion exchange exchangers (particle/intraparticle diffusion) (Abdelwahab et al, 2013);
- ❖ stoichiometric chemical exchange of ions on the ionized functional group in the ion exchanger (reaction rate) (Abdelwahab et al, 2013);
- ❖ diffusion of exchanged ions out of the exchanger and its diffusion through the bulk away from the loaded counter ions (Abdelwahab et al, 2013);

From the above mentioned stages, the ion exchange process can be a result of mass transfer or chemical process or a combination of the two distinct processes (Abdelwahab et al., 2013). It must also be noted that ion exchange operations are accomplished in cyclic operations divided into three stages namely loading, elution/stripping and regeneration. The ion exchange materials are moved from one section to the other depending on their state (loaded, eluted, and regenerated). Cyclic ion exchange processes are optimised by using ion exchange materials having high selectivity towards the ions of interest (Zagorodni, 2007; Nasef and Ujang, 2012).

2.2.2 Structure and properties of ion exchangers

Usually polymers are used to make ion exchange materials and various polymers are cross linked to form a three-dimensional polymeric structure to prevent them from dissolving in solution (Zagorodni, 2007). Zagorodni (2007) further states that the difficulty experienced by ions and water molecules when penetrating inside the material can be reduced by making the matrix more flexible by using longer flexible cross-linking bridges. However, longer bridges increase the total weight of exchangers without increasing the ion exchange capacity since the bridges themselves do not contain functional groups. The functional groups at the inter-

phase boundary are the only groups that participate in the ion exchange process, unlike in solvent extraction where the groups are stationary within the phase (Zagorodni, 2007).

The degree of cross linking, which is the density of cross links between polymeric chains, influences the matrix structure, i.e., elasticity, swelling ability and motion of counter ions within the exchanger (Zagorodni, 2007). Highly cross-linked materials are harder and stable in most cases. However, diffusion rate in highly cross-linked material is slow resulting in a decrease of the overall ion exchange rate in such material. Low cross linked materials can have low stability with jelly-like structures. Nevertheless, they have the advantage of increased rate of ion exchange. A compromise between the desired stability and reactivity is usually made when selecting the most suitable material for practical applications (Zagorodni, 2007).

2.2.3 Selectivity and ion exchange materials

Selectivity of the adsorbent is an important characteristic in evaluating the feasibility of ion exchange processes (Ruthven and Ching, 1989). Selectivity may depend on differences in metal loading equilibrium or on the difference in loading kinetics which is not common (Ruthven and Ching, 1989).

Recovery of Cu^{2+} ions, for example, from industrial effluents or from leaching streams is an important application of ion exchange processes (Dabrowski et al., 2004). The streams have low pH values whereby conventional chelating ion exchangers (iminodiacetate and aminophosphonic groups) do not load Cu^{2+} ions. However, chelating ion exchangers capable of loading Cu^{2+} ions at low pHs (>1.5) have been prepared from N-(hydroxyalkyl) picolamine (Dabrowski et al., 2004). A type of ion exchange resin, Dowex XFS 4195, can adsorb Cu^{2+} ions from 1 M sulphuric acid, but a more concentrated acid is needed for stripping and regeneration purposes (Dabrowski et al., 2004). Another chelating ion exchanger with ability to adsorb Cu^{2+} ions at low pHs is Dowex XFS 4196 and can be regenerated by a less concentrated acid (Dabrowski et al., 2004). In addition, higher selectivity for Cu^{2+} ions is obtained using chelating phenol formaldehyde resin which consists of salicyldoxime and salicylaldehyde as the two subunits (Dabrowski et al., 2004).

The following are other examples where ion exchange processes are applied. Cobalt (Co^{2+} ions) electrolyte is seldom pure cobalt thus it requires purification prior to electrowinning. The following metals, Cu, nickel (Ni) and zinc (Zn) are the most common impurities efficiently removed by ion exchange processes (van Deventer, 2011). The typical concentration of Cu^{2+} and Zn^{2+} ions in Co^{2+} ions electrolyte solution is in the range of 50-200 mg/L and it needs to be reduced to 2mg/L, preferably lower (van Deventer, 2011). Aminomethylphosphonic acid resin is usually used for removing Zn^{2+} and Cu^{2+} ions from Co^{2+} ions electrolyte because it is more selective towards Zn^{2+} and Cu^{2+} ions than Co^{2+} ions (van Deventer, 2011). Examples of commercially available ion exchangers used for Zn^{2+} and Cu^{2+} ions removal include Amberlite IRA 747, Purolite S950, and Lewatit TP260 (van Deventer, 2011). From the studies conducted at Mintek it was found that aminomethylphosphonic acid resin was effective in removing Cu^{2+} ions and Zn^{2+} ions to concentrations below 0.002g/L (van Deventer, 2011).

Currently, the separation of Ni (II) from Co (II) electrolyte is done using resins impregnated with bis-picolylamine (van Deventer, 2011). An example of this type of resin is Dow M4195, which is used at Chambishi Metals Plc in Zambia, as well as at Vale's nickel refinery in Port Colborne, Canada (van Deventer, 2011). van Deventer (2011) further states that the Noranda Research Centre has found that Dow M 4195 kinetics of adsorption was slow, however, the loading profiles were improved at flow rate of 1.2 bed volumes per hour.

2.2.4 Capacity of ion exchange materials

Ion exchangers can be thought of as a “reservoir” comprising exchangeable counter ions which are essentially the amount of fixed charges that must be replaced by the counter ions from the solution (Helfferich, 1995; Zagorodni, 2007). Ion exchangers are, therefore, quantitatively characterized using their capacity (Helfferich, 1995; Zagorodni, 2007).

There are two main definitions of capacity, scientific capacity and apparent capacity. Scientific capacity is the number of functional groups per specified amount of material

(Helfferich, 1995). Apparent capacity is defined as the number of counter ions that are exchangeable per specified amount of material (Helfferich, 1995). The apparent capacity of weak acidic/basic ion exchange functional group is affected by pH in the ion exchanger which is greatly influenced by the pH of the solution (Helfferich, 1995). The degree of ionization of weak acidic functional groups increases with an increase in pH, thereby increasing the extent of ion exchange.

2.3 Fibrous ion exchangers

This study focuses on developing an IEF contactor, therefore, it is worthwhile to have a separate section that discusses IEF. The idea of fabricating ion-exchange materials in the form of fibres was first reported 30 years ago (Economy et al, 2002). IEF can exist in a variety of textile forms such as threads, cloth, belts, paper, nonwoven fabric, sew-knit fabric, etc. (Kosandrovich and Soldatov, 2012). However, the important forms used for industrial applications are staple fibres, nonwoven canvases, and short-cut fibres (Kosandrovich and Soldatov, 2012). Figure 2.1 shows staple and nonwoven IEFs.

The staple fibres are produced by cutting a bunch of parallel endless filaments into pieces with a length of 40–70 mm (Figure 2.2 a) (Kosandrovich and Soldatov, 2012). Staple fibres can be used in the ion exchange application or as raw materials for making nonwoven canvases, threads, felts, etc. The nonwoven materials are canvases manufactured from the staple fibres without application of spinning or weaving (Figure 2.2 b) (Kosandrovich and Soldatov, 2012). Nonwoven fibres are characterized by the surface density, measured by the mass per square metre and thickness (mm), and measured at standardized conditions (Kosandrovich and Soldatov, 2012). The study of Kosandrovich and Soldatov (2012) reveals that the short-cut fibres usually have a filament length of 0.25 – 1.5 mm.

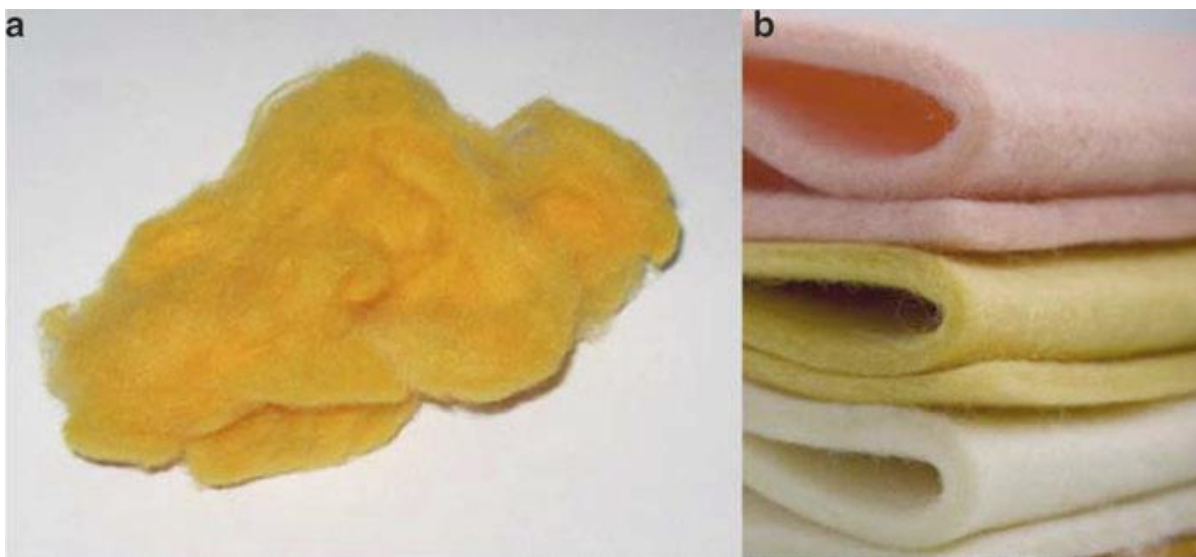


Figure 2. 1: Forms of IEF: (a) Staple fibre of anion exchanger FIBAN A-6. (b) Nonwoven fabrics of different FIBAN materials (Kosandrovich and Soldatov, 2012).

The methods that can be used to prepare ion exchange fibres are listed in Section 2.3.1. These methods entail the use of special polymers, composite fibres as well as grafting.

2.3.1 Fabrication of ion exchange fibres from special polymers

IEF can be made by combining special copolymers from monomers having groups that can dissociate and those which do not dissociate, and spinning solutions or melts of such copolymers with crosslinking agents (Kosandrovich and Soldatov, 2012). However, the synthesis of IEF using special polymers is costly and has not found a large scale application. IEFs with trade name Vion AN-1 are the only industrial fibre made from synthesis of special polymers and it is obtained by spinning of copolymer of 5-vinyl-2-methylpyridine and cross-linked with an epoxide oligomer (Kosandrovich and Soldatov, 2012).

2.3.2 Composite fibres

IEF can also be fabricated by mechanical mixing of inert fibre-forming polymer solutions or melts with evenly distributed IEB (Kosandrovich and Soldatov, 2012). The technology of spinning evenly distributed IEB of 3 – 5 mm size in the solution or melt of the fibre producing polymer can be utilized to make IEF comprised of at most 35% of the ion

exchange material (Kosandrovich and Soldatov, 2012). This technique is also applied by simply mixing a fibre producing polymer with a polymer that is easily changed to an ion exchanger after the fibre is made (Kosandrovich and Soldatov, 2012). Polymerization, copolymerization, or polycondensation of monomeric carriers of functional groups inside or on the surface of the parent fibre is used as well for preparing IEF (Kosandrovich and Soldatov, 2012). However, according to Kosandrovich and Soldatov (2012), IEF prepared this way do not possess good properties.

2.3.3 Grafting techniques for ion exchange fibre synthesis

Graft copolymerization is the most commonly used method for producing various types of IEF whereby the side chains containing the functional groups are grafted onto the chain of the main fibre-forming polymer (Kosandrovich and Soldatov, 2012). Grafting requires generation of free radicals or ions on the main polymer chain and are created using heat, ionizing radiation, or chemical reactions (Kosandrovich and Soldatov, 2012). Kosandrovich and Soldatov (2012) states that chemically inert fibres are used as parent material for grafting in order to withstand active chemicals used for functionalizing the material. Currently, several synthetic fibres, such as polyester, polyacrylonitrile and polypropylene, have been used as the parent fibres for the production of conventional IEF. However, amongst these synthetic fibres, polypropylene is widely used because of its low density, low cost, easy processing and ability to be modified to meet a variety of performance characteristics (Ji et al., 2011). To ensure that the mechanical strength is sufficiently high, the polystyrene-based ion exchange fibres are enhanced by the introduction of cross-linking group (Yoshioka and Shimamura, 1983).

2.4 Ion exchange operations

The common forms of ion exchange exchangers are granular beads, membranes, fibres, and hydrogels (Nasef and Ujang, 2012). For these polymer forms to be applied, a suitable engineering system with a set of operating parameters that can be manipulated to control their performance is required (Nasef and Ujang, 2012). Accordingly, the ion exchange systems take various configurations depending primarily on the physical form of ion

exchange material. The volume of solution and concentration of ionic species to be treated also play a role in the selection of system configuration (Nasef and Ujang, 2012).

There are three basic operating methods for ion exchangers consisting of batch, column and moving bed configurations (DuHamel and Graczyk, 1997). Batch or column methods are normally used for achieving separation when ion exchange material is in resin/bead form whereas plate and frame modules/cells are favoured upon using membrane/sheet forms (Nasef and Ujang, 2012).

2.4.1 Batch

In a batch method, the resin and solution are mixed in a batch tank, the exchange reaction is allowed to come to equilibrium, and then the resin is separated from the solution (Hamdaoui, 2009; Nasef and Ujang, 2012). The degree to which the exchange takes place is limited by the selectivity of the resin for the ions of interest in solution. As a result, the loading of ions onto the exchanger is hindered unless the preference for the ions in solution is higher than for the counter ions in the resin (Nasef and Ujang, 2012). Batch regeneration of the resin is chemically inefficient; therefore, it is often used in laboratories for fundamental sorption equilibrium and kinetic studies (Nasef and Ujang, 2012; Hamdaoui, 2009). For this reason the batch method is seldom used for industrial applications.

2.4.2 Fixed packed bed column

Ion exchange operations are usually carried out in fixed packed bed columns for industrial applications. Fixed packed bed columns operations is comparable to a number of batch reactors arranged in series (Nasef and Ujang, 2012). Column operations aim at utilizing the ion exchange by taking advantage of the limitation of selectivity of the resin (Nasef and Ujang, 2012). Single column operation necessitates storage reservoir unit to accumulate the feed solution during elution, regeneration and rinsing (Zagorodni, 2007). Therefore, multiple column systems are used to favour high selectivity. Columns are operated in either down flow, up flow, or counter flow modes or combinations of the different modes (Nasef and Ujang, 2012). Many fixed packed bed columns are operated in down flow mode whereby the feed to be treated is passed down through the bed of ion exchangers. The down flow

operation reduces the frequency at which the resins hit the interior walls of columns, thereby minimizing mechanical deterioration of resins. Moreover down flow operations as opposed to up flow does not alter the resin packing in a way that results in channelling of the feed solution. Column counter flow is when loading and elution are carried in down flow and up flow manner respectively or vice versa.

Fixed bed ion exchange (FBIX) is not suitable for separating concentrated components from each other (Chinn et al., 1992). This is due to the fact that the resin bed in FBIX is in equilibrium with the feed solution at the end of the loading step. As a result, achieving a good separation depends on favourable equilibrium loading of one of the concentrated components (Chinn et al., 1992). Even if equilibrium loading is favourable, the mixing of entrained concentrated feed together with flush result in inefficiencies of the operation (Chinn et al., 1992). In addition, fixed beds pressure drops can be significantly increased thereby reducing ion exchange rate. Consequently, FBIX systems have been restricted to the recovery of dilute components (Chinn et al., 1992).

2.4.3 Recoflo technology

Recoflo technology is an improvement to the fixed packed bed column, it uses fine mesh resins beads, and the bed is fully packed and regeneration is carried out in a counter current manner (Sheedy, 1998). Counter current in this case means that the regenerating solution is passed through the bed in the direction opposite to that of the solution to be treated. The recoflo technology is commercially applied in the following areas:

- ❖ separation of strong minerals from dissolved metal salts (Sheedy, 1998);
- ❖ purification, removal and recycle of dissolved metals in the surface finishing industry (Sheedy, 1998);
- ❖ production of highly purified water (Sheedy, 1998).

The use of fine mesh resins improves the exchange kinetics since the rate of exchange is inversely proportional to square of the particle diameter. As opposed to the fixed bed packed column, the bed depths are reduced and the remaining resin bed participates in the exchange. The configuration of the bed does not allow backwash in the system, so when treating solid containing material a proper filtration system must be installed. Moreover, fine mesh resins are expensive and difficult to obtain (Sheedy, 1998).

2.4.4 Fluidised bed column

The fluidized bed column operation is used when the raw feed contains suspended solids (Zagorodni, 2007; Nasef and Ujang, 2012). The presence of free-pass ways between beads allows the solid suspended particles to be transferred through the column giving fluidized bed column the advantage of processing solid-containing solution without any pre-treatment (Zagorodni, 2007; Nasef and Ujang, 2012). The ability of fluidised bed columns to handle solids makes them favourable for applications in biochemical filtration processes; such as fermentation broth where treated solutions are highly contained with suspended solids (Nasef and Ujang, 2012). The main disadvantage of fluidized bed is the inherent longitudinal mixing of the treated solution and the suspended ion exchanger in the column (Zagorodni, 2007).

2.4.5 Moving beds

The moving beds are the most cost effective methods applied for ion exchange operations. Moving beds operate by simply providing motion to ion exchangers and solution so that they flow within the system (Nasef and Ujang, 2012). The ion exchangers are contacted counter currently with the feed and eluent streams (Gold et al., 1975; Nasef and Ujang, 2012). At large scale operations, the separation is conducted using loop reactors which combine all the cyclic ion exchange process, incorporating elution and regeneration in a single unit (Zagordni, 2007). The advantage of this operation is a product of uniform quality at less space, capital, and labour (Gold et al., 1975; Nasef and Ujang, 2012). However, the necessity to circulate the bed around the sections (adsorption, regeneration, etc.) poses a problem during operation (Gold et al., 1975; Nasef and Ujang, 2012). An example of a contactor that uses moving beds is the Higgins contactor and it is the most successful of the moving bed reactors (Zagorodni, 2007). A diagram illustrating a Higgins contactor for water deionisation

is shown on Figure 2.2. The contactor has four parts namely the deionisation section, regeneration section, propulsion section, and expansion section labeled 1, 2, 3 and 4 as depicted on far right sketch on the figure (Zagorodni, 2007).

Regardless of being the most successfully simulated moving bed reactor, the Higgins contactor has difficulties in providing circular motion of the exchanger and the process is unstable (Zagorodni, 2007). Furthermore, there is a problem of longitudinal mixing at points of circular transportation and there is also deterioration of ion exchange resins due to the continuous exploitation (Zagorodni, 2007).

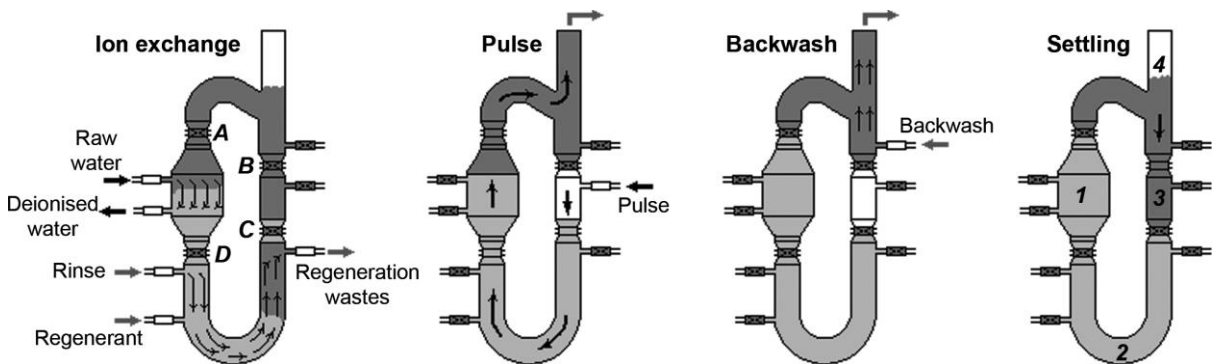


Figure 2. 2: Higgins contactor in water deionization process (Zagorodni, 2007).

2.4.6 Cascade columns

Columns arranged in a cyclic manner in cascade operations are used as an improvement to the moving bed technology (Zagorodni, 2007). The cascade technology operation is characterised with higher stability, increased lifetime of exchangers and has no axial mixing (Zagorodni, 2007). This technology allows the reduction of column sizes, but this in turn requires a larger operating space, and many control points and number of units. The arrangement and operation of the cyclic cascade technology is shown on Figure 2.3 below.

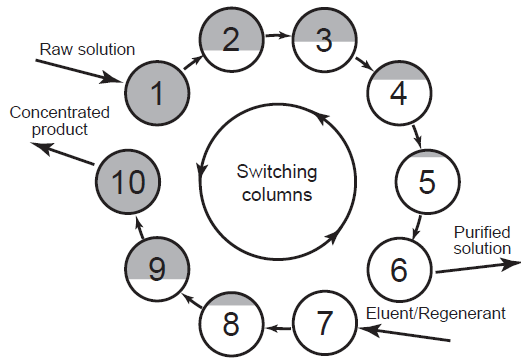


Figure 2. 3: Cascade technology employing cyclic columns.

2.4.7 Ion exchange membranes

Membranes are also used to carry out ion exchange processes. Ion exchange membranes are defined as thin sheets or films of ion exchange material that are used to separate ions by allowing either cations or anions to pass through (Kariduraganavar et al., 2012). Ion exchange membrane requires the membrane to be housed in a vessel called module (Nasef and Ujang, 2012). Support and protection from operating pressures, daily wear and tear caused on the operating environment is provided by the module, and it allows the application of control strategy over the system performance.

There are three things required to make ion exchange membranes, i.e., it must be a membrane, and it must be insoluble in solvents and must contain fixed charges within the membrane (Sata, 2004; Kariduraganavar et al, 2006). Membrane ion exchangers are produced by introducing functional groups into a polymer; thereafter, the polymer is turned into an insoluble membrane (Sata, 2004; Kariduraganavar et al, 2006). After turning the polymers into an insoluble membrane, a polymeric membrane is produced in which ion exchange groups (functional groups) are embedded; the polymers containing reactive groups are reacted with diamines, for example, to introduce anion exchange groups and form cross links in the process (Sata, 2004; Kariduraganavar et al, 2006).

Membrane modules are usually configured as plate-and-frame, spiral wound, tubular and hollow fibre (Nasef and Ujang, 2012). The plate-and-frame modules are the most employed membrane module for exchange operations (Nasef and Ujang, 2012). They have layers of

membranes divided by folded structural sheets referred to as corrugations (Nasef and Ujang, 2012). These corrugations run at right angles in alternating layers with feed material flowing in and retentate flowing out in one direction, while a carrier fluid flows in and permeate out in the other direction (Nasef and Ujang, 2012). The advantages of this system include ability to accommodate low levels of suspended solids and viscous fluids and the ability to replace membrane if needed (Nasef and Ujang, 2012). Its disadvantages include relatively low packing density, high initial cost, and difficulty of cleaning (Nasef and Ujang, 2012).

Common applications for plate-and-frame are in membranes used in electrodialysis and electrochemical processes while membranes applied for other processes have different configurations. Electrochemical membranes are applied for reduction of uranyl ions to uranous ion on the cathode (Kariduraganavar et al., 2012).

Ion exchange membranes have a higher mechanical strength when compared with IEF and IEB. Cationic IEB tend to be brittle and the anionic IEB are softer (Kariduraganavar et al., 2012). However, equipment required for membranes can be costly to construct and operate at large scale (Nasef and Ujang, 2012). Due to the cost associated with equipment and operation, the whole process may be uneconomical in the case where the desired product exists in low concentrations.

Table 2.1 summarises the advantages and disadvantages of various system configurations (batch, column, moving bed, membrane) for ion exchange.

Table 2. 1: Comparison of various ion exchange systems (Nasef and Ujang, 2012)

System configuration	Advantages	Disadvantages
Batch system	<ul style="list-style-type: none"> ❖ Easy to fabricate and operate ❖ Suitable for small scale ❖ Compatible with most ion exchangers ❖ Applicable for most kinds of treatments ❖ Can handle resins of any shape 	<ul style="list-style-type: none"> ❖ Manual operation may be cumbersome to operate with large volumes of waste ❖ The separation of liquid and ion exchange media is required ❖ Can only be operated at atmospheric pressures and ambient temperatures ❖ Once through use only
Conventional column system	<ul style="list-style-type: none"> ❖ Good throughput ❖ Simple to operate ❖ A wide variety of media are available ❖ Can be operated at elevated temperatures and pressures ❖ High decontamination factors are possible 	<ul style="list-style-type: none"> ❖ Large equipment can be costly ❖ The regeneration of media may require extra equipment ❖ There are difficulties in transporting inorganic ion exchangers through pipelines ❖ Requires prefiltration ❖ Small bed portion participates in the process at a time
Moving bed system	<ul style="list-style-type: none"> ❖ Continuous operation ❖ Achieves desired decontamination factors ❖ Requires less space for operations ❖ Less equipment required to supplement the operation ❖ Low pressure drop ❖ Requires no prefiltration 	<ul style="list-style-type: none"> ❖ Process is unstable ❖ Axial mixing problems ❖ Difficulty in providing circular motion ❖ Physical damage to ion exchangers
Membrane system	<ul style="list-style-type: none"> ❖ Applicable to waste treatment or concentration of metals ❖ Prefiltration is not necessary ❖ Does not require IEB ❖ Desired decontamination factors are possible 	<ul style="list-style-type: none"> ❖ Equipment can be costly to construct and operate on a large scale

2.5 Other ion exchange compatible systems

2.5.1 Diatomaceous earth filter

Diatomaceous earth (DE) filtration is a process that makes use of skeletal remains of small single celled organisms as filtration media (Bhardwaj and Mirliss, 2001). DE filtration removes solids from water and eliminates the need to use coagulant materials (Bhardwaj and Mirliss, 2001). The DE filter consists of a porous filter septum on which diatomaceous layer forms (Bhardwaj and Mirliss, 2001).

The filter media used in the diatomaceous can be replaced by media that allows for ion exchange process. An introduction of functional groups with higher affinity for the metal(s) of interest can make the system suitable for metal removal or recovery from dilute streams. Since the system does not require a separate prefiltration step, it can treat solid containing streams. However, the system will only allow loading, elution or backwashing at a time.

There are two types of DE filters: pressure and vacuum filters. Pressure filters have a pump on the influent stream and the filter media including the septum are enclosed within a vessel (Bhardwaj and Mirliss, 2001). Vacuum filters are open to the atmosphere and have a pump on effluent stream (Bhardwaj and Mirliss, 2001). Table 2.2 below outlines the characteristics of pressure and vacuum fliters.

Table 2. 2: Characteristics of pressure and vacuum filters (Bhardwaj and Mirliss, 2001).

Pressure filters	Vacuum filters
❖ Can handle high flow rates, allowing utilization of smaller, more compact filter units.	❖ Low capital fabrication cost
❖ Longer operations, leading to less amount pre-coat material and backwash water required due to less cycles for cleaning	❖ Low maintenance costs
❖ Less likelihood for disruption of media by gas bubbles	❖ Open to the atmosphere, allowing easy access and observation

2.5.2 Cartridge filters

Purolite (company with expertise in ion exchange resin technology) produces ion exchange cartridges from virgin polypropylene and using the recent heat welding techniques (Purolite, 2012). Ion exchange cartridge filters are composed of ion exchange material packed in a cartridge. For water treatment purposes, the ion exchange material used is selected based on the impurities that need to be removed. The operation of ion exchange cartridge filters is analogous to that of fixed packed bed.

2.5.3 Filter presses and belt filters

Filter presses and belt presses are used for solid liquid separation. Press filters consist of pressure plate and filter plates which are basically a cloth attached to plate frames (Sparks, 2012). The solid-liquid separation is conducted by introducing the slurry into the filter plates and the pressure is applied on the filter plate by pressure plate (Sparks, 2012). Belt filters utilise a cloth that moves continuously over at least two rollers and a vacuum under the cloth is created to ensure that filtration occurs (Sparks, 2012).

As early as 1955, it was suggested that ion exchange fibres fabricated into a belt moving on rollers can be used for continuous metal recovery from solutions (Muendel and Selke, 1955; Kotze, 1992). Actually, belt filters are more suitable for creating a continuous metal removal system. As the belt rotates, loading, elution and rinsing will be taking place simultaneous on the fibre belt.

2.6 Adsorption isotherms and kinetic models

2.6.1 Adsorption equilibrium isotherms

The Freundlich, Langmuir, Redlich and Peterson, Temkin, and the Dubinin–Redushkevich isotherm models are normally used to describe experimental equilibrium isotherms (Rengaraj et al., 2007; Gando-Ferreira et al., 2011; Hamdaoui, 2009; Ofomaja, 2010). The Freundlich isotherm model represented in Equation 2.1 is used to explain the observed phenomena during ion exchange process.

$$\log q_e = \log K_F + 1/n \log C_e \quad (2.1)$$

Where: C_e is the equilibrium concentration (mg/L);

q_e the amount of adsorbate per gram of the ion exchange resins;

K_F is the the Freundlich constant and

n is the Freundlich exponent

C_e , q_e , K_F and n are constants incorporating all factors affecting the adsorption process such as adsorption capacity and intensity (Rengaraj et al., 2007). The values of K_F and n are determined from the intercept and slope of the plot of $\log q_e$ and $\log C_e$, respectively. A strong linear relationship between $\log q_e$ and $\log C_e$ suggests that the adsorption follows Freundlich isotherm model (Rengaraj et al., 2007).

The Langmuir isotherm can be also applied to adsorption equilibrium during ion exchange with (Rengaraj et al., 2007). In particular, the Langmuir model (Equation 2.2) is applied to homogeneous sorption where the sorptions of the sorbate molecules onto the surface have the same sorption activation energy (Rengaraj et al., 2007). The Langmuir sorption isotherm is normally used to illustrate sorption of a solute from a liquid solution as follows:-

$$1/q_e = 1/Q_0 + 1/(bQ_0C_e) \quad (2.2)$$

Where C_e is the equilibrium concentration (mg/L);

q_e the amount adsorbed at equilibrium (mg/g);

Q_0 and b are Langmuir constants

Q_0 and b are related to adsorption capacity and energy of adsorption, respectively (Rengaraj et al., 2007). The values of Q_0 and b can be calculated from the slopes and intercepts of the Langmuir plots, respectively. The linear plots of $1/q_e$ versus $1/C_e$ with strong correlation confirm that the adsorption obeys Langmuir isotherm model.

Redlich and Peterson integrated the features of the Langmuir and Freundlich isotherms into a single equation and presented a general isotherm equation (Equation 2.3) provided below.

$$C_e/q_e = 1/(K_R) + a_R/(K_R) C_e^\beta \quad (2.3)$$

Where K_R , a_R and β are constants

The exponent, β , lies between 0 (Henry's law equation) and 1 (Langmuir form) (Rengaraj et al., 2007). Plotting C_e/q_e against C_e^β in Equation 5 to obtain the isotherm constants is impossible due to the three unknowns, a_R , K_R and β . A minimization procedure is, therefore, adopted to solve the above equation by maximizing the correlation coefficient between the theoretical data for q_e predicted from the above equation and the experimental data (Rengaraj et al., 2007).

The Temkin isotherm has been applied in the following form provided below (Equation 2.4):

$$q_e = RT/b \ln A + RT/b \ln C_e \quad (2.4)$$

Where $RT/b = B$ (2.5)

The constants A and b are determined from linear plots of q_e versus $\ln C_e$.

Dubinin and Radushkevich proposed another popular equation for the analysis of isotherm of a high degree of rectangularity (Equation 2.6 below) (Rengaraj et al., 2007).

$$\ln q_e = \ln q_s - B \varepsilon^2 \quad (2.6)$$

Where ε can be correlated as:

$$\varepsilon = RT \ln(1 + 1/C_e) \quad (2.7)$$

Where R is the gas constant (8.314 J/mol K);

T is the absolute temperature;

q_s is the Dubinin–Radushkevich isotherm constant related to adsorption capacity (mg/g)

The constant B provides the mean free energy E of sorption per molecule of the sorbate when it is transferred to the surface of the solid from infinity in the solution, and can be computed using the relationship in Equation 2.8 (Rengaraj et al., 2007):

$$E = 1/\sqrt{2B} \quad (2.8)$$

Linear plot of $\ln q_e$ versus ε^2 enables one to determine the constants q_e and E provided a strong linear relationship exists (Rengaraj et al., 2007).

2.6.2 Adsorption kinetic models

The kinetic parameters which are useful for the computation of adsorption rate, provides essential information for designing and modelling processes (Rengaraj et al., 2007). Therefore, it is important to analyse the effects of initial concentration, contact time, and adsorbent dosage from the kinetic perspective (Rengaraj et al., 2007). The kinetics of the adsorption data can be analyzed using various kinetic models such as pseudo-first-order and pseudo-second-order models as well as the Elovich model.

Equation 2.9 provided below is used to determine the rate constant for pseudo-first-order chemical sorption (Rengaraj et al, 2007; Bakiya lakshmi and Sudha, 2012).

$$\log(q_e - q_t) = \log(q_e) - k_1 t / 2.303 \quad (2.9)$$

Where:-

q_e - Amount of metal adsorbed at equilibrium

q_t - Amount of metal adsorbed at time t

k_1 - First order adsorption rate constant

t - Time

The pseudo-second order reaction is greatly influenced by the amount of metal on the adsorbent's surface and the amount of metal adsorbed at equilibrium (Rengaraj et al, 2007). The rate is directly proportional to the number of active surface sites (Rengaraj et al, 2007; Bakiya lakshmi and Sudha, 2012). Equation 2.10 provided below is used to describe pseudo-second order chemical sorption.

$$t/q_t = 1/(k_2 q_e^2) + t/q_e \quad (2.10)$$

$$rate = k_2 q_e^2 \quad (\text{Initial sorption rate})$$

Plot of t/q_t vs t are used to determine rate constant values (k_2) and amount of metal adsorbed at equilibrium (q_e) from intercepts and slopes, respectively.

The Elovich model is also used to describe the dynamic behaviour of ion exchange processes and it is expressed in Equation 2.11 as follows (Abdelwahab et al., 2013; Özacar and Sengil, 2005):

$$dq_t / dt = \alpha e^{-\beta q_t} \quad (2.11)$$

To simplify the Elovich model, $\alpha\beta$ is assumed to be greater than 1 and the following boundary conditions, $q_t = 0$ at $t = 0$ and $q_t = q_t$ at $t = t$ are applied (Abwdelwahab et al., 2013). Equation 2.11 then becomes:-

$$q_t = 1/\beta \ln(\alpha\beta) + 1/\beta \ln t \quad (2.12)$$

where α is the initial sorption rate (mg/g min), and the parameter β is related to the extent of surface coverage and activation energy for chemisorption (g/mg). A strong linear relationship between q_t and $\ln t$ illustrates that the data follows the Elovich kinetic model.

Chapter 3: Materials and Methods

3.1 Introduction

This chapter describes the materials and the procedures followed during batch experimental tests and sample analysis. The experimental tests were aimed at generating parameters required for designing an ion exchange contactor. This chapter also includes sources of materials used in the study. Details of the experimental data are provided in Table A.1 – A.5 of Appendix A.

3.2 Material acquisition

Ion exchange fibres (IEFs) referred to as Fiban X-1 were selected as the ion exchange material for this study. Fiban X-1 consists of iminodiacetate and carboxylic acid group attached to the polyacrylic matrix (Soldatov et al., 2011). The selected IEFs are generally referred to as chelating ion exchangers (Yahorova et al., 2010; Soldatov et al., 2011). The chemical representation of structure of Fiban X-1 is shown in Figure 3.1.

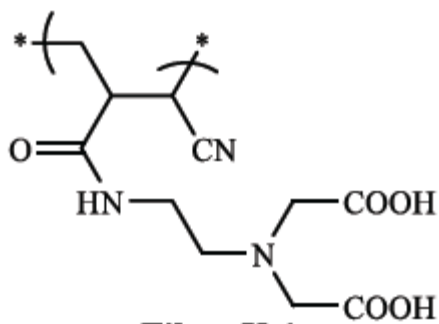


Figure 3. 1: Chemical structure of Fiban X-1 (Yahorova et al., 2013).

The ion exchange materials were purchased from the Institute of Physical Organic Chemistry (IPOC, Minsk, Belarus). Metal sulphate salts of the following elements: copper (Cu^{2+} ions), cobalt (Co^{2+} ions), nickel (Ni^{2+} ions), zinc (Zn^{2+} ions), manganese (Mn^{2+} ions) and

magnesium (Mg^{2+} ions) were also used for the test work. These metal sulphate salts were supplied by Merck, South Africa.

3.3 Fibre preparation

The IEFs were converted to H^+ form by washing with 2 M H_2SO_4 for 2 hours at room temperature. Acid of about 10 times the volume of IEFs was contacted with IEFs in a sealed bottle and was mixed by rolling on rollers for 2 hours. After 2 hours of contact, IEFs were separated from the acid by vacuum filtration. The IEFs were then washed with de-ionized water to remove entrained acid. Thereafter, the IEFs were left to dry in air for 24 hours. The characteristics of the fibres used in this study are listed in Table 3.1 below. The data in Table 3.1 is as provided by studies conducted by Soldatov et al. (1999) and the supplier, IPOC.

Table 3. 1: Characteristics of Fiban X-1 cationic ion-exchange fibres (Soldatov et al., 1999; Kosandrovich and Soldatov et al., 2012; Institute Of Physical Organic Chemistry of NASB, 2009).

Characteristics	Values/description
Physical form	Staple form
Maximum compression	0.24 kg/dm ³
Volume density	0.07 – 0.10 kg/dm ³
Effective diameter	10 – 40 μ
Colour	yellow
Matrix	Acrylic
Functional group	Carboxylic group, Iminodiacetic group
Ionic form as shipped	H^+
Total cationic capacity	3.74 meq/g
Moisture holding capacity	0.6 g H_2O /g
pKa	9.3
ΔpK	1.0
Temperature range	0 – 80 °C

3.4 Reagent and solution preparations

Caustic soda (NaOH) and sulphuric acid (H_2SO_4) solutions of 1 M and 2 M, respectively, were prepared from NaOH pellets and H_2SO_4 solution both with an assay of 98%. NaOH is commonly used for increasing pH of a solution in laboratory tests (Alyüz and Veli, 2009;

Ofamaja, 2010; Yahorova et al., 2010). On the other hand, H₂SO₄ is commonly used to decrease pH of solution in laboratory tests (Yahorova et al., 2010). About 2M HCl was prepared using 30 % HCl solution. HCl is used for eluting loaded metals from ion exchangers (Kose and Ozturk, 2008). An equimolar (2 mM) feed solution was prepared from metal sulphates of Cu²⁺ ions, Co²⁺ ions, Ni²⁺ ions, Zn²⁺ ions, Mg²⁺ ions and Mn²⁺ ions. The amounts of salts and solutions used to prepare the reagents are given in Table 3.2.

Table 3. 2: Mass of sulphate salts used to prepare the equimolar multicomponent solution.

Element	Mass of element required (g)	Mass % of element in the salt	Mass of salt required (g)	Assay of salt (g)	Actual salt mass required (g)	Amount of metal in ppm
Ni	0.235	0.223	1.051	0.990	1.062	117
Co	0.236	0.210	1.124	0.975	1.153	118
Zn	0.262	0.227	1.150	1.015	1.133	131
Mg	0.097	0.202	0.481	0.660	0.730	49
Mn	0.220	0.325	0.676	0.990	0.683	110
Cu	0.254	0.254	0.999	0.998	1.001	127

3.5 Effect of pH on extraction (s-curves)

Volumes of 100 mL of feed solution composed of Cu²⁺, Co²⁺, Ni²⁺, Zn²⁺, Mg²⁺ and Mn²⁺ ions with each at a concentration 2mM were contacted with 2 g of fibre in the pH range of 1.5-5.0 to determine how selectivity varies with pH. NaOH or H₂SO₄ was used to control pH from 1.5 to 5.0 accordingly within 0.5 pH increment. The tests were run for 24 hours and the final pH readings were noted. The IEFs were separated from the solution by vacuum filtration as stated in Section 3.3. Thereafter, the IEFs were washed with 100 mL of deionised water so as to remove entrained solution. The washed fibre sample was then stripped with 200 mL of 2 M HCl solution by agitation in a beaker for 4 hours. The eluted IEFs were separated from the eluent by filtration and then washed with deionized water. The volumes of the eluent were measured. Samples of effluent solutions, wash water used to wash the loaded IEFs, eluent solution and wash water used to wash the eluted IEFs were collected and analysed for

various metals. The washed IEFs were dried and stored for re-use. A schematic representation of the experimental set up is shown in Figure 3.2.

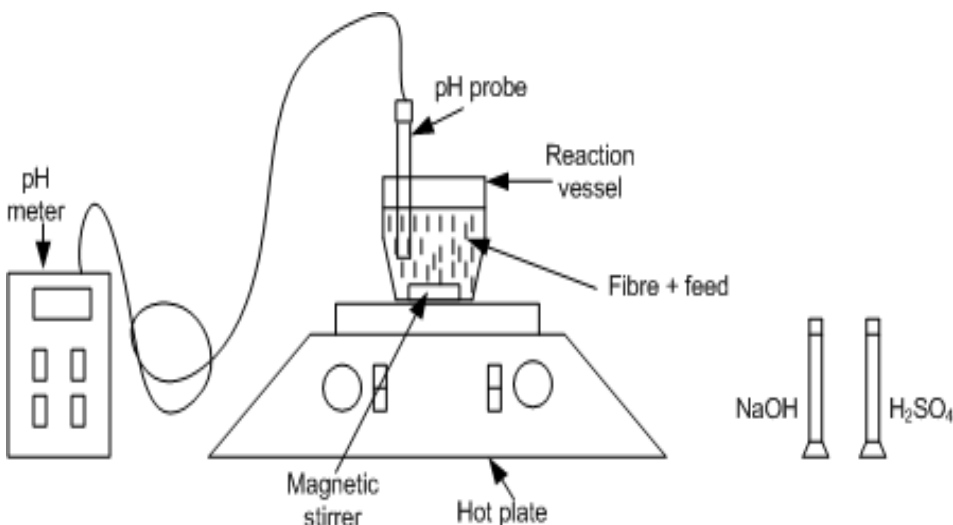


Figure 3. 2: Schematic experimental set up for loading tests.

3.6 Maximum loading capacity of copper

The tests for maximum Cu²⁺ ions loading were done to determine the amount of Cu²⁺ ions that could be loaded per g of IEFs at an optimum pH. A volume of 3.6 L containing 2mM (127 mg/L) Cu²⁺ ions was contacted with 0.5 g of fibre for 24 hours. The volume was selected to ensure that there was excess amount of Cu²⁺ ions ions in solution with respect to the capacity of IEFs given by the supplier. The pH of solution was controlled at 3 (selected optimum pH for Cu²⁺ ions loading from s-curve test as stated in Chapter 4). After the contact time the IEFs were separated from solution and washed. The washed IEFs were eluted with 100 mL of 2 M HCl solution for 4 hours as described above. Samples were collected and analysed as stated in the previous section. The fibres were dried and stored for re-use.

3.7 Generation of equilibrium adsorption isotherms

Adsorption equilibrium isotherms were generated for the loading of Cu^{2+} ions onto the IEFs by contacting fibre with synthetic Cu^{2+} ions (127 mg/L) solution at various solutions to fibre mass ratios as shown in Table 3.3.

Table 3. 3: Solution to fibre mass ratio for the equilibrium isotherm experiment and the mass of copper in the solutions used.

Mass ratio of solution to fibre (g/g)	mass of copper in solution (mg)
200	25
600	38
800	51
1200	76
2000	127
3600	220
4000	254

The solutions containing the fibres were mechanically agitated using a magnetic stirrer (Heidolph 036110550 MR Hei-Tec Digital Hot Plate Stirrer) at 300 rpm. The pH values for the individual experiments were controlled at the selected optimum pH of 3.0 obtained from s-curve experiments (see Chapter 4). NaOH or H_2SO_4 were used accordingly to control the pH at 3.0. The IEFs were separated from the solution by filtration and washed with de-ionised water. The washed fibre samples were then stripped by contacting with 100 mL of 2 M HCl solution for 4 hours in a batch system. The eluted IEFs were washed and separated by filtration. The fibres were dried and stored for re-use.

3.8 Elution test work

Prior to stripping, 1 gram of IEFs was loaded with copper by contacting the fibre with a 127 mg/L Cu^{2+} ions solution for 24 hours. The loading was conducted at the optimal pH of 3.0 (see Chapter 4). This was repeated for 4 samples of IEFs. The samples were collected and separation was done as described above in Section 3.5.

The loaded fibre samples were then used for eluent concentration evaluation test work. Concentrations of 0.1 M, 0.5 M, 1 M, 1.5 M and 2 M of HCl was used to strip the metal ions

from the fibre. The various concentrations of HCl were contacted with IEFs in a magnetically stirred beaker for 4 hours in a batch system. Samples were collected and separation was done as described in previous sections.

3.9 Kinetic tests

Kinetic tests were conducted at the optimum pH. About 2 g of IEFs was contacted with 0.8 L of 127 mg/L Cu^{2+} ions solution in a beaker where it was magnetically stirred. Samples of 5 mL from the solution were collected at the following time intervals: 5 min; 10 min; 15 min; 20 min; 30 min; 40 min; 50 min; 60 min; 2 hrs; 3 hrs; 4 hrs; 8 hrs; 10 hrs and the last sample was collected after 24 hrs. The IEFs were separated and washed and then eluted with 200 mL of 2M HCl as described previously (see Section 3.5). The larger volume of acid used was to ensure complete elution of Cu^{2+} ions from the IEFs. The IEFs were then separated, washed and stored for re-use.

3.10 Sample analysis

Analysis of samples for Cu^{2+} ions and other metal ions was done using AAS (Varian, SpectrAA 220 Fast Sequential). A picture of the Varian, SpectrAA 220 Fast Sequential is shown in Figure A.1 of Appendix A. The AAS measures the amount of light absorbed by the atoms in the excited state and in this way the concentration of samples referred to as analyte was determined. A certain amount of light absorbed by atoms corresponds to a specific concentration of elements. The mass extracted based on adsorption was calculated using the concentration of barren solutions and the wash water used to wash the loaded IEFs.

Standard solutions containing Zn^{2+} , Cu^{2+} , Co^{2+} , Ni^{2+} , Mg^{2+} and Mn^{2+} ions at 1.6, 8, 12, 12, 20 and 60 mg/L were used to calibrate the AAS. Samples collected from the experiments were diluted 5, 10 and 20 times with 4% HNO_3 . The diluted samples were aspirated to the atomizer using the embedded pump in the AAS machine. When the samples were atomized, the lamps for Cu^{2+} , Co^{2+} , Ni^{2+} , Zn^{2+} , Mn^{2+} and Mg^{2+} passed light through the atomized sample from which the concentration of each metal was determined depending on the amount

of light absorbed. The volumes and concentrations of feed, barren solution and wash water were substituted into Equation 3.1 to determine percentage loading or extraction based on adsorption.

$$\begin{aligned} \text{mass \% extraction} &= \frac{m_{\text{feed}} - m_{\text{barren}} - m_{\text{wash}}}{m_{\text{feed}}} \times 100\% \\ &= \frac{V_{\text{feed}}C_{\text{feed}} - V_{\text{barren}}C_{\text{barren}} - V_{\text{wash}}C_{\text{wash}}}{V_{\text{feed}}C_{\text{feed}}} \times 100\% \quad (3.1) \end{aligned}$$

Where m_{feed} is the mass of Cu^{2+} ions in feed solution; m_{barren} is the mass of Cu^{2+} ions in treated feed solution; m_{wash} is the mass of Cu^{2+} ions in wash water from washing the loaded IEFs. V_{feed} and C_{feed} are the feed volume and feed concentration of ions; V_{barren} and C_{barren} are the barren volume and barren concentration of ions; and V_{wash} and C_{wash} are the wash volume and concentration of ions in the wash water.

Chapter 4: Results and discussions

4.1 Introduction

Batch tests were conducted by contacting dilute Cu^{2+} ions solution with IEFs. The tests of the effects of pH on metal loading were conducted to determine the optimum operating pH and selectivity of IEFs for a solution containing Cu^{2+} , Co^{2+} , Ni^{2+} , Zn^{2+} , Mn^{2+} and Mg^{2+} . Maximum loading tests were carried out to determine the amount of Cu^{2+} ions that IEFs can load at the optimum pH. Equilibrium tests were conducted to generate the equilibrium curve that will be used in conjunction with the operating line to obtain the number of stages required to achieve the desired Cu^{2+} ions concentration in effluent solution. Lastly, the kinetics tests and elution tests were also conducted to determine the residence time and acid concentration required for complete elution, respectively.

A description of the experimental set up and procedures followed to perform the experiments are given in Chapter 3. The analytical technique used for determining the concentration of the metals in the solution samples is also given in Chapter 3. The models used for analysing the equilibrium and kinetics experimental data are outlined in Section 2.6 of the Literature Review (Chapter 2).

Experimental data and calculations for the results discussed in this section are provided in Appendix B. Raw and calculated data for the effects of pH on metal loading, maximum metal loading, equilibrium isotherm, elution tests and kinetic tests are provided in Tables B.1 – B.5, B.6 - B.7, B.8 – B.11, B.12 – B.14 and B.15 – B.18, respectively.

4.2 Effects of pH on metal loading

The effects of pH on metal extraction were investigated using an equimolar feed solution containing Cu^{2+} , Co^{2+} , Ni^{2+} , Zn^{2+} , Mn^{2+} and Mg^{2+} each at 2mM. The pH was varied from 1.5-5.0 at increments of 0.5. The general reaction that occurred during the adsorption of each metal is given as Reaction 4.1. The results showing how metal extraction varies with pH are given in Figure 4.1.



Where M^{n+} is the metal ion; R is the substrate; $-\text{CH}_2\text{N(CH}_2\text{COOH)}_2$ is the functional group (iminodiacetate); and $\text{R-CH}_2\text{-N(CH}_2\text{COOH)}_2$ is the IEF.

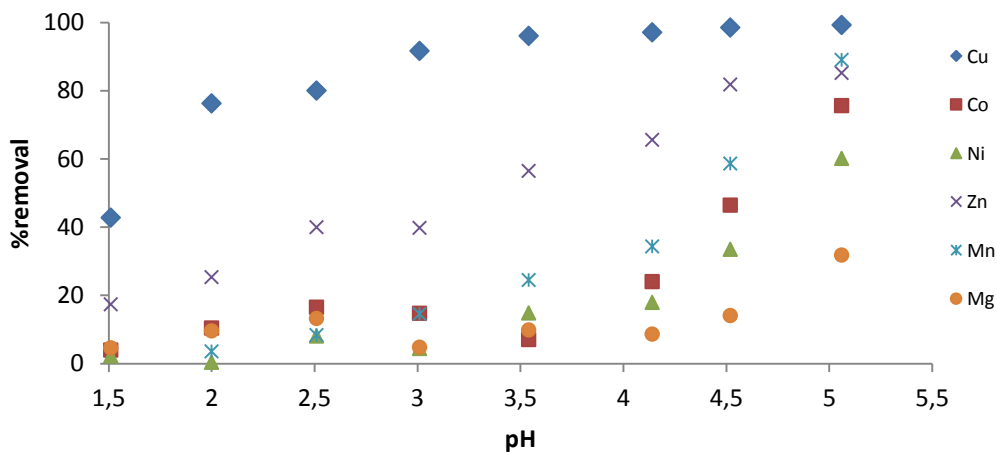


Figure 4. 1: Mass percentage of metal extracted (based on metal adsorbed) versus pH.

In general, the extraction of the metals in this study increases with an increase in pH as shown in Figure 4.1. An increase in pH of solution results in an increase in the degree of ionization of the weak acidic active groups as stated in literature (Helfferich, 1995). The more ionized the active groups, the higher the extent of ion exchange.

The results also indicate that the fibre has a higher selectivity for Cu^{2+} ions as illustrated by the higher extraction for copper metal at all the pH values studied. The higher selectivity towards Cu^{2+} ions could be attributed to stable complex formation between Cu^{2+} ions and the active groups on the IEFs. Cu^{2+} ions have a larger ionic radius which makes these ions hydrophobic, however, they have a smaller atomic radius compared to the other metals studied (Dean, 1992). As a result of the smaller atomic radius, Cu^{2+} ions diffused easily into the IEFs for ion exchange to occur.

In this study, Cu^{2+} , Mg^{2+} , Mn^{2+} and Ni^{2+} ions existed as divalent ions as the pH was kept at or below 5 (Takeno, 2005). On the other hand, Co^{2+} ions sometimes bond with OH^- ions to form $\text{Co}(\text{OH})_2(\text{aq})$ in the pH range of 0 - 14 (Takeno, 2005). The Co^{2+} ions that mainly existed as $\text{Co}(\text{OH})_2(\text{aq})$ was one of the reasons why less amounts of Co^{2+} ions were loaded onto the IEFs less amounts of Co^{2+} ions were loaded onto the IEFs (Takeno, 2005). Likewise, Zn^{2+} ions sometimes bond with OH^- ions to form $\text{Zn}(\text{OH})_2(\text{aq})$ in solution in the pH range 0 - 14 (Takeno, 2005). However, the higher loading of Zn^{2+} ions compared to Co^{2+} ions shows that the formation of $\text{Zn}(\text{OH})_2(\text{aq})$ was lower. Occasionally, at pHs above 4.0, Cu^{2+} ions form $\text{Cu}(\text{OH})^+$ in solution (Ji et al., 2011) which can also lead to lower extraction of Cu^{2+} ions as a result of a bigger radius of $\text{Cu}(\text{OH})^+$ as compared to Cu^{2+} (Dean, 1992).

A pH of 3 was selected as the optimum pH. At this pH, more Cu^{2+} ions were extracted compared to the other metals thus illustrating selective recovery of copper at this pH. In other words, the co-extraction of the other heavy metals was low at pH 3 as opposed to the co-extraction at pHs of 3.5 – 5.1 (see Figure 4.1). The selectivity order of the IEFs at pH 3.0 was as follows: - $\text{Cu}^{2+} > \text{Zn}^{2+} > \text{Co}^{2+} > \text{Mn}^{2+} > \text{Mg}^{2+} > \text{Ni}^{2+}$ as indicated by % removal results for pH 3.0 in Figure 4.1. Subsequent Cu^{2+} ions adsorption tests were, therefore, conducted at pH 3 in order to prevent precipitation effects and minimize co-loading of the other metals. However, the conducted subsequent tests were done using a synthetic solution containing Cu^{2+} ions only for the purpose of developing a metal recovery contactor.

4.3 Maximum metal loading

Maximum loading capacity of Cu^{2+} ions onto the fibre was determined at the optimum pH of 3.0. As stated by the supplier, the capacity of the IEFs in H^+ form is 3.74 mEq/g based on the number of ionizable functional groups and this is equivalent to 119 mg of Cu^{2+} ions per gram of IEFs (Soldatov et al., 2011). The results showed that a maximum of 62 mg of Cu^{2+} ions was loaded onto 1 g of fibre at pH 3.0 (Figure 4.2) The results from experiments previously conducted by Yahorova et al. (2010), showed that about 50 mg of Cu^{2+} ions could be loaded per gram of fibre. In other studies whereby chelating polymers, natural wool fibres and magnetic chitosan-isatin Schiff's base resin were used, the loading of Cu^{2+} ions was about 105 mg per gram of adsorbent used at pH of 5.0 (Jha et al., 2009; Cegłowski et al., 2015; Monier et al., 2010). However, at similar pHs, Jha et al. (2009) achieved Cu^{2+} ions loading of about 30 mg/g with feed composed of Cu^{2+} ions concentration at 300 mg/L. The low loading in this study and that of Yahorova et al.(2010) is attributed to the pH of 3 whereby the IEFs did not ionise completely to allow maximum loading (Lito et al., 2012). In addition, the functional groups in the IEFs in our study are weakly acidic which results in partial ionization only at low pHs (Helfferich, 1995; Soldatov et al., 2011). As mentioned in the previous section, the degree of ionization has an effect on the extent of ion exchange and the apparent capacity of weak acid fibres depends on pH. As the active groups ionize the apparent capacity of the fibre is increased. In general, the apparent loading capacity of weak acid fibres is expected to increase with an increase in pH.

4.4 Equilibrium Isotherm

The experiments for equilibrium isotherms were conducted at different solution to fibre ratio; the ratios were varied by changing the volume of the solution while keeping the mass of IEFs constant at 0.5 g. The equilibrium experimental results are shown on Figure 4.2. The results show that the equilibrium loadings increased with an increase in equilibrium concentration. The equilibrium loadings and concentration increased with an increase in solution to fibre ratio as a result of the equilibrium shift that ensured that the equilibrium constant does not change at constant temperature (Brown et al., 2011).

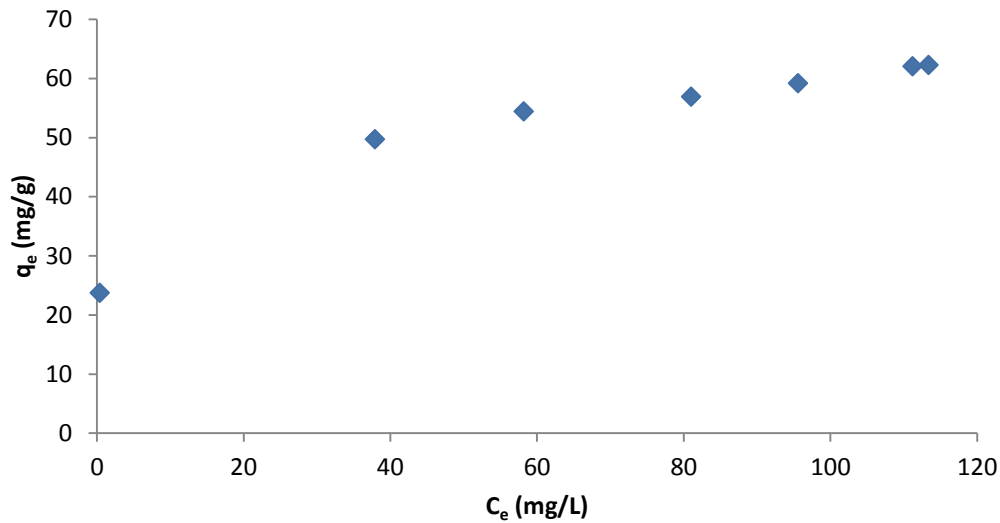


Figure 4. 2: Experimental equilibrium data points.

The linearised equilibrium models of the Langmuir, Redlich-Peterson, Dubinin and Radushkevich, Freundlich and Temkin equilibrium models were also fitted into the experimental data to determine the model that best describes the equilibrium sorption. Plots of the linearized Freundlich, Langmuir, Temkin, Dubin and Radushkevich, and the Redlich-Peterson equilibrium models fitted onto the experimental data are given in Figure 4.3 - 4.7, respectively. Correlation coefficients (R^2) for the correlated data corresponding to the equilibrium models are also provided on the respective figures.

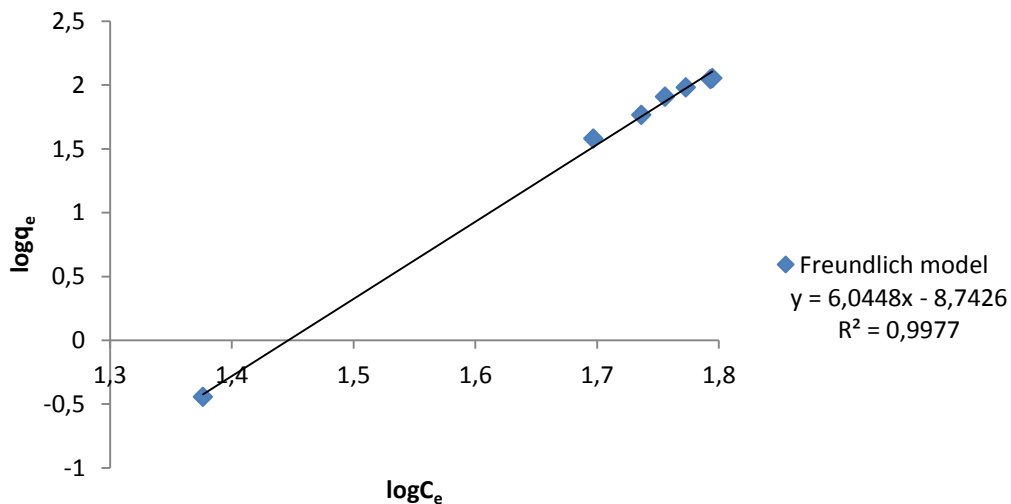


Figure 4. 3: Linearized Freundlich isotherm model fit into experimental data.

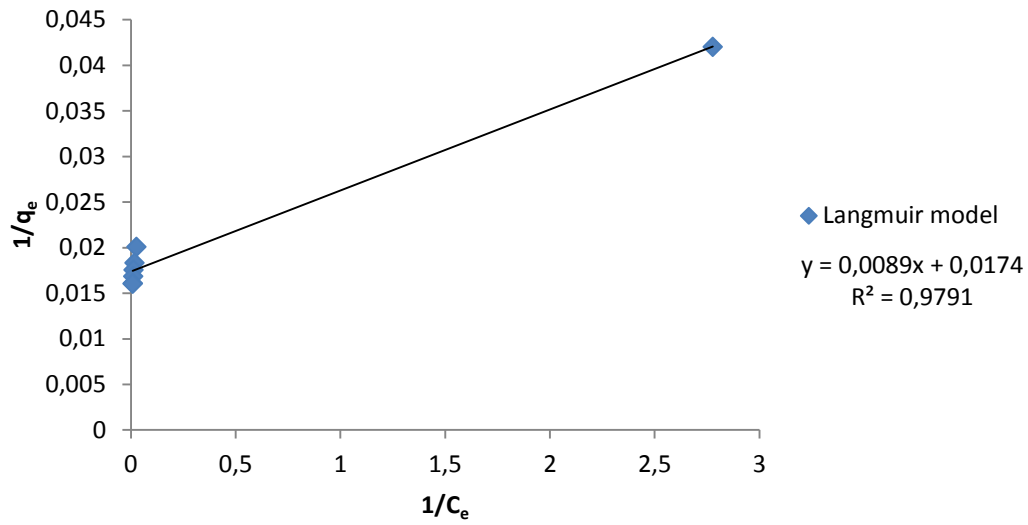


Figure 4. 4: Linearized Langmuir isotherm model fit into experimental data.

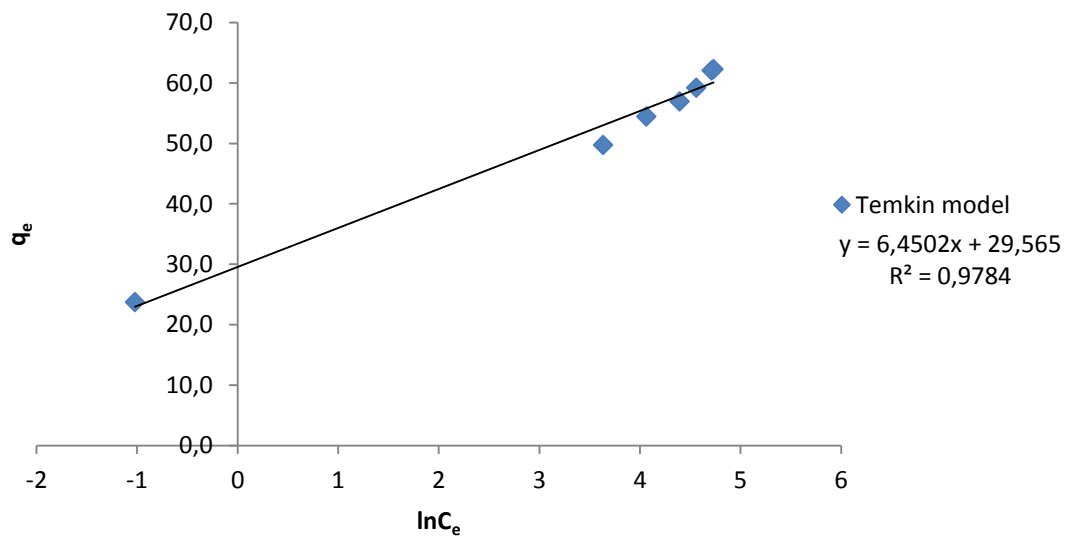


Figure 4. 5: Linearized Temkin isotherm model fit into experimental data.

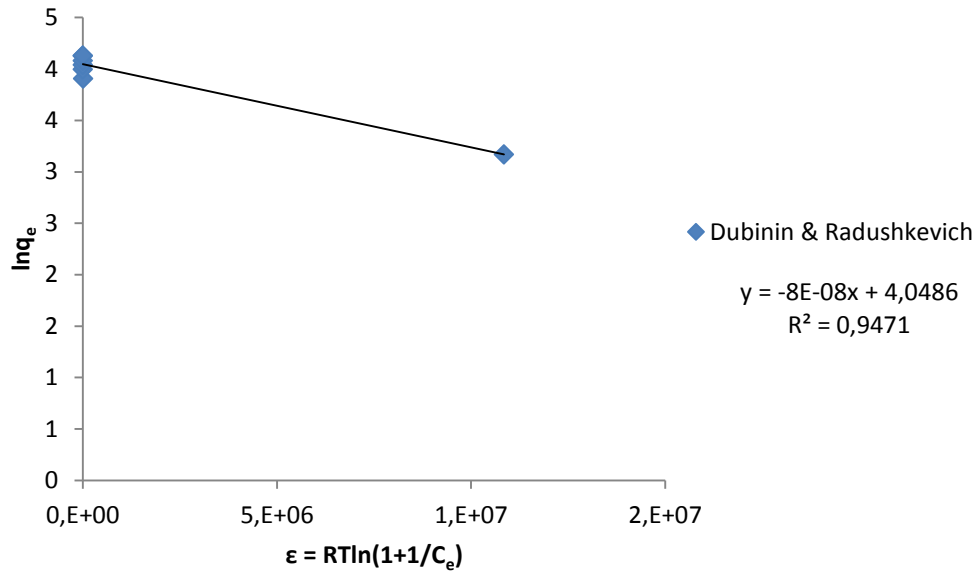


Figure 4.6: Linearized Dubinin and Radushkevich isotherm model fit into experimental data.

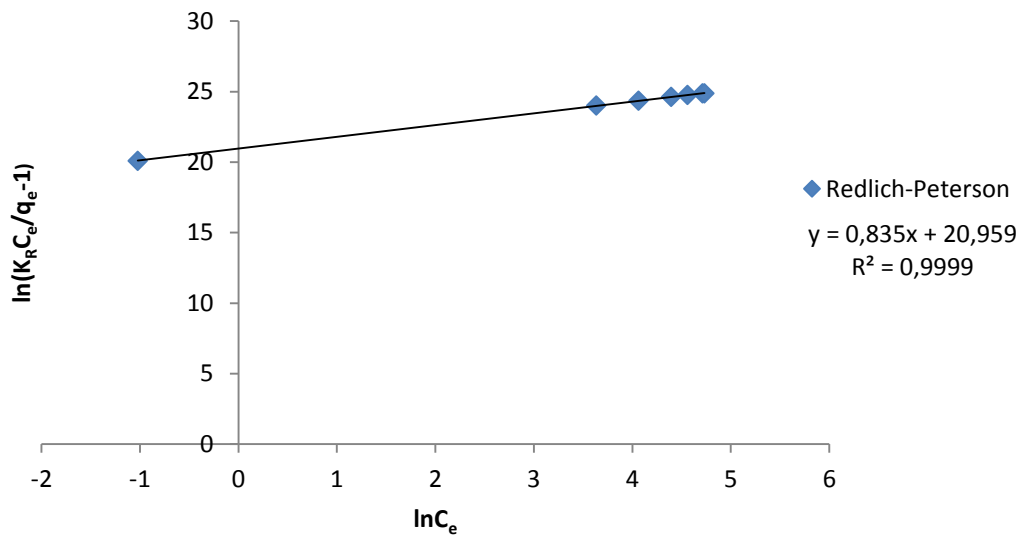


Figure 4. 7: Linearised Redlich-Peterson isotherm fit into experimental data.

The results show that the correlation coefficient between $\ln(K_R C_e / q_e - 1)$ and $\ln C_e$ used for fitting the Redlich-Peterson model was the closest to 1 when compared with the data used for the other models considered. However, the equilibrium loading predicted by the Redlich-Peterson model had the largest deviation from experimental equilibrium loadings when compared to the predictions by the Langmuir model and the Temkin model as listed in Table 4.1. The model with the second highest correlation coefficient between the data used was the Freundlich model. However, amongst the considered models, the metal equilibrium loading predicted from the Freundlich model had the largest deviations from the experimental equilibrium loading. The Temkin model was able to predict equilibrium loading with the least deviations from the experimental equilibrium loadings when with the other models considered. Therefore, the Temkin model was the most suitable model that could be used to predict the equilibrium behaviour of the Cu solutions and IEFs system in the study. The results in our equilibrium studies are in contrast with similar studies conducted using Fiban X-1, whereby equilibrium behavior was well described using Langmuir isotherm model (Soldatov et al., 2011). Other studies showed that the equilibrium behavior of Cu^{2+} ions removal using chelating polymers followed the Langmuir isotherm model (Monieret et al., 2010). In essence, the assumption associated with the Langmuir isotherm model of neglecting interaction between the loaded or adsorbed molecules (Cegłowski et al., 2015) was not applicable in our study.

The Temkin model assumes that heat of adsorption of all Cu^{2+} ions in the boundary layer decrease linearly rather than logarithmic with an increase in surface area (Foo and Hameed, 2010; Dada et al., 2012). Therefore, when operating at lower temperatures a larger surface area of IEFs will be required to improve metal loading (Helfferich, 1995) as it reduces the heat of adsorption.

Table 4. 1: Experimental equilibrium loading and the predicted loading using Redlich-Peterson, Freundlich, Langmuir model, Dubinin & Radushkevich and Temkin model.

Experimental	Redlich-Peterson	Freundlich	Langmuir	Dubinin & Radushkevich	Temkin
23.78	3.89	0.00	23.74	136.47	22.98
49.77	39.93	6.31	56.71	57.34	53.01
54.48	49.48	84.33	56.97	57.33	55.78
56.97	58.37	622.03	57.11	57.32	57.91
59.26	63.41	1693.84	57.17	57.32	58.98
62.10	68.39	4223.71	57.21	57.32	59.95
62.33	69.06	4754.72	57.21	57.32	60.08

4.5 Elution tests

Elution tests were conducted to evaluate the concentration of acid required to completely elute Cu^{2+} ions from IEFs. The mass of IEFs and volume of solution used was kept constant in all the individual experiments conducted. A volume of 200 mL Cu^{2+} ions feed solution was contacted with 1 g of IEFs to ensure equal amounts of Cu^{2+} ions are loaded onto the IEFs. Figure 4.8 illustrates how mass percentage of ions eluted varies with acid concentration used for elution (Raw data is provided in Table B. of Appendix B).

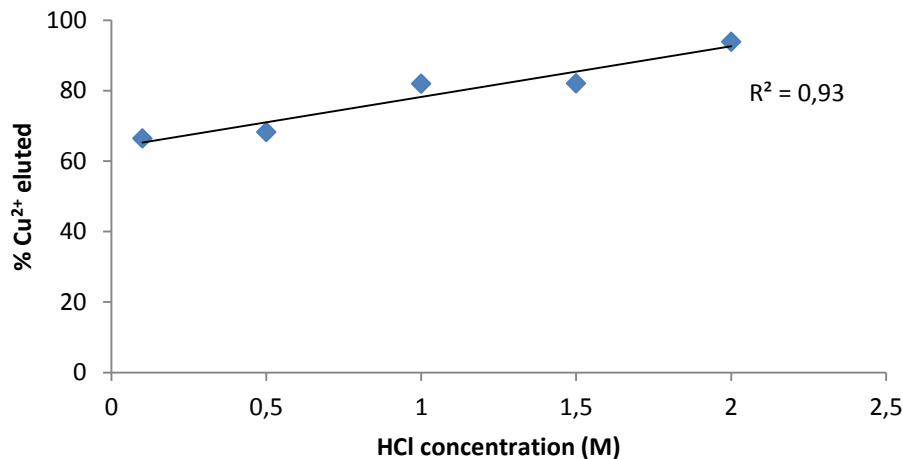


Figure 4. 8: Mass percentage eluted from IEFs versus hydrochloric acid concentration in molar units.

Figure 4.8 shows that the mass percentage of Cu^{2+} ions eluted increased proportionally with an increase in acid concentration used. Thus, there is a linear relationship between the acid concentration and mass percentage of Cu^{2+} ions eluted as illustrated by a correlation coefficient of 0.93. Acid concentration of 2M was able to elute 94% of mass of Cu^{2+} ions loaded onto the fibre and only 66% was eluted when 0.1M acid was used. Elution is an ion exchange process and it is affected by diffusion which depends on the concentration gradient of species involved (Helfferich, 1995). In this case, the extent of elution was lower at low acid concentrations and higher at high acid concentrations due to low and high acid concentration gradients, respectively. This can also be explained using Le Chatelier's principle. When less concentrated acid solutions are used for elution, a small amount of hydrogen ions will displace the loaded metal to establish equilibrium between the IEFs and solution with respect to pH (Helfferich, 1995). The percentage eluted when 1 M and 1.5 M acid was used, differed by 0.1%. This can be explained by the observed tendency of fibre strands to sometimes attach to each other instead of dispersing in solution thus preventing maximum exposure in solution and limiting extent of ion exchange (Helfferich, 1995; Inglezakis and Zorpas, 2012).

4.6 Kinetics test

Kinetic tests were conducted to determine the kinetic behavior of the Cu^{2+} ions removal by IEFs. The mass loaded onto the fibre increased with time as shown in Figure 4.9. The experimental results show that about 60% of metal in solution was loaded onto the IEFs within 5 minutes of contact and 80% was loaded onto the IEFs within an hour. Initially, loading rate was fast, but decreased with time due to lowered concentration gradient as the ion exchange occurred.

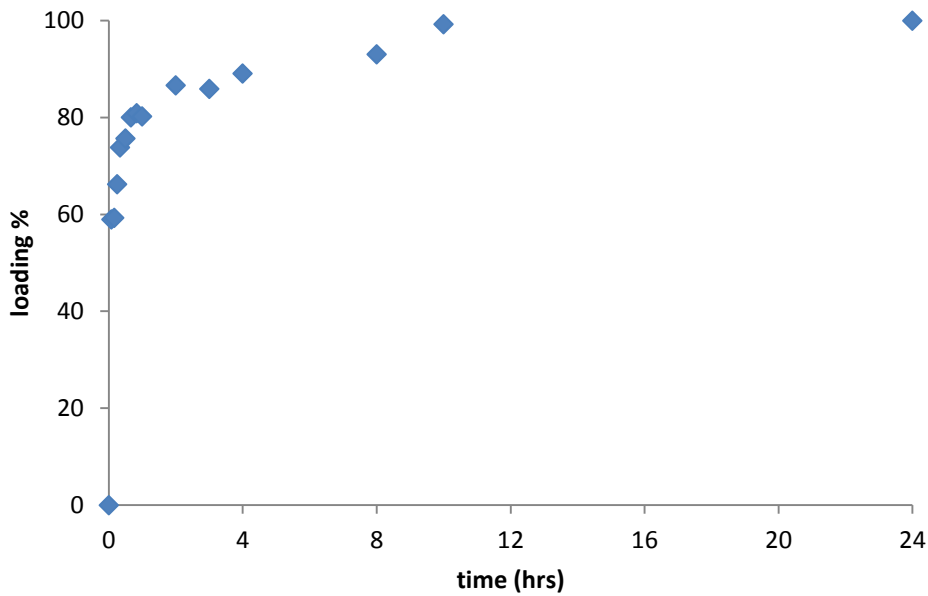


Figure 4. 9: Experimental loading of Cu^{2+} on IEF as a function of time.

The pseudo-first-order, pseudo-second-order and the Elovich kinetics models were fitted into the experimental data to check which model best describes kinetics of Cu^{2+} ions loading onto the fibre. Figure 4.10 shows the fit of pseudo-first-order kinetic model onto the experimental data, and Figure 4.11 shows the fit of pseudo-second-order kinetic model and the Elovich model fit is shown in Figure 4.12.

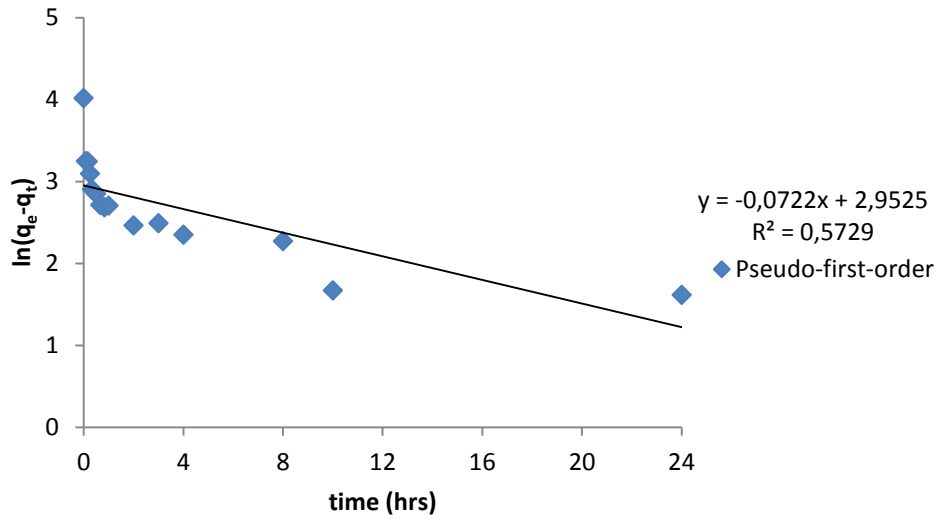


Figure 4. 10: Pseudo-first-order model fit on the kinetics experimental results.

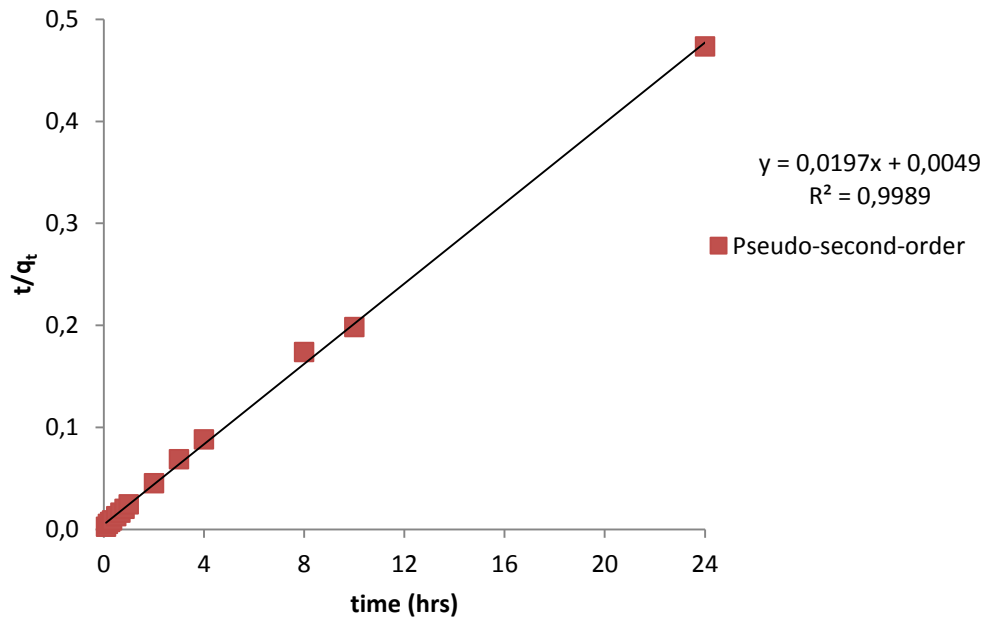


Figure 4. 11: Pseudo-second-order model fit on the kinetics experimental results.

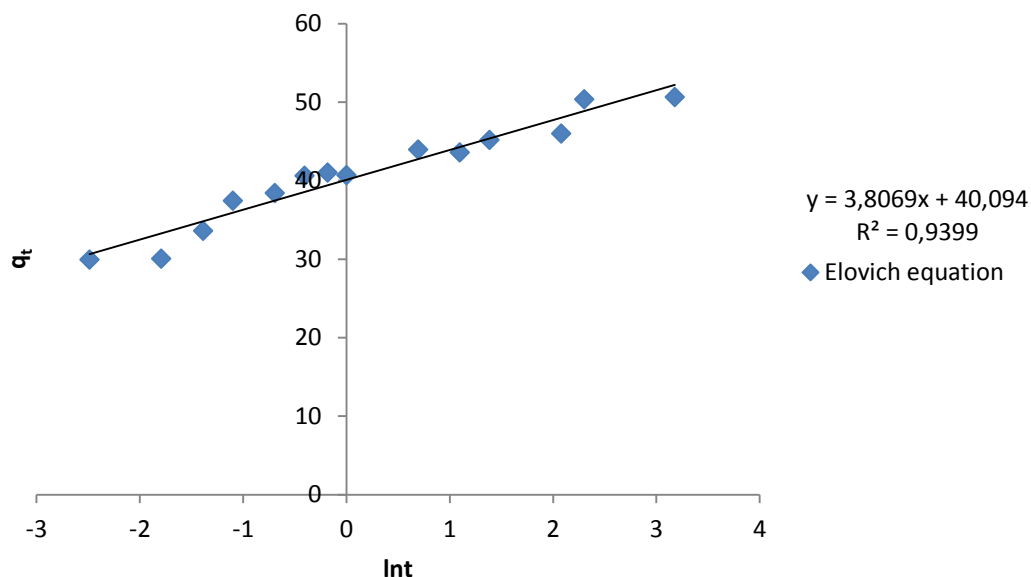


Figure 4. 12: Elovich model fit on the kinetics experimental results.

The best fit can be determined by a strong linear relationship of the data and the correlation coefficient is used to check the strength of the linear relationship. However, it is also necessary to compare the predicted loadings from the models with those obtained experimentally in order to validate the model.

The linear equations of the models were used to compute the parameters of the models and subsequently the parameters were used to predict loading as a function of time. The mass percentage of Cu^{2+} ions from experimental data and that predicted by the pseudo-first-order, pseudo-second-order and the Elovich models are listed in Table 4.2. Figures 4.10 - 4.12 shows that the pseudo-second-order had the largest correlation coefficients followed by the linear Elovich model and lastly the pseudo-first-order. However, the percentage loadings predicted by the pseudo-second order deviated more from the experimental loading as compared to predictions by the Elovich model (see Table 4.2). Nevertheless, the Elovich equation is commonly used for the chemisorptions kinetics between gases and solids (Cheung et al., 2000). Therefore, the pseudo-second-order was selected as the most suitable model that best describes the loading of copper onto IEFs used in this study. This is in agreement with previous batch studies for Cu^{2+} ions removal by chelating polymers, natural wool fibres and ion exchange resins (Monier et al., 2010; Jha et al., 2009; Ceglowski et al.,

2015; Monier et al., 2010). The reaction rate described with the pseudo-second order model depends on the amount of metal exposed to IEFs and it is directly proportional to the number of ionized functional groups (Rengaraj et al, 2007). In other words, according to the pseudo-second-order model, the kinetics of Cu^{2+} ions adsorption onto the IEFs was dependent on the amount of ions on the surface of IEFs and the amount of ions loaded at equilibrium (Rengaraj et al., 2007).

Table 4. 2: Mass percentage of Cu loaded from experimental data and that predicted using the pseudo-first-order, pseudo-second-order and the Elovich model.

experimental	pseudo-first-order	pseudo-second-order	Elovich
0	0	0	0
59	1	25	59
59	3	40	64
66	4	50	67
74	5	57	69
76	8	67	72
80	10	73	74
81	13	77	75
80	15	80	77
87	28	89	82
86	39	92	85
89	49	94	87
93	74	97	92
99	81	98	94
100	98	99	100

4.7 Summary

The optimum pH for selective removal of Cu^{2+} ions from dilute synthetic solution was found to be 3 and the selectivity order of the IEFs at pH 3.0 was as follows: - $\text{Cu}^{2+} > \text{Zn}^{2+} > \text{Co}^{2+} > \text{Mn}^{2+} > \text{Mg}^{2+} > \text{Ni}^{2+}$. Equilibrium loading of Cu^{2+} ions was 62 mg per gram of IEFs. However, this was lower than the maximum theoretical value of 119 mg of Cu^{2+} ions per gram of IEFs because at a pH of 3.0 the IEFs in this study did not ionise completely to allow maximum loading. The equilibrium sorption was found to exhibit the Temkin model behaviour. Therefore, the IEFs used in this study can be effectively applied at ambient

temperatures by increasing their surface area which lowers the heat of adsorption as suggested by the Temkin model. The percentage of metal eluted from IEFs increased with an increase in acid concentration. However, if large volumes of less concentrated acid solutions are used, the same percentage of elution as the low volume of highly concentrated acid solution can be achieved. Nevertheless, the use of less concentrated acid solutions at large volumes results in dilute Cu^{2+} ions solutions. Therefore, the use of highly concentrated acid solution is recommended. The kinetic behaviour of the system was best described using the pseudo-second-order model which means that the ion exchange rate in this study was directly proportional to the number of ionizable functional groups.

Chapter 5: Column tests

5.1 Introduction

Batch tests do not give data required to determine the superficial velocity (u) since batch operation does not simulate continuous processes. However, breakthrough tests conducted in columns allow computation of the U and contact time (CT) required for efficient continuous metal removal (Inglezakis, 2010; Inglezakis and Poulopoulos, 2006). Subsequently, the u and CT may be used for design purposes (Inglezakis, 2010; Inglezakis and Poulopoulos, 2006). In particular, the U and CT are used to determine the dimensions which will permit attainment of the same mass transfer rates in the desired contactor as in the column.

The controlling factors affecting the efficiency of ion exchange process in metal removal from solution in fixed bed columns have been carefully investigated (Soldatov et al., 1999). It was found that, metal loading efficiency onto IEFs depends on bed depth and flow rate (Soldatov et al., 1999). Density of the packing (i.e., IEFs packing) is also a controlling factor (Soldatov et al., 1999). However, variation in bed depth whilst keeping mass of the packing constant causes a variation in the packing density.

In this study, experimental tests were carried out to investigate the following variables:

- effect of bed packing density on loading,
- effect of feed flow rate on loading,
- effect of bed packing density on regeneration,
- effect of eluent flow rate on regeneration.

Empirical models were also used to describe the effluent concentration-time profile. In fact, the effluent concentration-time profile (breakthrough curve) is imperative for successful ion exchange column design (Kavak and Öztürk, 2004). The commonly used models for fixed bed columns are the Adams-Bohart model, Thomas model and the Yoon-Nelson model (Kavak and Öztürk, 2004; Nwabanne et al., 2012; Kalavathy et al., 2010). The Adams-Bohart model, Thomas model and the Yoon-Nelson model were fitted into the experimental

data fitted so as to determine the dynamic behaviour of the effluent concentration from the column.

5.2 Materials and Methods

5.2.1 Material acquisition, fibre and reagent preparation

The material acquisition was done as described in Section 3.2, Chapter 3. The IEFs were prepared by contacting with acid as described in Section 3.3 and the feed solution composed of 2mM Cu (127 mg/L Cu^{2+} ions) was prepared from CuSO_4 as stated in Section 3.4 (Chapter 3).

5.2.2 Experimental set up

The 1.4 cm diameter and 20 cm height column used in this study was packed with IEFs between two supporting layers of inert and porous cotton wool. At the bottom part of the column, the cotton wool was supported by a 45 micron screen placed on a plastic threaded cap. The column ends were closed with threaded caps connected to influent and effluent tubings. The feed solution was pumped from the beaker into the column using a peristaltic pump as shown in the paraphernalia in Figure 5.1. A magnetic stirrer was used to agitate the feed solution so as to ensure a feed with constant uniform concentration. The effluent solution from the column was collected in a graduated cylinder.

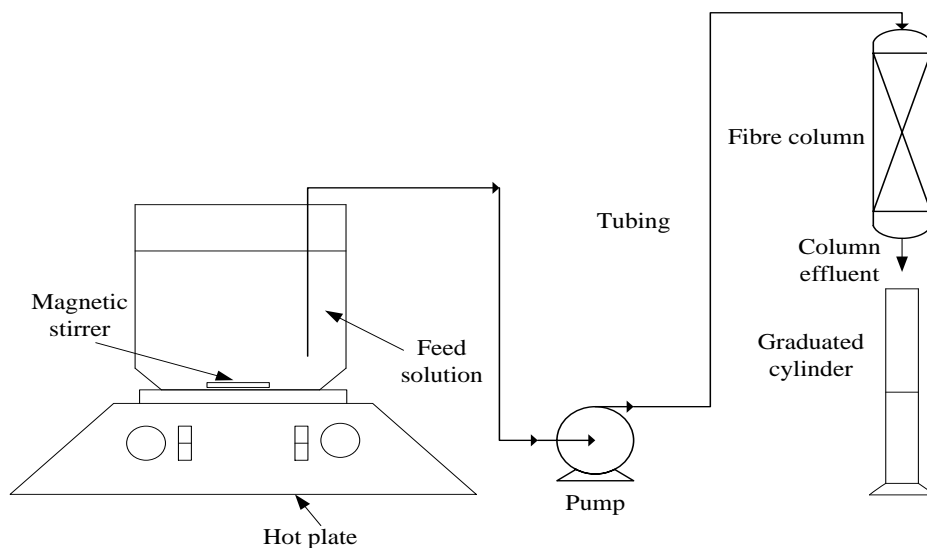


Figure 5. 1: Experimental set up.

5.2.3 Effect of bed packing density on Cu²⁺ ions removal and elution

The effects of bed packing density were investigated by passing 2000 mL of feed solution through a column packed with 2.56 g of IEFs at a constant flow rate of 8 mL/min. This was the lowest flow rate that could be attained in this study due to equipment limitation. In addition, lower flow rates favour metal loading and consequently column utilization (Helfferich, 1995). The bed packing density was initially set at 0.16 g/cm³ by compressing IEFs with inert and porous cotton wool. Effluent samples of volume equivalent to 250 mL were collected consecutively and the time taken for 250 mL of feed treated was recorded. The samples were analysed for Cu²⁺ ions using an atomic absorption spectrophotometer (AAS). De-ionised water of volume equivalent to 120 mL was then passed through the bed of IEFs at 8 mL/min to remove any entrained Cu²⁺ ions solution. Previous tests conducted at Mintek indicated that 4 bed volumes were sufficient for rinsing (Yahorova et al., 2010). In this study, 4 bed volumes were equivalent to 120 mL of de-ionised water.

After washing the bed of IEFs with de-ionised water, 105 mL of 2M HCl was passed through the column at 8 mL/min to elute the loaded Cu²⁺ ions. Preliminary tests indicated that 105 mL of 2M HCl was required to completely elute the Cu²⁺ ions. Therefore, samples of 15 mL were collected consecutively and the time taken for 15 mL of acid to pass through the bed was recorded. The samples were analysed for Cu²⁺ ions using an AAS. The bed of IEFs was washed again with 120 mL of de-ionised water at 8 mL/min to remove any entrained acid from the bed.

The above described procedure was repeated for bed packing density of 0.20, 0.28 and 0.37 g/cm³ while maintaining the flow rate constant at 8 mL/min. Each test was replicated 3 times.

5.2.4 Effects of feed and eluent flow rate on Cu²⁺ ions removal and elution

A feed solution of about 2000 mL containing 127 mg/L of Cu²⁺ ions was passed through a 2.56 g of staple IEFs with bed packing density of 0.16 g/cm³ at flow rate of 12 mL/min. The packing density of 0.16 g/cm³ was used because it gave a maximum Cu²⁺ ions removal (see Section 5.3.1 below). Effluent samples of volume equivalent to 250 mL were then collected

consecutively and the time taken for 250 mL of the treated feed to accumulate was recorded. The samples were analysed for Cu^{2+} ions using AAS. De-ionised water of volume equivalent to 120 mL was then passed through the bed of IEFs at 8mL/min to wash off any entrained Cu^{2+} ions solution.

After washing the bed of IEFs with water, 105 mL of 2M HCl was passed through the column at 8 mL/min to elute the adsorbed Cu^{2+} ions. Samples of 15 mL were collected consecutively and the time taken for 15 mL of acid to pass through the bed was recorded. The samples were analysed for Cu^{2+} ions using an AAS. The bed of the IEFs was washed again with de-ionised water to remove any entrained acid in the bed.

The above described procedure was repeated for flow rates of 17 and 28 mL/min while maintaining the bed packing density constant at 0.16 g/cm^3 . Each test was replicated 3 times.

5.3 Results and discussions

Bed volumes were used for comparing performance of IEFs with the same packing density and volume was expressed in litres or millilitres for comparing beds with different packing density as their bed volumes are not equal. For the results discussed in this section, reference should be made to Appendix C. Raw data and calculated data for column tests are provided in Table C1 – C65 and C66 – C70 in Appendix C, respectively.

5.3.1 Effect of packing density on Cu^{2+} ions removal

In this study, various packing densities were investigated at constant Cu^{2+} ions feed concentration and flow rate of 127 mg/L and 8 mL/min, respectively. Figure 5.2 shows the effects of packing density on Cu^{2+} ions removal. Generally, the removal of Cu^{2+} ions decreased with an increase in feed volume passed through the bed of IEFs. This was due to the reduction in the amount of freely available functional groups (in H^+ form) as the feed was passed which led to the reduction of Cu^{2+} ions removal (Helfferich, 1995). However, the removal of Cu^{2+} ions was the same after having passed 500 mL of feed in all the beds investigated. It was after passing 750 mL of feed that a significant difference in the Cu^{2+} ions

removal was observed. In addition, the results show that Cu^{2+} ions removal increased with a decrease in packing density from 750 mL of feed and more as shown in Figure 5.2. The Cu^{2+} ions removal was higher at low bed packing density (higher bed height) due to the increased residence time within the IEFs which led to an increased uptake of Cu^{2+} ions from the feed solution (Ahmad and Hameed, 2010; Kalavathy et al., 2010; Simate and Ndlovu, 2015). In this study, the mass of IEFs was kept constant at all beds investigated providing equal amount of active groups for all beds. Therefore, the increase in Cu^{2+} ions removal was due to the increase in bed surface area as the bed depth was increased to give a low packing density.

The breakthrough profile in Figure 5.2 also shows that only 75 % breakthrough of Cu^{2+} ions was reached in IEFs bed packing density of 0.16 g/cm^3 after treating about 2000 mL of feed as compared to 76 %, 90 % and 96 % reached in the 0.20 g/cm^3 , 0.28 g/cm^3 and 0.37 g/cm^3 , respectively. A lower breakthrough (C/C_f) indicates higher metal removal.

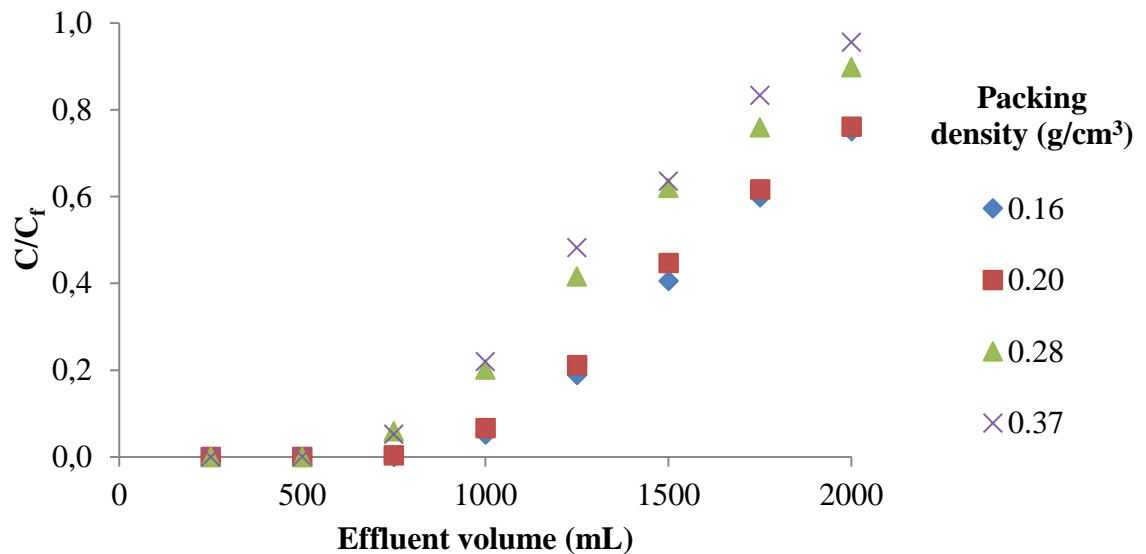


Figure 5. 2: Effluent concentration versus feed volume passed through various bed packing densities (IEFs mass 2.56 g) at constant flow rate of 8 mL/min.

5.3.2 Effect of feed flow rate on Cu²⁺ ions removal

The effect of feed flow rate on Cu²⁺ ions removal was investigated and the results are shown in Figure 5.3. The studied feed flow rates are 8, 12, 17 and 28 mL/min. The mass of IEFs and bed packing density were kept constant at 2.56 g and 0.16 g/cm³, respectively. The removal of Cu²⁺ ions was the same at volumes below 500 mL at all the flow rates studied. However, above 500 mL, the removal of Cu²⁺ ions decreased with an increased flow rate. The decrease of Cu²⁺ ions removal with increased flow rate is due to the reduced time for diffusion of Cu²⁺ ions between the feed and IEFs at high flow rates and vice versa (Ahmad and Hameed, 2010; Kalavathy et al., 2010; Yahaya et al., 2011). In other words, reduced contact time resulted in lower metal loading. As a consequence, the effluent concentration was higher at higher feed flow rates.

The breakthrough profile in Figure 5.3 shows that only 75 % breakthrough of Cu²⁺ ions was reached in IEFs when flow rate was 8 mL after treating about 2000 mL of feed as compared to 81 %, 83 % and 87 % reached in the 12, 17 and 28 mL/min, respectively. Once more, lower breakthrough (C/C_f) indicates high metal removal.

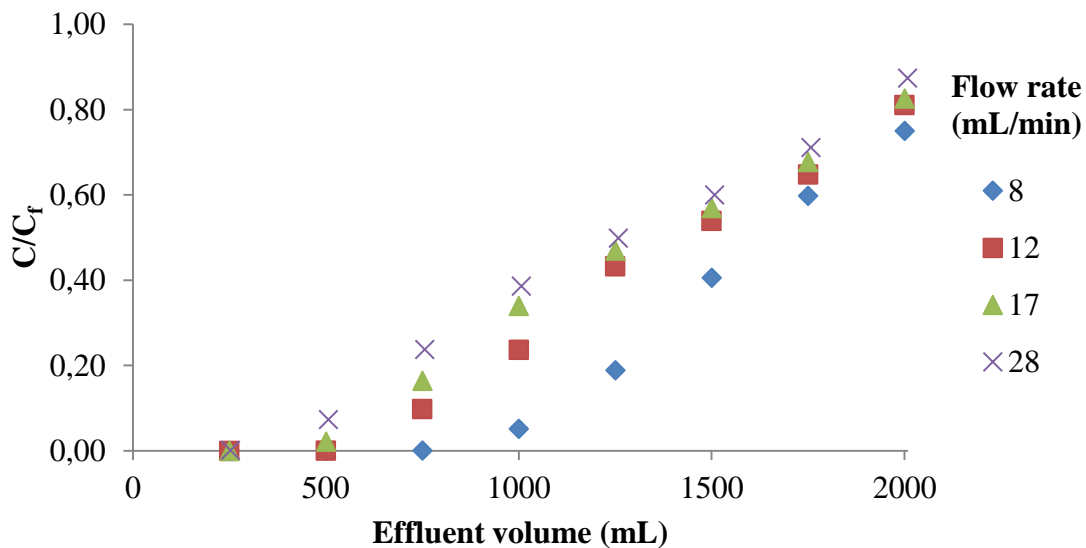


Figure 5. 3: Effluent concentration versus feed volume passed at various flow rates through a bed of 2.56 g IEFs adjusted to packing density of 0.16 g/cm³.

5.3.3 Effect of bed packing density on elution

The IEFs were eluted using 2 M HCl to investigate the effects of bed packing density on elution. Concentration of Cu^{2+} ions in the eluent was plotted against the volume of eluent that was passed through the loaded packed bed of IEFs. Initially, for all bed packing densities investigated, as shown in Figure 5.4, concentration of Cu^{2+} ions was minimal. Thereafter, about 99% of the loaded Cu^{2+} ions were eluted from the IEFs after passing 60 mL of acid. The IEFs were washed with de-ionised water prior to elution, therefore, the effluent volume of about 30 mL collected in the beginning during elution was the de-ionised water retained in the IEFs. As a consequence of the delayed contact between the acid and IEFs, Cu^{2+} ions began to report in the effluent solution after more than 30 mL was passed through the column of Cu^{2+} ions loaded IEFs.

The results presented in Figure 5.4, indicate that the loaded Cu^{2+} ions was completely eluted in all the beds after passing 80 mL of eluent through the column of Cu^{2+} ions loaded IEFs. Generally, the mass percentage of Cu^{2+} ions eluted increased with an increase in eluent volume. A higher eluent volume provided more H^+ ions available for exchange thereby increasing the extent of elution (Helfferich, 1995).

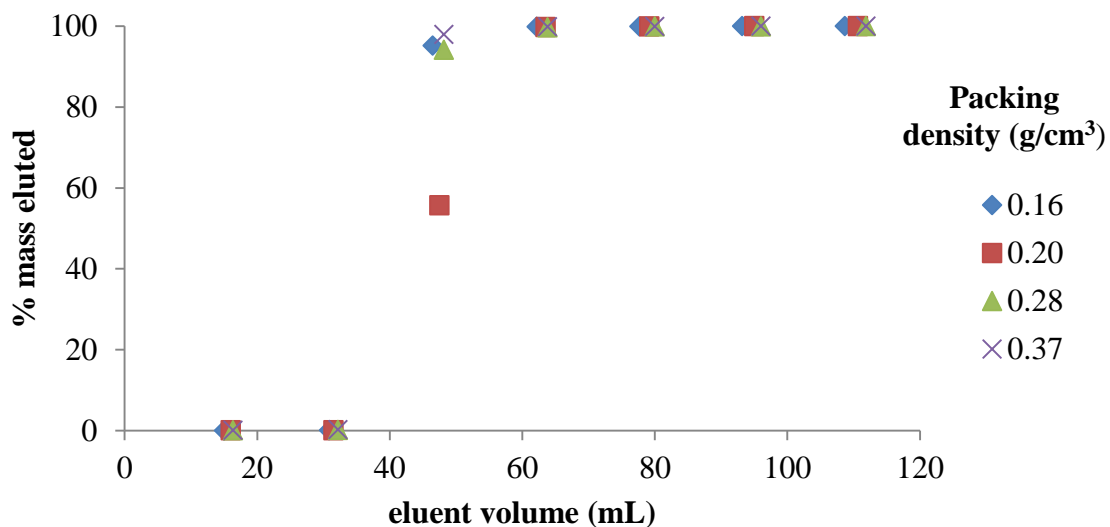


Figure 5. 4: Effect of bed packing density on elution of IEFs at constant flow rate and IEFs mass (8 mL/min and 2.56 g).

5.3.4 Effect of eluent flow rate on elution

Investigations on the effect of flow rate on elution were conducted at constant bed packing density and IEFs mass of 0.16 g/cm³ and 2.56 g, respectively and the results are shown in Figure 5.5. Generally, the mass percentage of Cu²⁺ ions eluted increased with eluent volume. As can be seen from Figure 5.5, the mass percentage of Cu²⁺ ions eluted per unit volume of eluent passed through the column was the same in all flow rates except after passing 45 mL. It is suspected that there may have been channelling in the beds before passing an eluent volume of 45 mL.

The loaded Cu²⁺ ions were eluted faster at higher eluent flow rate as compared to low flow rate. Elution of loaded ions depends on the driving force, which is the concentration gradient of ions between the IEFs and the eluent (Helfferich, 1995). In this study, higher eluent flow rate created a sufficient driving force faster than lower eluent flow rate which consequently led to faster elution of Cu²⁺ ions. Therefore, in this study, the Cu²⁺ ions were eluted faster with high eluent flow rates. In other words, elution rate of Cu²⁺ ions was proportional to the eluent flow rate.

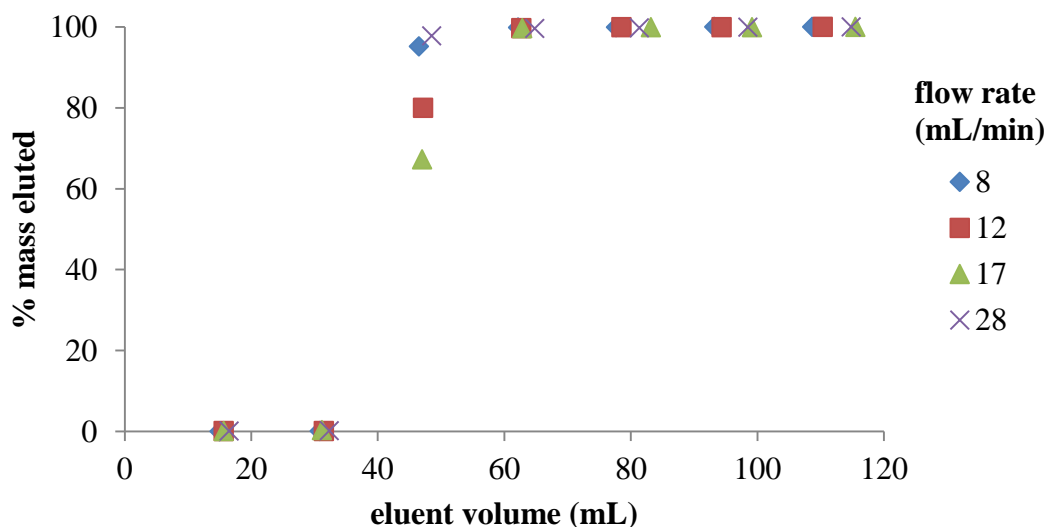


Figure 5. 5: Effect of flow rate on elution of IEFs at constant bed packing density and IEFs mass (0.16 g/cm³ and 2.56 g).

5.3.5 Computation of u and τ

The values of the superficial velocity (u) and the contact time (τ) were determined at flow rate and packing density of 8 mL/min and 0.16 g/cm³ where the lowest breakthrough was the lowest. Equation 5.1 and 5.2 were used to calculate u and τ , respectively. The values of u and τ were found to be 5.20 cm/min and 2.02 min, respectively.

$$u = Q_{feed} / A_{column} = (8mL / min) / (\Pi(1.4cm)^2 / 4) = 5.20mL / min.cm^2 \quad (5.1)$$

$$\tau = V_{bed} / Q_{feed} = ((\Pi(1.4cm)^2 / 4) \times 10.5cm) / (8mL / min) = 2.02min \quad (5.2)$$

Where u is the superficial velocity; Q_{feed} is the volumetric flow rate of the feed; A_{column} is the cross sectional area of the column; τ is the contact time and the V_{bed} is the volume of the IEF bed.

5.4 Model fitting

The effluent concentration-time profile (breakthrough curve) is imperative for successful ion exchange column design (Kavak and Öztürk, 2004) and empirical models are normally used to describe the effluent concentration-time profile. The commonly used models for fixed bed columns are the Adam-Bohart model, Thomas model and the Yoon-Nelson model (Kavak and Öztürk, 2004; Nwabanne et al., 2012; Kalavathy et al., 2010). The Adam-Bohart model, Thomas model and the Yoon-Nelson model were fitted into the experimental data to determine the dynamic behaviour of the effluent concentration from the column.

5.4.1 Thomas model

The Thomas model employs Langmuir isotherm for equilibrium and second order reversible reaction kinetics as it assumes plug flow behaviour in the bed (Ahmad and Hameed, 2010; Kalavathy et al., 2010). However, the Thomas model neglects the intraparticle diffusion as well as the external resistance during the ion exchange process (Kalavathy et al., 2010). The linearized Thomas model is expressed as follows:

$$\ln\left(\frac{C_o}{C_t} - 1\right) = \frac{k_{Th}q_o w}{Q} - k_{Th}C_o t \quad (5.3)$$

Where: -
k_{Th}: Thomas rate constant (mL/min mg)
q_o: equilibrium Cu uptake (mg/g)
C_o: feed concentration of Cu (mg/L)
C_t: effluent concentration of Cu (mg/L)
w: mass of IEFs (g)
Q: flow rate (mL/min).

The values of k_{Th} and q_o were determined from the slopes and intercepts of linear plots of ln(C_o/C_t-1) versus t. Values of C_o, C_t and t were measured experimentally. The least squares fit method was used to determine the slope and intercepts of the best fit line. The effect of

packing density and flow rate on the Thomas model parameters (k_{TH} and q_0) are listed in Table 5.1 and 5.2, respectively.

The determined correlation coefficients (R^2) ranged from 0.80-0.99 as it can be seen on Table 5.1 and 5.2. The R^2 value closer to 1 show that there is strong linear relationship between the data plotted.

The Thomas rate constant decreased with an increase in bed packing density from 0.16 – 0.28 g/cm^3 as listed in Table 5.1 which is in agreement with similar studies conducted by other researchers (Yahaya et al., 2011; Chowdhury et al., 2013; Malkovich and Nuhoglu, 2006; Simate and Ndlovu, 2015). The Thomas rate constant increased with a decrease in bed packing density (increase in bed height) as a result of the increased residence time in lower packing which increased Cu^{2+} ions uptake from solution (Pengthamkeerati and Satapanajaru, 2013). Amongst the flow rates studied, the Thomas rate constant was higher at a flow rate of 8 mL/min. However, the Thomas rate constant increased with flow rates from 8 – 28 mL/min as shown in Table 5.2. This is in agreement with the trend found in other studies (Aksu and Gonen, 2004; Chowdhury et al., 2013; Malkovich and Nuhoglu, 2006). As flow rate increased, more Cu^{2+} ions reached the functional groups on IEFs faster and in turn increased ion exchange rate (Pengthamkeerati and Satapanajaru, 2013). Conversely, the studies by Yahaya et al., (2011) shows that the Thomas rate constant decreased with an increase in flow rate.

The predicted maximum solid phase Cu^{2+} ions concentrations (q_0) were unrealistic as they were more than 500 times than the theoretical capacity of the IEFs (see Table 5.1 and 5.2). The Thomas model was inappropriate in this study because it does not incorporate external and internal diffusion (Kalavathy et al., 2010). Therefore, the rate limiting step of adsorption in this study may be either external and/or internal diffusion.

Table 5. 1: Effect of bed packing density on Thomas model parameters.

Packing density (g/cm³)	Flow rate (mL/min)	k_{TH} (mL/min mg)	q_o (mg/g)	R²
0.16	8	4.31E-04	8.43E+04	0.80
0.20	8	3.17E-04	8.16E+04	0.92
0.28	8	2.35E-04	6.96E+04	0.99
0.37	8	2.76E-04	6.52E+04	0.98

Table 5. 2: Effect of flow rate on Thomas model parameters.

Packing density (g/cm³)	Flow rate (mL/min)	k_{TH} (mL/min mg)	q_o (mg/g)	R²
0.16	8	4.31E-04	8.43E+04	0.80
0.16	12	2.61E-04	7.41E+04	0.98
0.16	17	3.17E-04	6.78E+04	0.98
0.16	28	4.86E-04	6.26E+04	0.98

5.4.2 The Yoon-Nelson model

According to the Yoon-Nelson model, the decrease in ion loading rate is proportional to the probability of ion removal by IEFs (Aksu and Gonen, 2004). In other words, the Yoon-Nelson model states that the loading rate decreases as metal ions are loaded onto the IEFs. In the current study, this could probably be due to a decrease in the differences of Cu²⁺ ions concentrations in solid and liquid phase as loading occurs. The linearised form of the Yoon-Nelson model is expressed in Equation (5.4) given below (Nwabanne and Igbokwe, 2012; Kalavathy et al, 2010; Trgo et al., 2011; Aksu and Gonen, 2004).

$$\ln\left(\frac{C_t}{C_o - C_t}\right) = k_{YN}t - \tau k_{YN} \quad (5.4)$$

Where: - C_t: effluent concentration of Cu (mg/L)

C_o: feed concentration of Cu (mg/L)

k_{YN} : Yoon-Nelson rate constant (1/min)

t: time (min)

τ : time required for 50% adsorbate breakthrough (min).

The Yoon-Nelson constant (k_{YN}) and the time required for 50% adsorbate breakthrough (τ) were obtained from slope and y-intercept plots of $\ln(C_t/(C_0-C_t))$ versus time.

Table 5.3 and 5.4 lists the Yoon-Nelson parameters at various bed depths and flow rates, respectively. The correlation coefficients (R^2) were at least 0.98 or more except for bed density of 0.16 and 0.20 g/cm³ cm which were 0.80 and 0.92, respectively.

The Yoon-Nelson rate constant generally increased with a decrease in bed packing density (increase in bed height) as listed in Table 5.3. High bed packing density reduced residence time which lowered Cu²⁺ ions uptake from solution. However, Aksu and Gonen (2004) found that the Yoon-Nelson rate constant decreased with an increase in bed height. Overall, the Yoon-Nelson constant increased with an increase in flow rate (see Table 5.4) which is in agreement with the results found by Aksu and Gonen (2004). Higher flow rates results in Cu²⁺ ions reaching the functional groups faster which may cause an increase in ion exchange rate (Helfferich, 1995).

The 50% breakthrough time (τ) decreased with an increase in bed packing density and flow rate as listed in Table 5.3 and 5.4 which is consistent with studies by Aksu and Gonen (2008). At low bed packing density, constant flow rate results in shorter feed retention times due to the shorter bed depth (Saad et al., 2014; Auta and Hameed, 2014). Flow rate is directly proportional to superficial velocity; therefore an increase in flow rate reduces feed retention time within IEFs thereby resulting in a shorter breakthrough time (Saad et al., 2014; Auta and Hameed, 2014). The 50% breakthrough times predicted by the Yoon-Nelson model were within the range of the 50% breakthrough times obtained experimentally as listed in Table 5.3 and 5.4.

Table 5. 3: Effect of bed depth on parameters of the Yoon-Nelson model.

Packing density (g/cm ³)	Flow rate (mL/min)	k _{YN} (1/min)	Yoon-Nelson τ (min)	experimental range of τ (min)	R ²
0.16	8	5.47E-02	212	192-223	0.80
0.20	8	4.02E-02	207	190-221	0.92
0.28	8	2.98E-02	179	159-191	0.99
0.37	8	3.51E-02	171	158-191	0.98

Table 5. 4: Effect of flow rate on parameters of the Yoon-Nelson model

Packing density (g/cm ³)	Flow rate (mL/min)	k _{YN} (1/min)	Yoon-Nelson τ (min)	experimental range of τ (min)	R ²
0.16	8	5.47E-02	212	192-223	0.80
0.16	12	3.31E-02	123	105-126	0.98
0.16	17	4.02E-02	80	72-87	0.98
0.16	28	6.17E-02	46	36-46	0.98

5.4.3 The Adam's-Bohart model

The Adam-Bohart model describes the relationship between C_t/C_o and t during continuous operation (Kalavathy et al., 2010). The Adam-Bohart model is normally used to describe the initial part of the breakthrough curve (Kalavathy et al., 2010). The simplified form of the Adam-Bohart model used in this study is referred to as the bed depth service time (BDST) (Goyal and Bhagat, 2010; Rajeshkannan et al., 2013). The BDST model equation is given below (Equation (5.5)).

$$\ln \frac{C_t}{C_o} = k_{AB} C_o t - k_{AB} N_o \frac{Z}{F} \quad (5.5)$$

Where: - C_t : effluent concentration of Cu (mg/L)

C_o : feed concentration of Cu (mg/L)

t: time (min)

k_{AB} : Adam-Bohart kinetic constant (L/mg min)

N_o : saturation concentration (mg/L)

Z: bed depth (cm)

F: linear velocity (cm/min)

The values of K_{AB} and N_o listed in Table 5.5 and 5.6 were determined from intercepts and slopes of the plot of $\ln C_t/C_o$ against t. The correlation coefficients (R^2) between the plots of $\ln C_t/C_o$ against t ranged between 0.71 and 0.95 as listed in Table 5.5 and 5.6 below.

The kinetic constant (k_{AB}) generally increased with a decrease in bed packing density (increase in bed height) as listed in Table 5.5. A decrease in packing density at constant flow rate increases residence time which enhances Cu^{2+} ions uptake from solution (Saad et al., 2014; Auta and Hameed, 2014). However, in studies by Saadi et al. (2013) the kinetic constant (k_{AB}) decreased with an increase in bed height. On the other hand, the Adam-Bohart rate constant (k_{AB}) increased with flow rate in the range 8-28 mL/min (see Table 5.6) which is congruent with studies by Zulfadhly et al. (2001) and Saadi et al. (2013). Once more, higher flow rates resulted in Cu^{2+} ions from solution reaching functional groups on IEFs faster (Saad et al., 2014; Auta and Hameed, 2014). Ideally, ion exchange occurs as counter ions in solution contact with ionized functional groups (Helfferich, 1995).

The predicted saturation concentration (N_o) increased with a decrease in bed packing density as a consequence of higher Cu^{2+} ions removal at higher bed packing density (see Table 5.5). The saturation concentration also increased with an increase in flow rate as a result of reduced contact time which negatively affected loading of Cu^{2+} ions onto IEFs (see Table 5.6). The saturation concentration was expected to be equivalent to the feed concentration. However, the saturation concentration predicted by the BDST model was more than 100 times that of the feed in all studied conditions because the BDST model neglects the effects of intra-particle mass and external film mass transfer resistance (Rajeshkannan et al., 2013; Goyal and Bhagat, 2010; Kalavathy et al., 2010).

Table 5. 5: Effect of bed depth on parameters of the BDST model.

Packing density				
(g/cm³)	Flow rate (mL/min)	k_{AB}	N_o (mg/L)	R²
0.16	8	3.61E-04	1.44E+04	0.71
0.20	8	2.43E-04	1.82E+04	0.82
0.28	8	1.28E-04	2.70E+04	0.87
0.37	8	1.33E-04	3.42E+04	0.83

Table 5. 6: Effect of bed depth on parameters of the BDST model.

Packing density				
(g/cm³)	Flow rate (mL/min)	k_{AB}	N_o (mg/L)	R²
0.16	8	3.61E-04	1.44E+04	0.71
0.16	12	1.49E-04	1.57E+04	0.89
0.16	17	1.59E-04	1.62E+04	0.90
0.16	28	2.07E-04	1.63E+04	0.95

5.4.4 Comparison of models

As indicated by the sum of absolute errors in Table 5.7 and 5.8, the effluent concentrations predicted by the Yoon-Nelson and Thomas models were the same in all experiments except for bed packing density and flow rate of 0.16 g/cm³ and 8 mL/min, respectively. However, the parameters of the Yoon-Nelson model were within the expected experimental range as listed in Tables 5.1-5.6. The parameters of the Thomas models, particularly the equilibrium uptake of IEFs were more than 500 times than the theoretical maximum uptake. The Thomas models parameters were unreasonable due the assumption that intraparticle diffusion and external resistance may be neglected. The effluent concentrations predicted by the BDST model had larger deviations from experimental effluent concentrations as listed in Table 5.7 and 5.8. In addition, the parameters of the BDST model were unrealistic as the saturation concentration (N_o) was more than 100 times that of feed (Table 5.1-5.6). As stated above, the BDST model is unsuitable for predicting effluent concentration in this study due to its

unaccountability of the effects of intra-particle mass and external film mass transfer resistance.

The plots of effluent Cu concentrations predicted by the Thomas, Yoon-Nelson and BDST models versus time are shown in Figure 5.7 – 5.13. The predicted Cu concentrations are compared with the effluent Cu concentrations obtained experimentally. For values of absolute deviations between experimental and predicted effluent Cu concentration (Thomas, Yoon-Nelson and BDST models) refer to Tables C.81 - C.87 in Appendix C.

Table 5. 7: Sum of absolute errors between experimental concentrations at various times and those predicted by the Thomas, Yoon-Nelson and Adam's Bohart model at various bed packing densities.

packing density (g/cm³)	Thomas	Yoon-Nelson	Adam-Bohart
0.16	67.58	69.43	355.34
0.20	45.83	45.83	164.85
0.28	26.25	26.25	110.88
0.37	32.34	32.34	132.11

Table 5. 8: Sum of absolute errors between experimental concentrations at various times and those predicted by the Thomas, Yoon-Nelson and Adam's Bohart model at various feed flow rates.

Flow rate (mL/min)	Thomas	Yoon-Nelson	Adam-Bohart
8.00	67.58	69.43	355.34
12.00	34.65	34.65	90.87
17.00	41.03	41.03	79.70
28.00	39.84	39.84	69.67

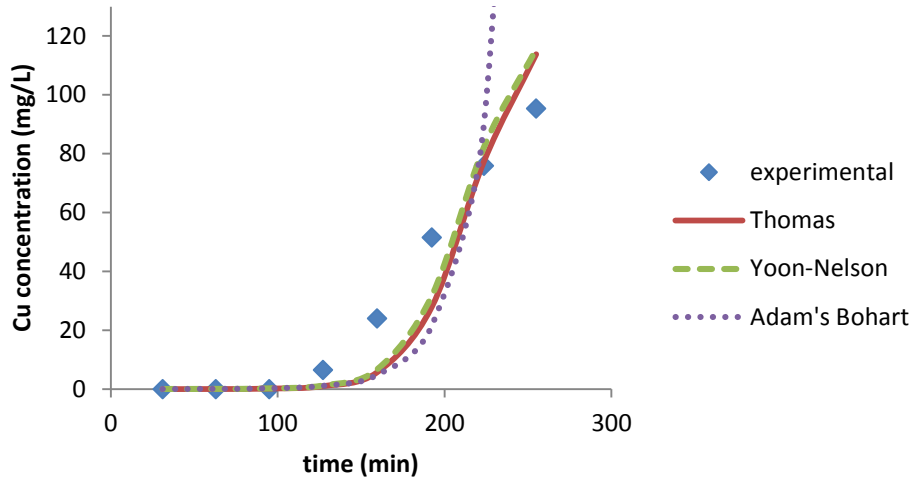


Figure 5. 6: Plot of Cu concentration from experiments and those predicted by the Thomas, Yoon-Nelson and Adam's Bohart model versus time at bed depth and flow rate of 10.5 cm and 8 mL/min.

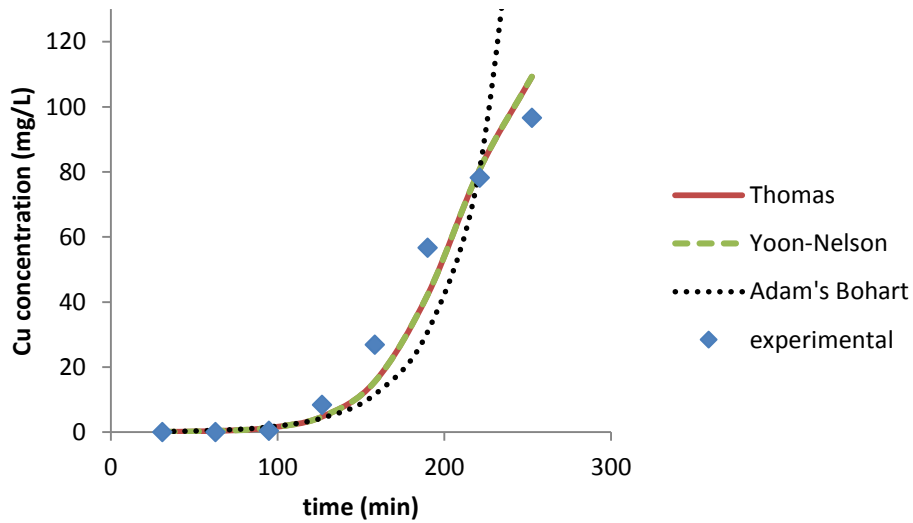


Figure 5. 7: Plot of Cu concentration from experiments and those predicted by the Thomas, Yoon-Nelson and Adam's Bohart model versus time at bed depth and flow rate of 8.5 cm and 8 mL/min.

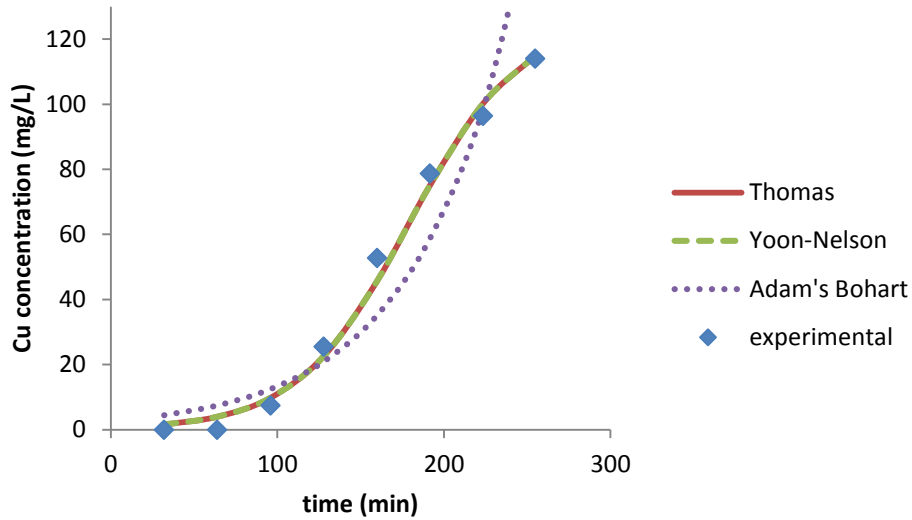


Figure 5. 8: Plot of Cu concentration from experiments and those predicted by the Thomas, Yoon-Nelson and Adam's Bohart model versus time at bed depth and flow rate of 6.0 cm and 8 mL/min.

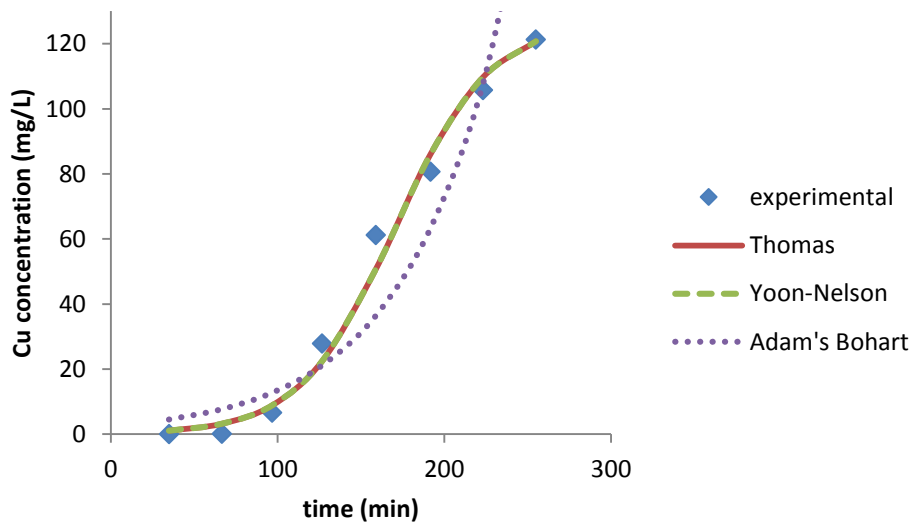


Figure 5. 9: Plot of Cu concentration from experiments and those predicted by the Thomas, Yoon-Nelson and Adam's Bohart model versus time at bed depth and flow rate of 4.5 cm and 8 mL/min.

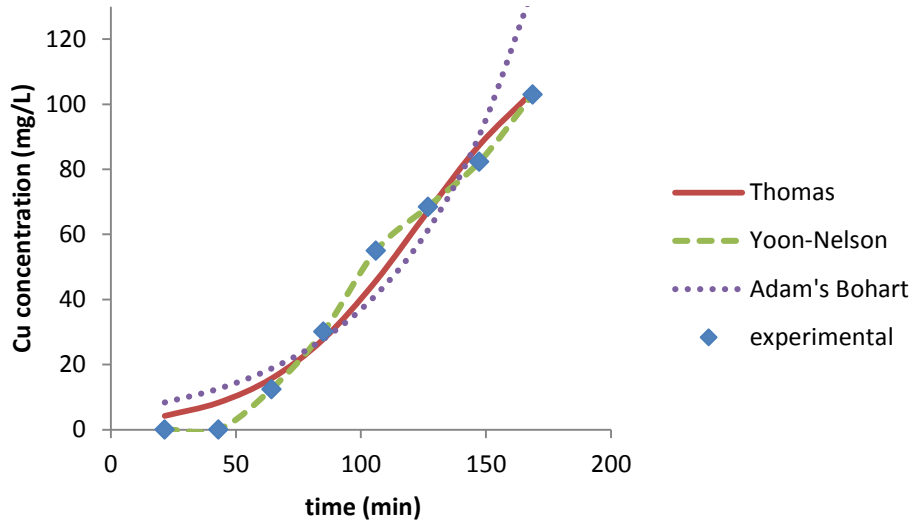


Figure 5. 10: Plot of Cu concentration from experiments and those predicted by the Thomas, Yoon-Nelson and Adam's Bohart model versus time at bed depth and flow rate of 10.5 cm and 12 mL/min.

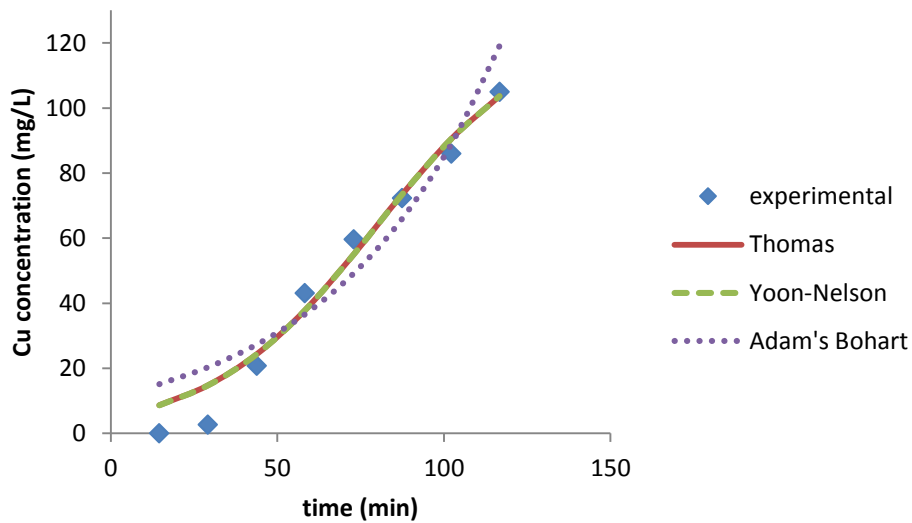


Figure 5. 11: Plot of Cu concentration from experiments and those predicted by the Thomas, Yoon-Nelson and Adam's Bohart model versus time at bed depth and flow rate of 10.5 cm and 17 mL/min.

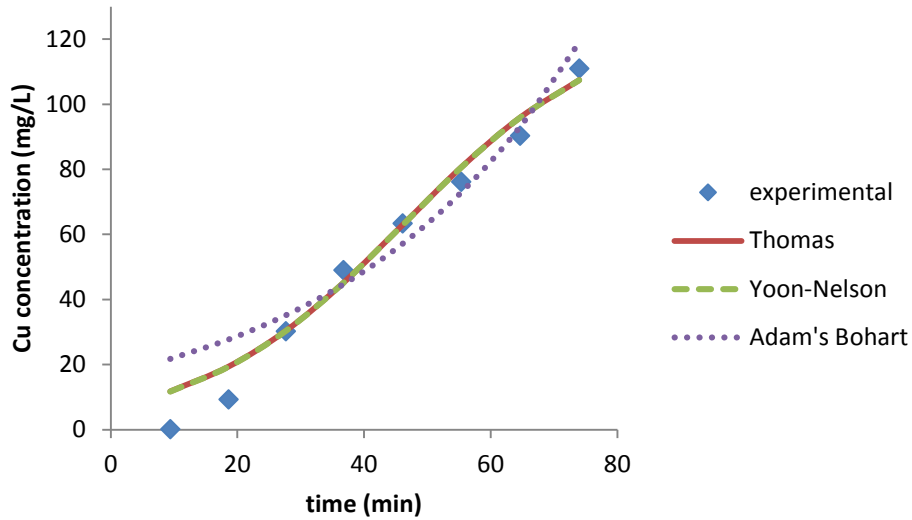


Figure 5. 12: Plot of Cu concentration from experiments and those predicted by the Thomas, Yoon-Nelson and Adam's Bohart model versus time at bed depth and flow rate of 10.5 cm and 28 mL/min.

5.5 Summary

Breakthrough tests were conducted using plastic columns packed with IEFs at lab scale. The tests were done to investigate effects of bed packing density and flow rate on Cu^{2+} ions removal and elution. The removal of Cu^{2+} ions was found to increase with a decrease in both bed packing density and feed flow rate due to the increased residence time within the IEFs. The elution rate increased with an increase in the eluent flow rate. In other words, the loaded ions were eluted at a rate proportional to the eluent flow rate. The required values of U and CT for the contactor design were found to be 5.20 cm/min and 2.02 min, respectively. Amongst the fitted empirical models, the Yoon-Nelson model was the most suitable model for predicting how effluent concentration during Cu^{2+} ions removal varies with time. This means that the Cu^{2+} ions removal decreased as more Cu^{2+} ions were loaded onto the IEFs.

Chapter 6: Fibre contactor design

6.1 Introduction

This Chapter discusses the selection and design of a continuous IEF contactor. The equilibrium data obtained in batch tests were used to determine the required adsorption stages of the contactor. The U and the CT obtained from column tests were used to size the proposed lab scale sorption pan of the contactor.

6.2 Choice of contactor(s)

Amongst the reviewed contactors compatible with IEFs, the belt and the table pan filter model were found to have the potential for continuous and practical removal of copper from dilute solutions. These systems can be designed to have simultaneous loading, elution and rinsing.

A semi-batch belt contactor shown in Figure 6.1 below was considered for continuous metal removal. The semi-batch belt contactor consists of a belt made of fibres which moves through baths of solutions where loading, elution and rinsing occurs (Karlson, 1975). As shown in Figure 6.1, there is at least more than 50% of the fibre belt that will not participate in the ion exchange process at a time due to the arrangement. In addition, the system does not operate in a counter current manner. The semi-batch belt contactor is also not continuous due to the necessity to halt operation during replacement of solutions in the baths. Furthermore, it is believed that the arrangement does not favour high mass transfer rates. Due to these reasons and many others, the semi-batch belt contactor was disregarded as it is inefficient and impractical.

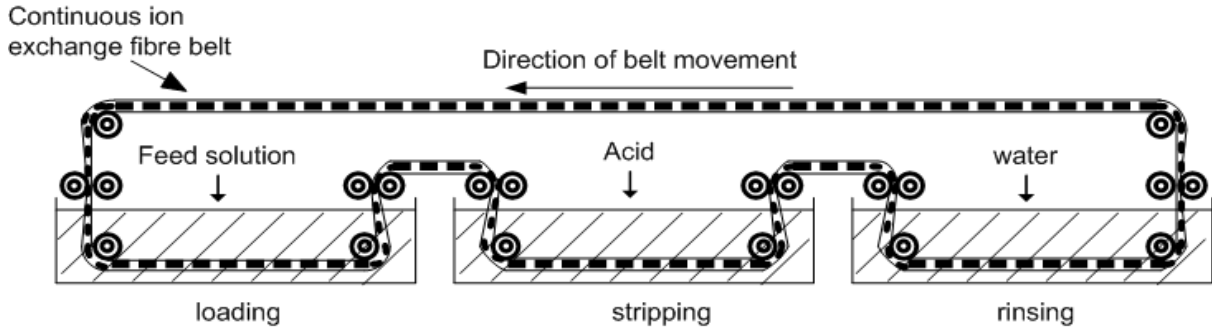


Figure 6. 1: Semi-batch belt contactor.

The horizontal moving belt contactor shown in Figure 6.2 below appears to have a realistic potential to operate continuously with loading, elution and rinsing occurring simultaneously (Muendel and Selke, 1955; Phelps and Ruthven, 2002; Brandani et al., 1999). The advantage of this arrangement is the ability to operate in a counter-current manner which increases ion exchange reaction rates. However, half of the belt will not be utilized for ion exchange operation in the arrangement of the horizontal belt as shown in Figure 6.2. This may result in increased cost associated with IEFs.

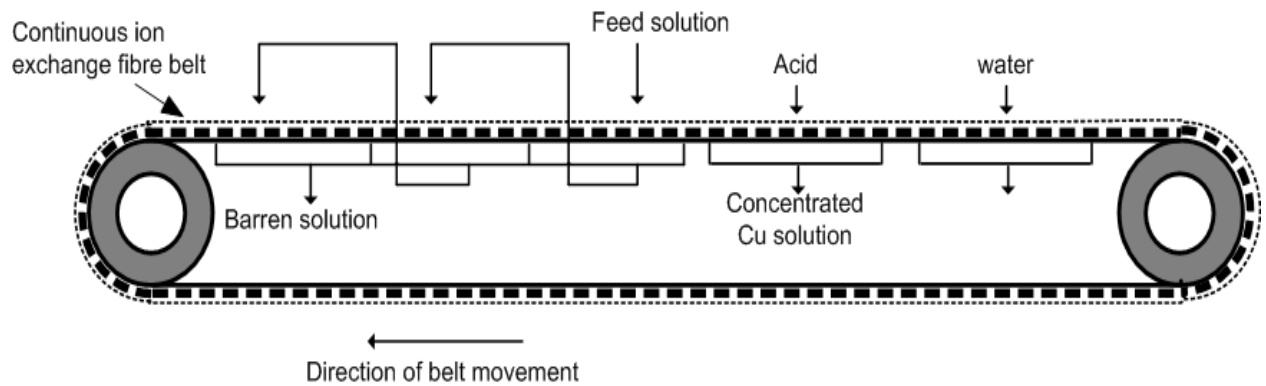


Figure 6. 2: Horizontal moving belt fibre contactor.

As an improvement to the above horizontal moving belt, it was proposed that elution and rinsing be conducted at the bottom section of the belt to maximize usage of the belt. Figure

6.3 below shows the improved horizontal belt contactor. As shown in Figure 6.3, the configuration necessitates operation between top and bottom part of the belt. However, processing on both sections (top and bottom) of the belt may result in a complex mechanical and/or physical arrangement of the system. The complexity in the moving belt contactor is due to the suctions required underneath the top and bottom sections as well as the introduction of rinsing and stripping solutions between the sections.

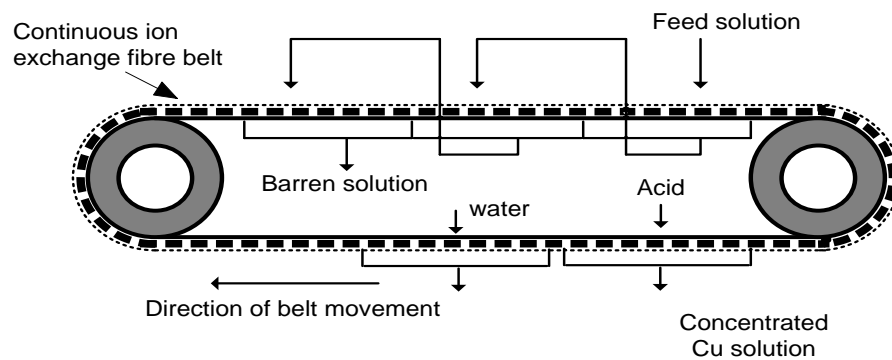


Figure 6. 3: Improved horizontal moving belt fibre contactor.

A continuous table pan ‘filter’ model normally used for solid-liquid separation in the phosphonic industry may be used for ion exchange purposes. The table pan filter consist of pans which are fitted with cloth through which solids are retained as liquid passes through thereby achieving separation (Wakeman and Wei, 1995; Nair, 2006). The IEFs can be embodied in the place of filter cloth through which feed can be passed for treatment purposes. The configuration of the table pan fibre contactor is shown in Figure 6.4 below. The contactor consists of sections containing IEFs with a vacuum created underneath to ensure that the solution passes through the IEFs. An advantage of the table pan ‘filter’ model is that the IEFs in various forms can be embodied into the sections. Thus, the table pan ‘filter’ model was regarded as the favourable contactor for IEFs.

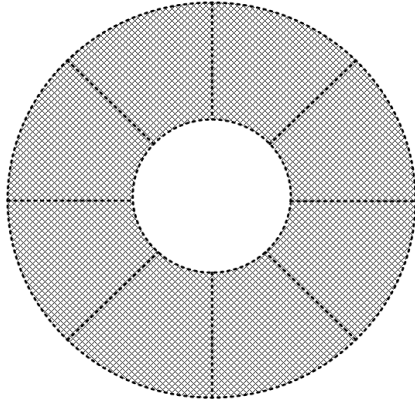


Figure 6. 4: Table pan fibre contactor.

6.3 Adsorption stages

The theoretical number of stages required to reduce feed concentration to 1.5 mg/L were determined using graphical techniques presented by Sherry (1993). As shown in Section 4.4, the Temkin model was found to best describe the equilibrium relationship between Cu in solid and liquid phase. Therefore, the Temkin isotherm model was used to plot the equilibrium curve. Material balance of Cu was used to determine the operating line. The Temkin isotherm and operating line equations are shown below as Equation 6.1 and 6.2, respectively (see detailed derivations of the two equations in Appendix D). The slope of the operating line is obtained as the ratio of the total cationic equivalence of the feed solution and the total cationic capacity (119 mg/g) of the IEFs. The operating line passes through the feed concentration and maximum loading obtained experimentally, respectively.

$$q_e = 0.486C_e - 1.740 \quad (6.1)$$

$$q_e = RT/b \ln (AC_e) \quad (6.2)$$

Where: $R = 8.314 \text{ Pa m}^3 \text{ mol}^{-1} \text{ K}^{-1}$

$T = 298 \text{ K}$

$b = 384.11 \text{ Pa m}^3 \text{ mol}^{-1} \text{ mg}^{-1} \text{ g}$

$A = 97.864 \text{ L/mg}$

The theoretical number of stages required to produce a barren solution containing Cu^{2+} ions at a concentration of 1.5 mg/L is shown in Figure 6.5. The required stages were determined by the number of right angled triangles formed between the operating line and equilibrium curve as shown in Figure 6.5. As shown in Figure 6.5, 3 adsorption stages are needed to reduce feed concentration to 1.5 mg/L at most. The technique that was used is analogous to the McCabe-Thiele method that is commonly used in liquid- liquid extraction, distillation, etc., problems.

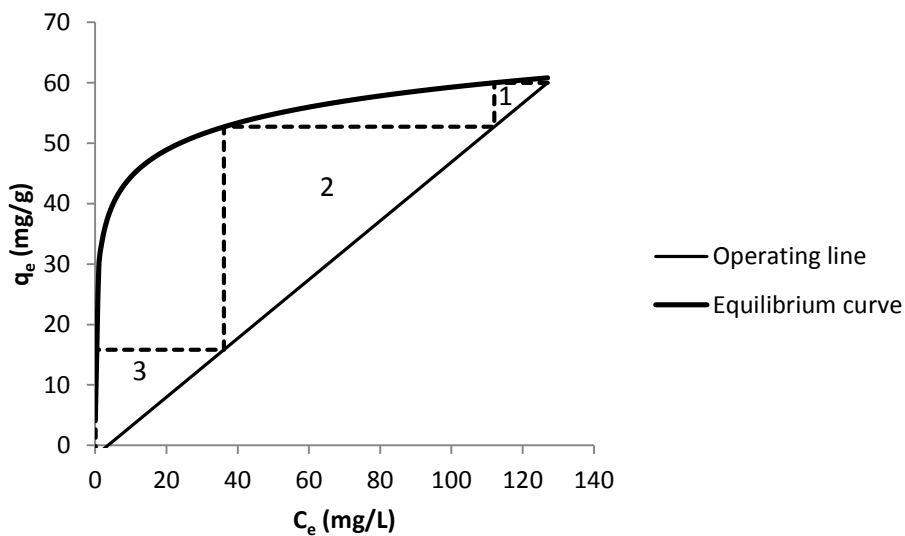


Figure 6. 5: Graphical representation of the number of theoretical adsorption stages required to produce a barren solution.

As stated above, a continuous ion exchange sorption comprises of loading, elution and rinsing. Kinetic tests (Chapter 4) showed that 80% loading occurs within the first hour of contact. Therefore, it was assumed that 80% equilibrium will be attained during continuous operation; therefore 4 actual adsorption stages are required. Contrary to loading, elution of the loaded Cu^{2+} ions was faster as observed in elution studies (Chapter 4). In addition, the loaded IEFs were completely eluted with about 5 bed volumes of 2 M HCl in a single stage. Therefore, two elution stages will be required to ensure that all ions loaded onto the IEFs are eluted. The IEFs will be rinsed before and after the two elution stages to remove entrained feed solution and acid solution, respectively. As a result, the total number of sorption sections required is 8. A schematic diagram showing the top view of the sections required for sorption is shown in Figure 6.6 below.

The operation of the table pan IEF contactor is similar to the cascade columns usually referred to as the carousel system. However, the proposed IEF contactor will allow easy packing of IEFs and limit number of control points required in the system since less adsorption sections are required.

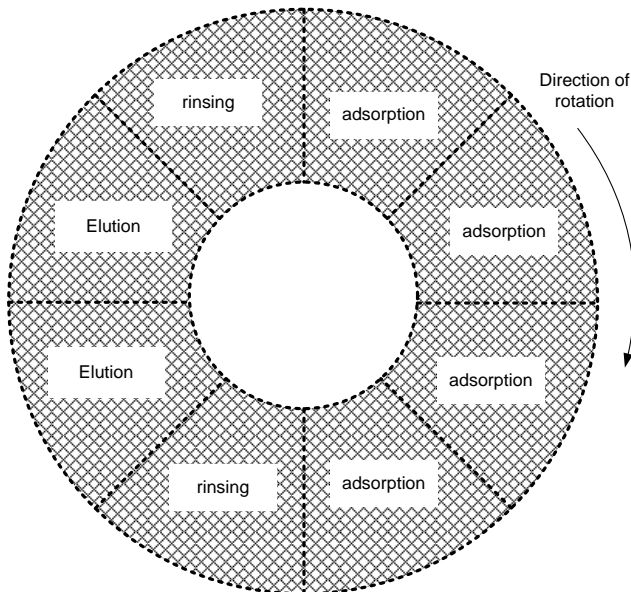


Figure 6. 6: Schematic top view diagram of the IEF contactor sections.

The batch tests conducted showed that the elution and rinsing stages were faster than the adsorption stage. Consequently, the duration of each cycle will depend on the residence time required to reach maximum metal loading.

6.4 Design of IEF sorption pan

The scale-up design approach was used to transfer the ion exchange technology from fixed bed columns to the proposed table pan IEF contactor. The design method by Gaikwad et al. (2010) was incorporated into the scale-up method to determine some of the parameters. The scale-up design approach developed by Fornwalt and Hutchins (1966) uses the U and τ obtained from column tests to size the desired contactor (Inglezakis, 2010; Inglezakis and Poulopoulos, 2006). In this study, the U was defined as the ratio of feed flow rate to cross sectional area of the column used in laboratory tests (Inglezakis, 2010; Inglezakis and Poulopoulos, 2006). The τ was defined as the quotient of the IEF bed volume and the feed flow rate (Inglezakis, 2010; Inglezakis and Poulopoulos, 2006). The mass transfer characteristics obtained in column tests can be obtained in the table pan IEF contactor provided that the U and τ are kept constant (Inglezakis, 2010; Inglezakis and Poulopoulos, 2006). The parameters of the proposed sorption pan are listed in Table 6.1 below. Detailed calculations for determining parameters of the sorption pan are provided in Appendix D.

Table 6. 1: IEF contactor specifications*

Parameters	
$\rho_{b,packing}$ (g/cm ³)	0.16
$A_{contactor}$ (cm ²)	18.86
θ	45°
r (cm)	4
R (cm)	8.00
R-r (cm)	4.00
V_{bed} (cm ³)	198.00
h_{bed} (cm)	10.5
$H_{contactor}$ (cm)	12.5
$V_{contactor}$ (cm ³)	235.72
m_{IEFs} (g)	31.36
q_e (mg Cu/g IEF)	74.51
$t_{breakthrough}$ (min)	188
$V_{breakthrough}$ (mL)	18400
V_{eluent} (mL)	1286
$V_{rinse\ water}$ (mL)	1470

*Detailed calculations are provided in Appendix D.

6.5 Mechanical design of IEF pan

The pressure drop in packed IEFs must not be more than 20 kPa, therefore, the bed height must not exceed 20 cm as recommended in practice (Kosandrovich and Soldatov, 2012).

Clear polyvinyl chloride (PVC) was selected as material for construction of the IEF pan. Clear PVC is cost effective, corrosion resistant and can withstand temperatures of up to 60 °C. This material of construction will ensure that contactor is always operated within the operating temperature range of the IEFs. The working temperature range for the selected IEFs is 0 to 80°C.

The IEFs packing on the contactor will be supported by a 45 micron screen so that they are not washed out of the pan. The screen placed to prevent IEFs from being washed out will be supported by the bottom closure of the pan discussed in the next paragraph. A 45 micron screen will also be placed inside the top closure to prevent any particles from clogging the IEF packing. A porous piston with screen size of 45 microns may be used to set the bed height to various values when required (Soldatov et al., 1999) or alternatively an inert and porous cotton wool.

The top part of the contactor was designed to have a flanged opening connected to a threaded cap that allows connection with tubing. The flanged opening will also easy opening in case the packed IEFs need to be replaced. The bottom part was designed to be conical to ensure the treated solutions exit the contactor. Moreover, the bottom part was also designed to have a valve for controlling liquid outflow and consequently the liquid level on top of the packed IEFs. The mechanical diagram of the designed contactor segment is shown in Figure 6.7.

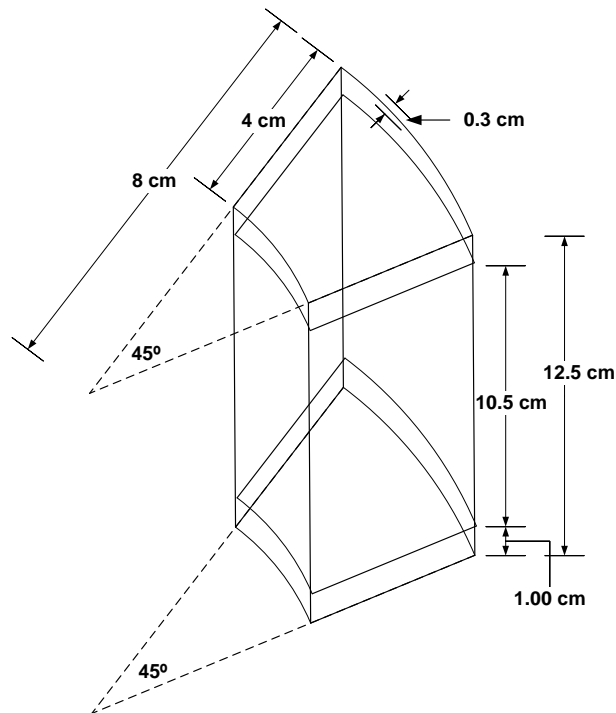


Figure 6.7: Mechanical design diagram of the IEF sorption sector.

6.6 Summary

A rotating contactor similar to the table pan 'filter' model was selected for continuous ion exchange sorption characterized with simultaneous loading, rinsing and elution. The number of equilibrium adsorption stages was determined. A lab scale sorption sector of the contactor was sized and a mechanical diagram was provided. Although the IEF contactor will operate continuously, it will rotate once per cycle which has a duration equivalent to the breakthrough time. Each rotation cycle will shift the sorption sectors to the position of the subsequent sorption sectors with respect to the selected direction of rotation.

Chapter 7: Contactor testing

7.1 Introduction

The IEFs contactor pan designed in Chapter 6 was constructed and tested in this study. Fabrication of the contactor was conducted at Mintek, (South Africa). The designed contactor operates similarly to ion exchange columns. However, the designed contactor has a different shape from columns which allows it to be compatible with continuous structure of table pan ‘filter’ model as discussed in Chapter 6.

In this study, the contactor pan was tested by passing feed solution through the packed IEFs. After loading of Cu^{2+} ions, the IEFs were eluted using acid thereby generating the elution profile of the contactor. The tests conducted included comparison of the effect of density in the designed contactor.

The determination of the adsorption mechanisms is imperative. An understanding of the adsorption mechanisms allows one to select the most suitable model for describing the process. Therefore, the Thomas, Yoon-Nelson and Adam’s Bohart models were also fitted onto the breakthrough profile of the contactor.

7.2 Materials and Methods

7.2.1 Material acquisition, fibre and reagent preparation

The material acquisition was done as described in Section 3.2, Chapter 3. The IEFs were prepared by contacting with acid as described in Section 3.3 and the feed solution composed of 2mM Cu^{2+} ions was prepared from CuSO_4 as stated in Section 3.4 (Chapter 3).

7.2.2 Experimental set up

The manufactured IEF contactor was packed with 31.36 g of IEFs such that the packing density was 0.16 g/cm^3 . Packing density of 0.16 g/cm^3 corresponds to the packing density in column tests with an optimum breakthrough time. The contactor was configured vertically by

clamping it on a stand. The solution was pumped from the tank downwards into the contactor using a peristaltic pump. As stated in Chapter 3, downward flow is often employed in ion exchange columns for both loading and elution. The feed solution in the beaker was continuously mixed using an electric stirrer connected to an impeller. The effluent solution from the column was collected into a graduated cylinder. A schematic sketch of the experimental set up is provided in Figure 7.1 below. The actual image of the contactor is given in Figure E.1 found in Appendix E.

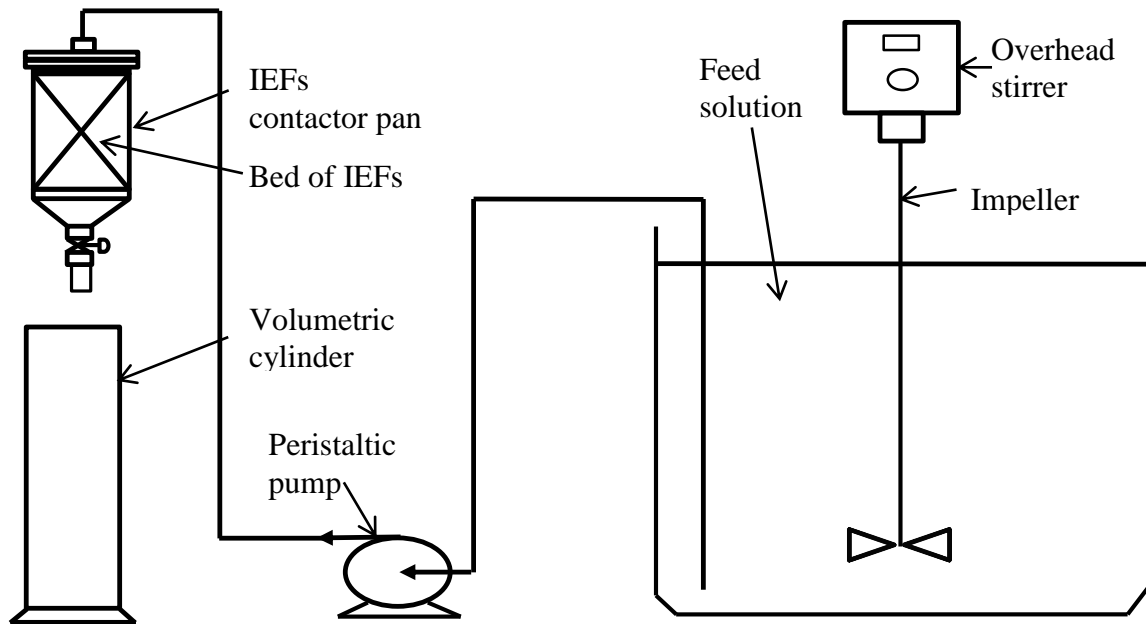


Figure 7. 1: Schematic presentation of the experimental set up for contactor testing.

7.2.3 Experimental procedure

The breakthrough profile of Cu on the IEFs packed bed in the designed table pan contactor was generated by passing feed solution containing 127 mg/L of Cu through the bed. Results from column breakthrough tests (Chapter 5), indicated that u of 5.2 cm/min prolongs the breakthrough time. Therefore, the feed solution was pumped at a flow rate of 98 mL/min so that u of 5.2 cm/min could be attained within the contactor. Feed solution volume of 30 L was passed through the contactor. Samples were collected consecutively after passing 2 L of

feed solution through the IEFs and time taken to collect 2 L was measured and recorded. The samples were then analysed for the concentration of Cu^{2+} ions using an AAS.

Prior to regeneration of IEFs, 2 L of deionised water was passed through the contactor pan to remove any entrained feed solution within the IEFs bed.

Similar to column tests, the washed IEFs bed was then regenerated by 2 M of HCl. The HCl acid solution of volume of about 1280 mL was passed through the Cu loaded bed of IEFs at 98 mL/min in order to maintain the u of 5.2 cm/min. Samples were collected after contacting the loaded bed with 160 mL of acid. The time taken to pass 160 mL of solution (consecutively) was noted and samples were analysed for Cu^{2+} ions.

Similar to column tests, the IEFs bed was then washed with 2L of deionised water so as to remove any entrained acid. The deionised water was passed at a flow rate of 98 mL/min. The experiment was replicated 3 times to check reproducibility of the results.

7.3 Results and discussions

For the results discussed in this section, reference should also be made to Appendix E. Please note that in this study, a bed volume is equivalent to the quotient of the volume of solution treated and volume of the packed bed of IEFs. Bed volumes were used for comparing performance of IEFs with the same packing density and volume was expressed in litres or millilitres for comparing beds with different packing density as their bed volumes were not the same.

7.3.1 Breakthrough profile of the IEFs table pan contactor

The breakthrough profile of Cu^{2+} ions through the designed IEF contactor pan was generated by passing through 124 bed volumes of 127 mg/L of Cu^{2+} ions solution. Generally, as shown in Figure 7.2, the breakthrough of Cu^{2+} ions in the contactor increased as feed was continuously passed through the bed of IEFs. As more feed solution was passed through the bed of IEFs, the amount of ionised functional groups in H^+ form decreased and resulted in

less Cu^{2+} ions uptake from the feed solution (Helfferich, 1995). The breakthrough profile in Figure 7.2 shows that Cu^{2+} ions concentration was noticeable in the contactor effluent after treating more than 30 bed volumes as compared to 60 bed volumes in the column. The figure also shows that in the contactor 50 % breakthrough was reached after treating 60 bed volumes as compared to about 100 bed volumes in the column. This was due to unequal distribution of the feed solution within the contactor and consequently Cu^{2+} ions escaped through to the effluent as they continued contacting with functional groups which had already loaded Cu^{2+} ions.

Overall, the loading of Cu^{2+} ions in the designed contactor was 45 mg/g of fibre as compared to the 54 mg/g of fibre obtained in column tests at packing density of 0.16 g/cm^3 . Once more, this was due to unequal distribution of the feed solution within the contactor pan and consequently Cu^{2+} ions escaped through to the effluent as the feed solution continued contacting with functional groups which had already loaded Cu^{2+} ions.

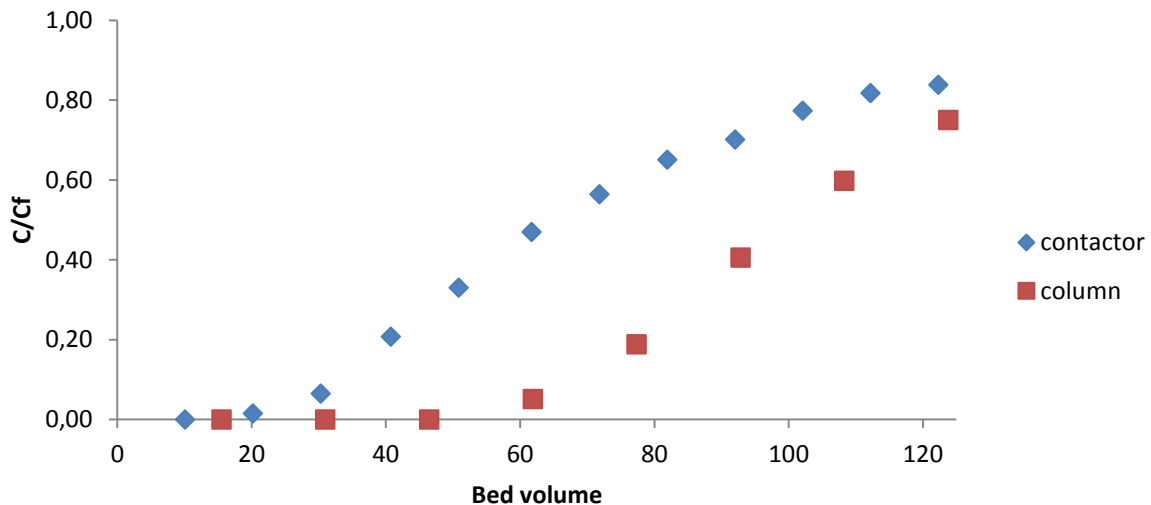


Figure 7. 2: Breakthrough profile of the IEFs contactor and column at 0.16g/cm^3 .

7.3.2 Comparison of contactor and column packing density profile

The packing densities of the IEFs in the contactor were set to 0.16 , 0.28 and 0.37 g/cm^3 to compare with column test results (Chapter 5). The results that show the comparison of the

contactor and column at packing densities of 0.16, 0.28 and 0.37 g/cm³ are given in Figure 7.2, 7.3 and 7.4, respectively. Figure 2 shows that the 50% breakthrough of Cu²⁺ ions for the contactor with packing density of 0.16 g/cm³ occurred after treating 67 bed volumes of feed solution as compared to 100 bed volumes which was treated using column. For packing density of 0.28 g/cm³, 50% breakthrough of Cu²⁺ ions for the contactor occurred after treating 107 bed volumes of feed solution as compared to 150 bed volumes which was treated using column (Figure 7.3). In other words, IEFs packed in the contactor treated less amount of feed when compared with IEFs at the same density in columns. Once more, this was attributed to the uneven feed distribution. Similar results were found when IEFs with packing density of 0.37 g/cm³ in the contactor were compared with IEFs in the column with the same packing density (Figure 7.4).

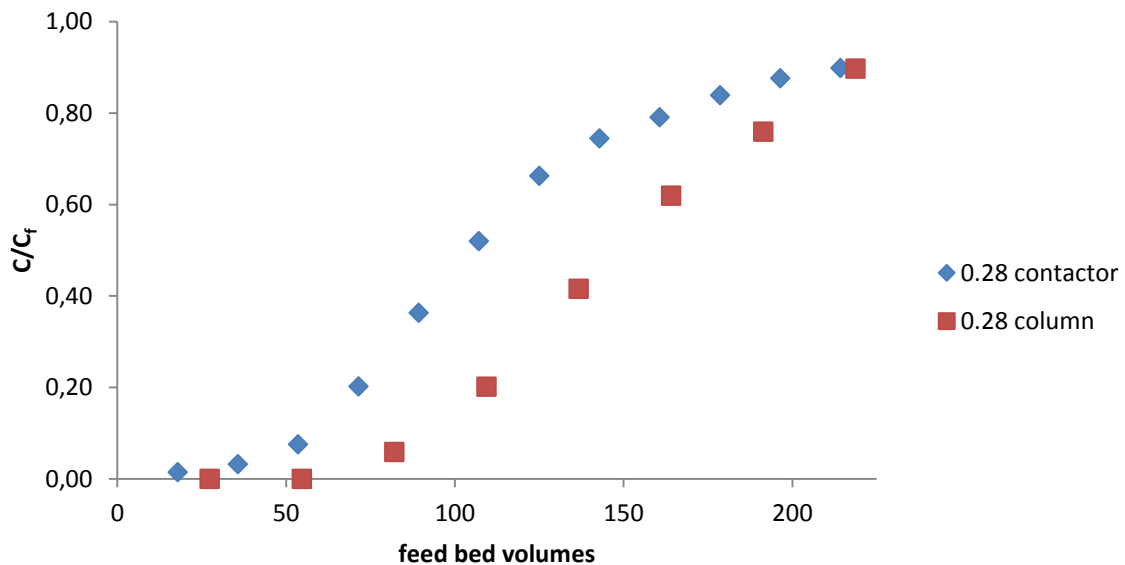


Figure 7. 3: Breakthrough profiles of the contactor and the column at 0.28g/cm³.

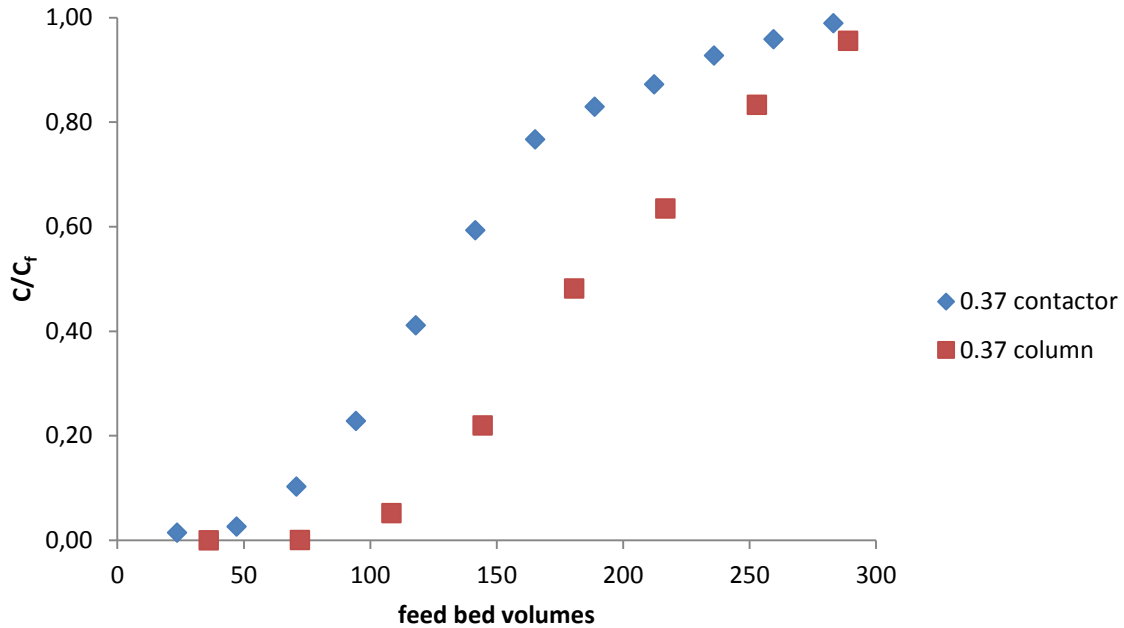


Figure 7. 4: Breakthrough profile of the contactor and column at 0.37g/cm³.

7.3.3 Elution profile of the contactor

The IEFs packed into the contactor pan were eluted using 2 M HCl solution. The elution profile of the contactor is shown in Figure 7.5. The IEFs were washed with deionised water prior to elution, therefore, the effluent bed volume of 0.8 collected from the contactor in the beginning during elution was the de-ionised water retained within the IEFs, and hence the Cu²⁺ ions concentration was zero. Cu²⁺ ions reported in the effluent stream after passing about 1.6 bed volumes of eluent. Figure 7.5 also shows that the concentration of Cu²⁺ ions reached 7 100 mg/L after passing about 1.6 bed volumes of eluent through the contactor and, thereafter, the concentration decreased until it reached zero showing that Cu²⁺ ions were being eluted from the IEFs. The results in Figure 7.5 also show that about 4.1 bed volumes of eluent were required for complete elution.

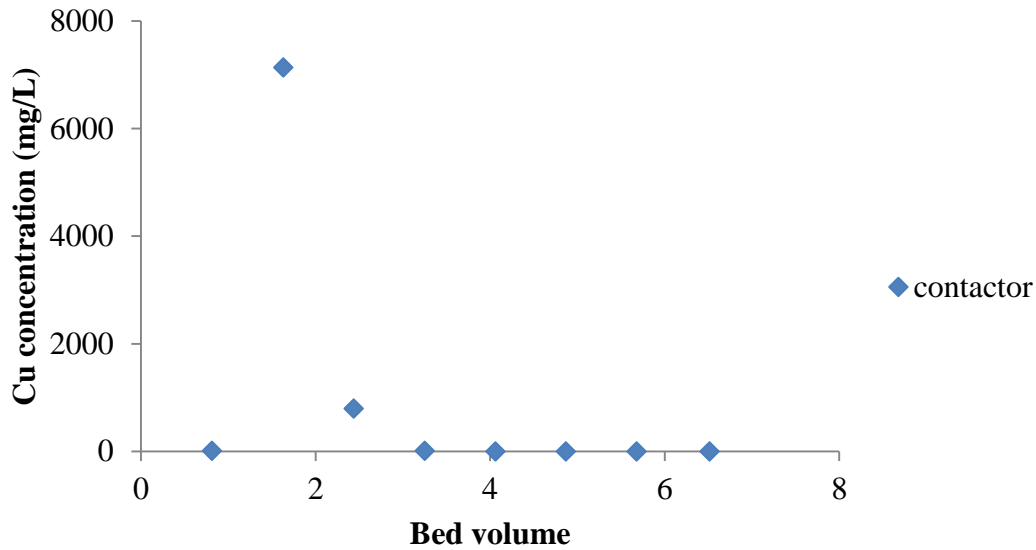


Figure 7. 5: Regeneration profile of the IEFs contactor.

7.3.4 Model fitting into the IEFs contactor pan

The Thomas, Yoon-Nelson and the Adams-Bohart model were fitted into the breakthrough profile of the contactor as previously done for column breakthrough profiles. The designed contactor has a different shape from the column; however, it was necessary to check whether any of the models would predict the dynamic behaviour of the Cu^{2+} ions loading onto the IEFs.

The effluent Cu^{2+} ions concentrations predicted by the three models are shown in Figure 7.6. Both the Yoon-Nelson and Thomas model poorly predicted the effluent concentration. Moreover, the Thomas model parameter, q_0 (maximum Cu loading), was about 100 times more than the maximum attainable loading (see Table 7.1) obtained in column tests. Similarly, the Yoon-Nelson parameter, τ (time required for 50% adsorbate breakthrough), was outside the experimental range (see Table 7.2). The Adam-Bohart model also poorly predicted the effluent concentration with correlation coefficient (R^2) of 0.52 as compared to 0.71 obtained for both Yoon-Nelson and Thomas model. In addition, the saturation concentration (N_0) predicted by the Adam-Bohart model was more than 100 times of the highest reachable concentration in the effluent stream as shown in Table 7.3.

The poor predictions by the fitted models could be attributed to the shape of the contactor pan. The models were developed using columns which differs from the shape of the designed contactor pan (Nwabanne and Igbokwe, 2012; Kalavathy et al., 2010; Aksu and Gonen, 2004; Srivastava et al., 2008).

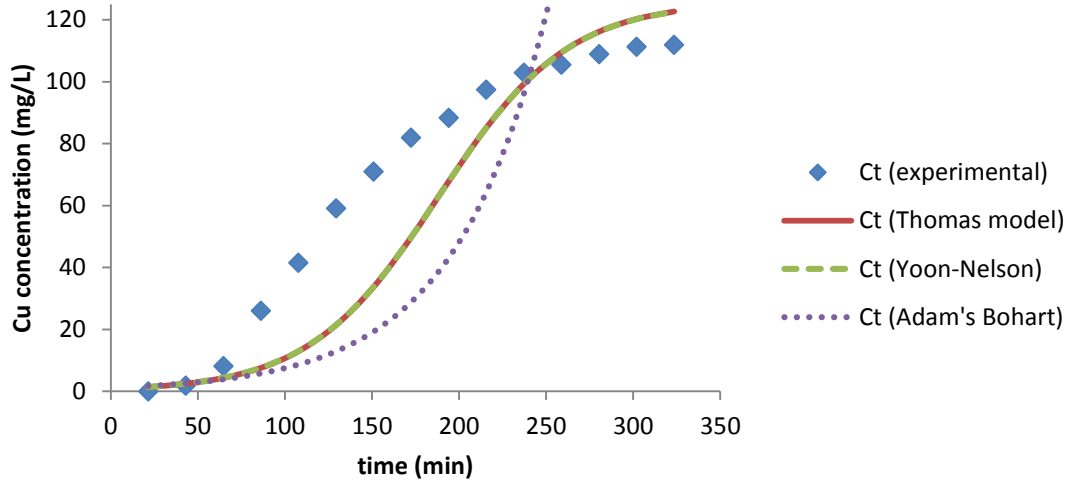


Figure 7. 6: Plot of experimental Cu concentration and that predicted by the Thomas, Yoon-Nelson and Adam's Bohart model versus time for the IEFs contactor.

Table 7. 1: Thomas model parameters for the IEFs contactor pan.

k_{TH} (mL/min mg)	experimental q_0 (mg/g)	predicted q_0 (mg/g)	R^2
0.000214	69	70451.54	0.71

Table 7. 2: Yoon-Nelson model parameters for the IEFs contactor pan.

k_{YN} (1/min)	τ (min)	experimental range of τ (min)	R^2
0.0269	188.31	130-152	0.71

Table 7. 3: Adam's Bohart model parameters for the IEFs contactor pan.

k_{AB} (L/mg min)	Experimental N_0 (mg/L)	N_0 (mg/L)	R^2
0.000148	127	14917.93	0.52

7.4 Summary

The study showed that the contactor was able to remove 45 mg of Cu^{2+} ions/g of fibre from the feed solution as compared to 54 mg Cu^{2+} ions/g of fibre obtained in column tests. Loading of Cu^{2+} ions onto the designed table pan contactor was found to be lower due to the higher cross sectional area which consequently resulted in uneven distribution. Similar to column tests, the effect of packing density was also investigated and it was found that Cu^{2+} ions removal was high at low packing density. In contrast to column Cu breakthrough, the Yoon-Nelson model was unable to predict the breakthrough of Cu^{2+} ions in the designed IEF contactor pan.

Chapter 8: Conclusions and recommendations

8.1 Conclusions

8.1.1. Introduction

A review of the literature in this study has shown that amongst the traditional wastewater treatment methods, ion exchange methods have been found to be very effective in removing impurities from solutions. Undoubtedly, granular ion exchange beads are the most common and widely used in ion exchange processes. However, another form of ion exchange materials called IEFs have been found to be more effective than granular ion exchange beads because they possess larger surface areas and shorter diffusion paths which improve the rate of ion exchange. The main aim of this study was to develop a continuous ion exchange contactor for Cu^{2+} ions removal from dilute solutions using IEFs. The WHO recommended a maximum concentration of Cu^{2+} ions in portable water of 1.5 mg/L. It is, therefore, of significant importance that Cu^{2+} ions in industrial waste effluent streams is reduced to minimal amounts. It is also worthwhile to minimise Cu^{2+} ions in waste streams because of its industrial importance. As a result, a contactor based on the table pan 'filter' model was selected for continuous ion exchange sorption and is characterized with simultaneous loading, elution and regeneration.

To develop the continuous IEFs contactor characterised with continuous and simultaneous loading, elution and rinsing of Cu^{2+} ions, the objectives of the study were defined as follows:-

- ❖ Determine whether the selected IEFs have a higher selectivity for Cu^{2+} ions.
- ❖ Establish equilibrium and kinetics of the selected IEFs.
- ❖ Determine the required superficial velocity and contact time using columns for the contactor design.
- ❖ Theoretically evaluate various designs of the horizontal ion exchange belts and other compatible systems and select the most suitable one for this application.

- ❖ Investigate the Cu^{2+} ions loading and elution duties on IEFs packed in a column.
- ❖ Design and test the sorption section of the selected IEFs contactor.

8.1.2. Batch tests

The batch tests conducted allowed establishment of the equilibrium and kinetic data for Cu^{2+} ions loading onto IEFs referred to as Fiban X-1. The tests also revealed the selectivity of the IEFs in dilute solutions amongst metal ions namely, Cu^{2+} , Co^{2+} , Ni^{2+} , Zn^{2+} , Mn^{2+} and Mg^{2+} .

Generally, the loading of the tested metal ions onto the IEFs used increased with an increase in pH. This trend was attributed to an increase in ionization of weak acid functional group on the IEFs which in turn increased the apparent loading capacity. The IEFs used were found to have a higher selectivity for Cu^{2+} ions in dilute solutions containing Cu^{2+} , Co^{2+} , Ni^{2+} , Zn^{2+} , Mn^{2+} , and Mg^{2+} . The optimum operating pH was 3.0. From the conducted tests at pH 3.0, there was minimal co-loading of the other metals while the loading of Cu^{2+} ions was higher. Therefore, the batch tests illustrated that the IEFs can selectively load Cu^{2+} ions at lab scale from dilute solutions containing other metals such as Co^{2+} , Ni^{2+} , Zn^{2+} , Mn^{2+} and Mg^{2+} .

Maximum loading of Cu^{2+} ions onto IEFs was 62 mg per gram of IEFs and it was obtained at the optimum operating pH of 3.0. Amongst the fitted equilibrium models (linearised equilibrium models of the Langmuir, Redlich-Peterson, Dubinin and Radushkevich, Freundlich and Temkin equilibrium models), the equilibrium sorption was found to exhibit the Temkin model behaviour. The Temkin model assumes that the heat of adsorption of all Cu^{2+} ions in the boundary layer decreases linearly rather than logarithmic with an increase in surface area. Therefore, the IEFs used in this study can be effectively applied at ambient temperatures by increasing their surface area which lowers the heat of adsorption.

The study found that the percentage of metal eluted from IEFs increased with an increase in acid concentration. However, if large volumes of less concentrated acid solutions are used, the same percentage of elution as the low volume of highly concentrated acid solution can be

achieved. Nevertheless, the use of less concentrated acid solutions at large volumes results in dilute Cu^{2+} ions effluent solutions. Therefore, the use of highly concentrated acid solution is recommended. The kinetic behaviour of the system was best described using the pseudo-second-order model which means that the ion exchange rate in this study was directly proportional to the number of ionizable functional groups.

8.1.3. Choice of contactor type and column tests

A contactor based on the table pan ‘filter’ model was selected for continuous loading and elution of Cu^{2+} ions. This type of contactor allows IEFs basically in any form to be embodied into the sections. Using the McCabe-Thiele technique and assuming that 80% equilibrium will be attained during continuous operation, it was found that 4 actual loading stages were required to reduce Cu^{2+} ions concentration to levels below 1.5 mg/L. For the purposes of this study, only a lab scale sorption section of the contactor was designed.

Initially, plastic columns packed with IEFs were used to test the feasibility of the proposed IEF contactor. The results showed that the effluent Cu^{2+} ions concentration decreased with a decrease in bed packing density for the same amount of feed volume passed at constant flow rate. Effluent Cu^{2+} ions concentration was also found to decrease with a decrease in feed flow rate for the same amount of volume that was passed through the IEF column at constant packing density. The amount of Cu^{2+} ions loaded onto the IEFs was higher at lower packing densities and flow rates due to the increased contact duration. Longer contact durations favoured Cu^{2+} ions loading as more Cu^{2+} ions were allowed to diffuse into the IEFs. The maximum Cu^{2+} ions loading attained was obtained at a packing density and flow rate of 0.16 g/cm³ and 8 mL/min, respectively.

In this study, the loaded Cu^{2+} ions were eluted with 2 M HCl. There was no significant difference in elution rates for IEFs packed at various packing densities eluted at constant acid flow rate. On the other hand, the elution rate increased with an increase in acid flow rate. The same amount of acid volume was required to completely elute the loaded Cu^{2+} ions from the IEFs irrespective of packing density and acid flow rate.

The Yoon-Nelson model was found to be the most suitable for describing the loading of Cu^{2+} ions onto IEFs packed in the column under the conditions in this study. Other models considered were the Thomas model and the Adam-Bohart model. As stated in literature, the Yoon-Nelson model assumes that the rate of decrease in the probability of loading of each ion is proportional to the probability of ion loading and the probability of ion breakthrough on IEFs. This means that the Cu^{2+} ions removal decreased as more Cu^{2+} ions were loaded onto the IEFs.

8.1.4 Design of the table pan contactor

Data collected from column test results (i.e., superficial velocity and contact time at the optimum flow rate (8mL/min) and packing density (0.16 g/cm³), respectively) was used to size the proposed contactor pan. The scale up approach technique was followed in determining the dimensions of the contactor pan.

The dimensions of the contactor were as follows: the height of the contactor was 12.5 cm; the height of the IEFs bed was 10.5 cm with packing density of 0.16 g/cm³; the inner and outer radius were 4 and cm, respectively; the volume of the contactor and the IEFs bed were 235 and 198 cm³, respectively.

8.1.5 Contactor testing

The study showed that the contactor was able to remove 45 mg of Cu^{2+} ions/g of fibre from the feed solution as compared to 54 mg Cu^{2+} ions/g of fibre obtained in column tests. Loading of Cu^{2+} ions onto the designed contactor pan was found to be low due to the higher cross sectional area which consequently resulted in uneven distribution. The IEFs loaded with Cu^{2+} ions were successfully eluted with 4.1 bed volumes of 2 M HCl as compared to the 4.8 bed volumes which was required to completely elute the entire loaded Cu^{2+} ions in the column. While the loading of Cu^{2+} ions was low, the designed contactor is promising as it was able to remove Cu^{2+} ions from the feed solution and the IEFs could be completely eluted for reuse. In contrast to column Cu breakthrough results, the Yoon-Nelson model was unable to predict the breakthrough of Cu^{2+} ions in the designed IEF contactor pan.

8.2 Recommendations

From the findings in the study and for further development of the IEF contactor, the following recommendations are proposed.

Batch tests

The batch tests conducted in this study only investigated the equilibrium and kinetic behaviour for dilute solutions comprised of solely Cu^{2+} ions. Further studies can be focused on investigating the equilibrium and kinetic behaviour for multi-component dilute solutions. The results from the multi-component studies can then be used to design IEFs contactors which can effectively treat multi-component waste streams.

Contactor design and testing

The results obtained from testing the designed contactor showed that the IEFs arranged as in the proposed contactor can be effectively used for Cu^{2+} ions loading provided that the feed is evenly distributed. However, loading of Cu^{2+} ions using the proposed contactor as tested in this study was demonstrated at lab scale. It is, therefore, suggested that scale-up studies be conducted to investigate the effectiveness of the contactor at a larger scale. Once the scale-up studies demonstrate that the IEF contactor is effective at large scale, mathematical and linear driving force (LDF) models which will allow simulations to be carried out must be fitted into the data. Moreover, mathematical and LDF models may be derived to account for the shape of the designed contactor. The model that best describes the process at large scale can also be used for process optimization and optimal large scale design. In addition, the most suitable model will also be used for economic evaluation of the ion exchange sorption process at large scale. This approach will minimise costs as the actual large scale contactor will be manufactured once the design has been tested with experiments simulating its operation.

It is also suggested that the design of the contactor should include a feed distributor to prevent uneven distribution of solution to be treated.

References

Abdelwahab, O., Amin, N.K., El-Ashtoukhy, E-S.Z., 2013. Removal of zinc ions from aqueous solution using a cation exchange resin. *Chemical engineering research and design* 91(1), 165–173.

Ahmad, A., A., Hameed, B., H., 2010. Fixed-bed adsorption of reactive azo dye onto granular activated carbon prepared from waste. *Journal of Hazardous Materials* 175, 298-303.

Aksu, Z., Gonen, F., 2004. Biosorption of phenol by immobilized activated sludge in a continuous packed bed: prediction of breakthrough curves. *Process Biochemistry* 39, 599-613.

Alluri, H. K., Ronda, S. R., Settalluri, V.S., Bondili, J. S., Venkateshwar, P., 2007. Biosorption: An eco-friendly alternative for heavy metal removal. *African Journal of Biotechnology* 6 (25), 2924-2931

Al-Orthman, Z.,A., I, Naushad, Mu., 2011. Determination of ion-exchange kinetic parameters for the poly-o-methoxyaniline Zr(IV) molybdate composite cation-exchanger. *Chemical Engineering Journal* 166, 639–645.

Alyüz, B., Veli, S., 2009. Kinetics and equilibrium studies for the removal of nickel and zinc from aqueous solutions by ion exchange resins. *Journal of Hazardous Materials* 167, 482–488.

Auta, M., Hameed, B., H., 2014. Chitosan–clay composite as highly effective and low-cost adsorbent for batch and fixed-bed adsorption of methylene blue. *Chemical Engineering Journal* 237, 352–361.

Bakiya Lakshmi, K., Sudha P.N., 2012. Adsorption of Copper (II) ion onto chitosan/sisal/banana fiber hybrid composite. *International Journal Of Environmental Sciences* 3(1), 453-470.

- Bhardwaj, V., Mirliss, M., J., 2001. Diatomaceous earth filtration for drinking water. Tech brief: A national drinking water clearinghouse fact sheet. Available at: http://www.nesc.wvu.edu/pdf/dw/publications/ontap/2009_tbdiatomaceous_dwfsom39.pdf. [Accessed: July 2013].
- Bochenek, R., Sitarz, R., Antos, D., 2011. Design of continuous ion exchange process for wastewater treatment. *Chemical Engineering Science* 66, 6209-6219.
- Brandani, S., Austin, K., Ruthven, D., 1999. The flow pattern and residence time distribution for an endless belt solid liquid contactor. *Chemical Engineering Science* 54, 417-432.
- Brown, T., E., LeMay, H., E., H., Bursten, B., E., Murphy, C., Woodward, P., 2011. *Chemistry: The Central Science*. Prentice Hall, United States of America.
- Bryan, W.,L., 1962. Ion exchange fabrics, US Patent US3062379 A.
- Cegłowski, M., Schroeder, G., 2015. Removal of heavy metal ions with the use of chelating polymers obtained by grafting pyridine–pyrazole ligands onto polymethylhydrosiloxane. *Chemical Engineering Journal* 259,885-893, doi: <http://dx.doi.org/10.1016/j.cej.2014.08.058>.
- Cheung, C., W., Porter, J., F., McKay, G., 2000. Sorption kinetics for the removal of copper and zinc from effluents using bone char. *Separation and Purification Technology* 19, 55–64
- Chin, A., F., McAndrew, R.,T., Hummel, R.,L., Mouland, J.,E., 1992. Application of short bed reciprocating flow ion exchange to copper/zinc separation from concentrated leach solutions. *Hydrometallurgy* 30, 431-444.
- D' Alelio G., F., 1944. Production of synthetic polymeric compositions comprising sulphonated polymerizates of poly-vinyl aryl compounds and treatment of liquid media therewith. US Patent 2,366,007.
- Dabrowski, A., Hubicki, Z., Podkoscielny, P., Robens, E., 2004. Selective removal of the heavy metal ions from waters and industrial wastewaters by ion-exchange method. *Chemosphere* 56, 91–106.

Dada, A.,O., Olalekan, A.,P., Olatunya, A.M., Dada, O., 2012. Langmuir, Freundlich, Temkin and Dubinin–Radushkevich Isotherms Studies of Equilibrium Sorption of Zn²⁺ Unto Phosphoric Acid Modified Rice Husk. *Journal of Applied Chemistry* 3, 38-45.

Dai, X.,Simons, A., Breuer, P., 2012. A review of copper cyanide recovery technologies for the cyanidation of copper containing gold ores. *Minerals Engineering* 25, 1-13.

Dean, J.A, 1992. Lange’s handbook of chemistry. Mcgraw Hill. Available at http://materias.qi.fcen.uba.ar/file.php/16/Tablas/Radios_atomicos_e_ionicos.pdf. [Accessed July 2013].

Dominguez, L., Benak, K. R., Economy, J., 2001. Design of high efficiency polymeric cation exchange fibers. *Polymer for Advanced Technologies* 12, 197-205

DuHamel, D., Graczyk, K., 1997. Ion exchange. Operating methods. Available at: <http://www.rpi.edu/dept/chem-eng/Biotech-Environ/IONEX/methods.html>. [Accessed: March 2013].

Economy, J., Dominguez, L., Mangun, C. L., 2002. Polymeric Ion-Exchange Fibres. *Industrial & Engineering Chemistry Research* 41, 6436-6442

Foo, K.,Y.,Hameed, B.,H., 2010. Insights into the modeling of adsorption isotherm systems. *Chemical Engineering Journal* 156, 2-10.

Frost, F., A., 1969. The development, kinetics and dynamics of a continuous ion exchanger. PhD Thesis, University of the Witwatersrand, Johannesburg.

Gaikwad, R., W., Sapkal, V., S., Sapkal, R., S., 2010. Ion exchange system design for removal of heavy metals from acid mine drainage wastewater. *Acta Montanistica Slovaca* 15 (4), 298-304.

Galan, B., Castaneda, D., Ortiz., I., 2005. Removal and recovery of Cr(IV) from polluted ground waters: A comparative study of ion-exchange technologies. *Water research* 39, 4317-4324.

- Gando-Ferreira, L., M., Romão, I., S., Quina, M., J., 2011. Equilibrium and kinetic studies on removal of Cu^{2+} and Cr^{3+} from aqueous solutions using a chelating resin. *Chemical Engineering Journal* 172, 277–286.
- Gold, H., Todisco, A., Sonin, A. A., Probst, R. F., 1975. The Avco continuous moving bed ion exchange process and large scale desalting. *Desalination* 17 (1), 111-120.
- Górka, A., Bochenek, R., Warchoń, J., Kaczmarski, K., Antos, D., 2008. Ion exchange kinetics in removal of small ions. Effect of salt concentration on inter-and-intraparticle diffusion. *Chemical Engineering Science* 63, 637 – 650.
- Goyal, M., Bhagat, M., 2010. Dynamic adsorption of Pb (II) ions from aqueous solution using activated carbon beds. *Indian Journal of Engineering and Materials Sciences* 17, 367-372.
- Gyabaah, M., 1998. Comparison of the performance of contacting equipment for the removal of ammonium ions from waste streams using ion exchange. Masters Dissertation, University of the Witwatersrand, Johannesburg
- Hamdaoui, O., 2009. Removal of copper (II) from aqueous phase by Purolite C100-MB cation exchange resin in fixed bed columns: Modelling. *Journal of Hazardous Materials* 161, 737–746.
- Harland, C., E., 1994. Ion exchange: Theory and Practice. 2nd edition, The Bath Press, Great Britain.
- Hekmatzadeh, A., A., Karimi-Jashani, A., Talebbeydokhti, N., 2012. Mass transfer modelling of nitrate in an ion exchange selective resin. *World academy of science, Engineering and technology* 61, 660-665.
- Helferich, F., G., 1995. Ion exchange. Dover Publications, New York.
- Huang, J., Zhang, X., Bai, L., Yuan, S., 2012. Polyphenylene sulphide based anion exchange fibre: Synthesis, characterization and adsorption of Cr(IV). *Journal of Environmental Sciences* 24(8), 1433-1438.

Inglezakis, V., J., 2010. Ion Exchange and Adsorption Fixed Bed Operations for Wastewater Treatment - Part II: Scale-Up And Approximate Design Methods. *Journal of Engineering Studies and Research* 16 (3), 42-50.

Inglezakis, V., J., Pouloupoulos, S., G., 2006. Adsorption, Ion Exchange and Catalysis: Design of Operations and Environmental Applications. Elsevier, the Netherlands.

Inglezakis, V., J., Zorpas, A., 2012. Fundamentals of Ion Exchange Fixed-Bed Operations. In: Inamuddin and Luqman (eds.) *Ion exchange technology I: theory and materials*. Netherlands: Springer, pp. 121-161.

Institute of Physical Organic Chemistry of NABS, 2009. Available from: http://ifoch.bas-net.by/en/research/fiban/X1_1.html. [Accessed: April 2014].

Jaskari, L., Vuorio, M., Kontturi, K., Jose´ A. Manzanares, J.A., Hirvonen, J., 2001. Ion-exchange fibers and drugs: an equilibrium study. *Journal of Controlled Release* 70, 219–229

Jha, M., K., Nguyen, V., Lee, J., Jeong, J. Yoo, J., 2009. Adsorption of copper from the sulphate solution of low copper contents using the cationic resin Amberlite IR 120. *Journal of Hazardous Materials* 164 (2–3), 948-953.

Ji, Z., Bei, Y., Liu, Q., 2011. Removal of Copper Ions from Aqueous Solution with a Weak Cation Exchanger by Radiation-Induction Grafting Acrylic Acid onto Polypropylene Fibre. *International Journal of Industrial Chemistry*, 2(1), 23-26.

Kalavathy, H., Karthik, B., Miranda, L., R., 2010. Removal and recovery of Ni and Zn from aqueous solution using activated carbon from *Hevea brasiliensis*: Batch and column studies. *Colloids and Surfaces B: Biointerfaces* 78, 291-302.

Kariduraganavar, M. Y., Kittur, A.A., Kulkarni, S.S., 2012. Ion Exchange Membranes: Preparation, Properties, and Applications. In: Inamuddin and Luqman (eds.) *Ion exchange technology I: theory and materials*. Netherlands: Springer, pp. 233-276.

Kariduraganavar, M.,Y., Nagarale, R.,K., Kittur, A.,A., Kulkarni, S.,S., 2006. Ion-exchange membranes: preparative methods for electro dialysis and fuel cell applications. *Desalination* 197, 225-246

Karlson, E., L., 1975. Twin belt ion exchange system. Patent: US 3910842 A

Kavak, D., Öztürk, N., 2004. Adsorption of boron from aqueous solution by sepirolite: II. Column studies. II. Uluslararası Bor Sempozyumu 23-25, 495-500.

Khan, A.,A., Akhtar, T., 2011. Synthesis, characterization and ion-exchange properties of a fibrous type ‘polymeric-inorganic’ composite cation-exchanger Nylon-6, 6 Sn (IV) phosphate: Its application in making Hg(II) selective membrane electrode. *Electrochimica Acta* 54, 3320–3329.

Ko, Y.,G., Choi, U.,S., 2007. Observation of metal ions adsorption on novel polymeric chelating fiber and activated carbon fibre. *Separation and Purification Technology* 57, 338–347.

Ko,Y.G., Chun, Y.J., Choi, U.S., 2011. Removal of Cu(II) and Cr(IV) ions from aqueous solution using chelating fibre packed column: Equilibrium and kinetic studies. *Journal of Hazardous Materials* 194, 92-99.

Kosandrovich, E. G., Soldatov, V. S., 2012. Fibrous Ion Exchangers. In: Inamuddin and Luqman (eds.) *Ion exchange technology I: theory and materials*. Netherlands: Springer, pp. 299-371.

Kose, T., E., Ozturk, N., 2008. Boron removal from aqueous solutions by ion-exchange resin: Column sorption–elution studies. *Journal of Hazardous Materials* 152, 744–749.

Kotze, M., 1992. The status of ion-exchange fibers for metallurgical applications. *The Journal of The Minerals, Metals & Materials Society* 44 (5), 46-50.

Ladeira, A., C., Q., C.A. Morais, C.,A., 2005. Uranium recovery from industrial effluent by ion exchange-column experiments. *Minerals Engineering* 18, 1337–1340.

Lee, I-H., Kuan, Y-C., Chern J-M., 2007. Equilibrium and kinetics of heavy metal ion exchange. *Journal of the Chinese Institute of Chemical Engineers* 38, 71–84.

Lito, P., F., Cardoso, S., P., Loureiro, J., M., Silva, C., M., 2012. Ion Exchange Equilibria and Kinetics. . In: Inamuddin and Luqman (eds.) *Ion exchange technology I: theory and materials*. Netherlands: Springer, pp. 51-120.

Lopes, C.B., Lito, P. F., Cardoso S.P., Pereira E., Duarte A.C., Silva, C.M., 2012. Metal Recovery, Separation and/or Pre-concentration. In: Inamuddin and Luqman (eds.) *Ion exchange technology II: applications*. Netherlands: Springer, pp. 237-322.

Monier M., Ayad, D., M., Sarhan, A., A., 2010. Adsorption of Cu(II), Hg(II), and Ni(II) ions by modified natural wool chelating fiber. *Journal of Hazardous Materials* 176 (1–3), 348-355. Doi: <http://dx.doi.org/10.1016/j.jhazmat.2009.11.034>.

Muendel, C., H., Selke, W., A., 1955. Continuous Ion exchange with an Endless belt of phosphorylated Cotton. *Engineering, Design, and Process development*, 47(3), 374-379.

Nair, M., P., S., 2006. Equipment: Tilting pan filters – the industrial work-horses of filtration, *Filtration & Separation*, 43, 10, 28-30.

Nasef, M.M., Ujang, Z., 2012. Introduction to Ion Exchange Processes. In: Inamuddin and Luqman (eds.) *Ion exchange technology II: applications*. Netherlands: Springer, pp. 1-39

Nesteronok, P., V., Soldatov, V., S., 2011. Acid–base properties of ion exchangers: V. Synthesis and properties of ion exchangers on the base of modacrylic polyacrylonitrile–vinylchloride fibers. *Reactive and Functional Polymers* 71, 1033–1039.

Ntimbani, R., N., Simate, G., S., Ndlovu, S., 2015. Removal of copper ions from dilute synthetic solution using staple ion exchange fibres: Equilibrium and kinetic studies. *Journal of Environmental Chemical Engineering* 3 (2), 1258-1266.

Nwabanne, J., T., Igbokwe, P., K., 2012. Kinetic modeling of heavy metals Adsorption on fixed bed column. *International Journal of Environmental Research* 6(4), 945-952.

Ofamaja, A.E., 2010. Equilibrium studies of copper ion adsorption onto palm kernel fibre. *Journal of Environmental Management* 91, 1491-1499.

Özacar M., Sengil, I.A., 2005. A kinetic study of metal complex dye sorption onto pine sawdust. *Process Biochemistry* 40, 565–572.

Palacios, V.M., Caro, I., Perez, L., 2001. Application of Ion Exchange Techniques to Industrial Process of Metal Ions Removal from Wine. *Adsorption* 7, 131–138

Park, J-S., 2012. Structure, Synthesis, and General Properties of Ion Exchangers. In: Inamuddin and Luqman (eds.) *Ion exchange technology II: applications*. Netherlands: Springer, pp. 211- 231.

Parodi, A., Vincent, T., Pilsniak, M., Trochimczuk, A. W., Guibal, E., 2008. Palladium and platinum binding on an imidazol containing resin. *Hydrometallurgy* 92, 1-10

Pengthamkeerati, P., Satapanajaru, T., 2013. Analysis and modeling of column operations on reactive dye removal onto alkaline-treated biomass fly ash. *Desalination and Water Treatment*, 1-8.

Perry, R., H., Green, D., H., Maloney, J., O., 1997. *Perry's Chemical Engineer's handbook*. McGraw-Hill, United States of America

Phelps, D., S., C., Ruthven, D., M., 2002. Mass transfer performance of an endless belt counter-current ion exchanger for liquid phase adsorption. *Separation and Purification Technology* 27, 243–256.

Purolite, 2012. Ion Exchange Resin Cartridges. Polysciences Inc. Available at: https://acs.expoplanner.com/files/acsfall12/ExhibFiles/1043_3141_PolyPuroliteCartridgeBroch_05012012.pdf. [Accessed: July 2013].

Rajeshkannan, R., Rajasimman, M., Rajamohan, N., 2013. Packed Bed Column Studies for the Removal Of Dyes Using Novel Sorbent. *Chemical Industry & Chemical Engineering Quarterly* 19 (4), 461 - 470

removal from cobalt electrolyte. The Southern African Institute of Mining and Metallurgy, Base Metals Conference. South Africa, 283-298.

Rengaraj, S., Yeon, J. W., Kimb, Y., Jung, Y., Haa, Y.K., Kima, W.H., 2007. Adsorption characteristics of Cu(II) onto ion exchange resins 252H and 1500H: Kinetics, isotherms and error analysis. *Journal of Hazardous Materials* 143, 469–477.

Rio Tinto, 2011. Copper fact sheet. Available from: http://www.riotinto.com/documents/corpPub_Copper.pdf. [Accessed: May 2013].

Rodelo, G., Gomez, A., Ruiz-Mandriquez, A., 2002. Biosorption of Pb(II) by *Thiobacillus ferrooxidans*. *Revista Internacional de Contaminacion Ambiental* 18 (1), 33-37.

Rodrigues, A., E., 1983. Dynamic of Ion exchange processes. In: Liberti and Helfferich (eds.) *Mass transfer and kinetics of ion exchange*. The Netherlands: Applied Sciences 71, 259-312.

Ruthven, D.M., Ching, C.B., 1989. Counter-current and simulated counter-current adsorption separation processes. *Chemical engineering science* 44 (5), 1018-1038

Saad, D., M., Cukrowska, E., Tutu, H., 2014. Column adsorption studies for the removal of U by phosphonated cross-linked polyethylenimine: modelling and optimization. *Applied Water Science*, [Accessed: March 2014].

Sata, T., 2004. Chapter 1: Introduction. *Ion Exchange Membranes: Preparation, Characterization, Modification and Application*. The Royal Society of Chemistry, United Kingdom

Sherry, H., 1993. The design of ion-exchange processes. *Zeolites* 13, 377-383.

Simate, G. S., Ndlovu, S., 2015. The removal of heavy metals in a packed bed column using immobilized cassava peel waste biomass. *Journal of Industrial and Engineering Chemistry* 21, 635-643.

Sinnott, R., Towler, G. 2008. Chemical Engineering Design Principles, Practice and Economics of Plant and Process Design. UK: Elsevier Butterworth-Heinemann

Slater, M., J., 1979. Continuous ion exchange plant design methods and problems. Hydrometallurgy 4, 299-316.

Soldatov, V., S., Zelenkovskii, V., M., Orlovskaya, L., A., 2011. Sorption of bivalent ions by a fibrous chelating ion exchanger and the structure of sorption complexes. Reactive & Functional Polymers 71, 49–61.

Soldatov, V., S., Polus, Z., Pawlowska, Z., Maczka, I., Alexander Shunkevich, A., Kasandrovich, E., Polikarpov, A., 2004. A Strong Acid Nonwoven Filtering Medium for Deep Air Purification. Fibres & Textiles 4 (48), 56-61.

Soldatov, V., S., Shunkevich, A., A., Elinson, I., S., Johann, J., Iraushekc, H., 1999. Chemically active textile materials as efficient means for water purification. Desalination 124 (1-3), 181-192

Sparks, T., 2012. Solid-liquid filtration: understanding filter presses and belt filters. Filtration+ Separation 49(4), 20-24.

Srivastava, V., C., Prasad, B., Mishra, I., M., Mall, I., D., Swamy, M., M., 2008. Prediction of Breakthrough Curves for Sorptive Removal of Phenol by Bagasse Fly Ash Packed Bed. Industrial and Engineering Chemistry Research 47, 1603-1613.

Sud, D., 2012. Ion Exchange Membranes: Preparation, Properties, and Applications. In: Inamuddin and Luqman (eds.) Ion exchange technology I: theory and materials. Netherlands: Springer, pp. 373-401.

Szlag, D.C., Wolf, N.J., 1996. Recent advances in ion exchange materials and processes for pollution prevention. Clean Products and Processes 1, 117–131.

Takeno, N., 2005. Atlas of Eh-pH diagrams: Intercomparison of thermodynamic databases. National Institute of Advanced Industrial Science and Technology. Geological Survey of Japan Open File Report No.419.

Tanaka, Y., 2007. Chapter 1: Preparation of Ion Exchange Membranes. Membrane Science and Technology, 12, 3-16.

Trgo, M., Medvidovic, V., N., Peric, J., 2011. Application of Mathematical models to dynamic removal of lead on natural zeolite clinoptilolite in a fixed bed column. Indian Journal of Chemical Technology 18, 123-131.

Van Deventer, J., 2011. Selected Ion Exchange Applications in the Hydrometallurgical Industry. Solvent Extraction and Ion Exchange 29, 695–718.

Wakeman, R., J., Wei, X., 1995. Simulating the performance of tilting pan filters, Filtration & Separation 32 (10), 979-984.

Yahaya, N., K., E., M., Abustan, I., Latiff, M., F., P., M., Bello, O., S., Ahmad, M., A., 2011. Fixed-bed Column Study for Cu²⁺ ions Removal from Aqueous Solutions using Rice Husk based Activated Carbon. International Journal of Engineering & Technology IJET-IJENS 11(1), 186-190.

Yahorava, V., Kotze, M., Auerswald, D., 2013. Evaluation of different adsorbents for copper

Yahorava, V., Thulare, T., Kotze, M., du Prees, R., 2010. Development of ion exchange fibre processes for hydrometallurgy. Mintek Internal Report: Hydrometallurgy Division.

Yoshioka, T., Shimamura, M, 1983. Studies of polystyrene-based Ion exchange fibre. I. The preparation and fundamental characteristics of polystyrene based ion exchange fibre. Bulletin of the Chemical Society of Japan 56(12), 3726- 3729.

Zagorodni, A. A., 2007. Chapter 12 - Ion Exchange Purification and Separation, Ion Exchange Materials, Elsevier, Oxford, 263-281.

Zagorodni, A. A., 2007. Chapter 14 - Technological Schemes of Ion Exchange, Ion Exchange Materials, Elsevier, Oxford, 297-314.

Zhang, S., Chen, S., Zhang, Q., Li, P., Yuan, C., 2008. Preparation and characterization of an ion exchanger based on semi-carbonized polyacrylonitrile fibre. *Reactive & Functional Polymers* 68, 891–898.

Appendix A

Solution preparation

The synthetic solution containing equimolar ions of Cu, Co, Ni, Zn, Mn and Mg at 2mM was prepared from sulphate salts of the metals stated above. Table A.1 below shows the mass of each sulphate salt used to prepare 2 L of the multi-component solution.

Table A. 1: Mass of sulphate salts used to prepare the multicomponent solution.

Element	Mass of element required (g)	Mass % of element in the salt	Mass of salt required (g)	Assay of salt (g)	Actual salt mass required (g)	Amount of metal in ppm
Ni	0.235	0.223	1.051	0.990	1.062	117
Co	0.236	0.210	1.124	0.975	1.153	118
Zn	0.262	0.227	1.150	1.015	1.133	131
Mg	0.097	0.202	0.481	0.660	0.730	49
Mn	0.220	0.325	0.676	0.990	0.683	110
Cu	0.254	0.254	0.999	0.998	1.001	127

Caustic soda (NaOH) was used as a pH adjusting agent and was added when the pH needed to be increased. A solution of NaOH at 1 M was prepared from NaOH pellets of assay 98%. Table A.2 shows the mass of pellets required to prepare 1 L of 1 M NaOH.

Table A. 2: Mass of NaOH pellets required to prepare 1L of 1 M NaOH.

	Concentration desired (M)	desired Volume (L)	MW	mass required (g)	Assay	Salt mass required (g)
NaOH	1.00	1.00	40.00	40.00	0.98	40.80

Sulphuric acid (H₂SO₄) was also used as a pH adjusting agent. It was added when the pH needed to be increased and it was prepared from the 98% H₂SO₄ solution. Table A.3 contains summary of calculations for preparing 1 L of 1 M H₂SO₄.

Table A. 3: Volume of 98% sulphuric acid required to prepare 2 M sulphuric acid.

amount desired (M)	volume desired (L)	% of acid in solution	volume of mixture	density of mixture (g/mL)	concentration of mix (M)	volume required (mL)
1.00	1.00	98.00	2.50	1.84	18.38	54.40

Hydrochloric acid (HCl) was prepared to be used for elution purposes. A solution of 2 M HCl was prepared from 37% HCl solution. Table A.4 below summarises the calculations for preparations and lists the volume require to prepare 2 L 2 M HCl.

Table A. 4: Volume of 37% HCl solution required to prepare 2 L of 2 M HCl.

concentration desired (M)	% of acid in solution	volume of mixture	density of mixture (g/mL)	Concentrationn of mixture (M)	volume required (mL)
2.00	37.00	20.00	1.19	12.06	331.60

IEFs preparations

Ion exchange fibres (IEFs) were converted to H⁺ form by contacting with 1 M sulphuric acid. Acid that was 10 times the volume of IEFs was contacted with IEFs in a sealed bottle and was mixed by rolling on rollers for 2 hours. After 2 hours of contact, IEFs were separated from acid by vacuum filtration. The IEFs were then washed with de-ionized water to remove entrained acid. Thereafter, the IEFs were left to dry in air for 24 hours. Table A.5 below shows the mass of IEFs and volume of acid contacted to convert the IEFs to H⁺.

Table A. 5: Mass of IEFs and acid volume contacted for conversion.

Mass of IEFs (g)	Volume of IEFs (L)	Volume of acid (L)
17	0.2	2

Analysis

Analysis of samples for Cu^{2+} ions and other metal ions was done using AAS (Varian, SpectrAA 220 Fast Sequential). The AAS measures the amount of light absorbed by the atoms in the excited state and in this way the concentration of samples referred to as analyte was determined. A certain amount of light absorbed by atoms corresponds to a specific concentration of elements. The mass extracted based on adsorption was calculated using the concentration of barren solutions and the wash water used to wash the loaded IEFs.

Standard solutions containing Zn^{2+} , Cu^{2+} , Co^{2+} , Ni^{2+} , Mg^{2+} and Mn^{2+} ions at 1.6, 8, 12, 12, 20 and 60 mg/L were used to calibrate the AAS. Samples collected from the experiments were diluted 5, 10 and 20 times with 4% HNO_3 . The diluted samples were aspirated to the atomizer using the embedded pump in the AAS machine. When the samples were atomized, the lamps for Cu^{2+} , Co^{2+} , Ni^{2+} , Zn^{2+} , Mn^{2+} and Mg^{2+} passed light through the atomized sample from which the concentration of each metal was determined depending on the amount of light absorbed. The volumes and concentrations of feed, barren solution and wash water were substituted into Equation (A. 1) to determine percentage loading or extraction based on adsorption.

$$\begin{aligned} \text{mass \% extraction} &= \frac{m_{\text{feed}} - m_{\text{barren}} - m_{\text{wash}}}{m_{\text{feed}}} (100\%) \\ &= \frac{V_{\text{feed}}C_{\text{feed}} - V_{\text{barren}}C_{\text{barren}} - V_{\text{wash}}C_{\text{wash}}}{V_{\text{feed}}C_{\text{feed}}} (100\%) \quad (\text{A.2}) \end{aligned}$$

Where m_{feed} is the mass of Cu^{2+} ions in feed solution; m_{barren} is the mass of Cu^{2+} ions in treated feed solution; m_{wash} is the mass of Cu^{2+} ions in wash water from washing the loaded IEFs. V_{feed} and C_{feed} are the feed volume and feed concentration of ions; V_{barren} and C_{barren} are the barren volume and barren concentration of ions; and V_{wash} and C_{wash} are the wash volume and concentration of ions in the wash water.

The atomic absorption spectroscopy machine that was used for analysis is shown in Figure A.1.



Figure A. 1: Image of the atomic absorption spectroscopy used for sample analysis.

Appendix B

Multicomponent batch tests

Table B. 1: Data for multicomponent batch test.

pH	fibre mass, (g)	filtrate Voume, (mL)	Final pH	NaOH Volume (mL)	H ₂ SO ₄ Volume mL	Desired acid (mL)	Concentrated Eluent (mL)
1.5	2	100	1.5	-	4.60	200	180
2.0	2	100	2.0	-	2.20	200	181
2.5	2	100	2.5	-	0.50	200	185
3.0	2	100	3.0	-	-	200	183
3.5	2	100	3.5	2.10	-	200	192
4.0	2	100	4.1	6.70	-	200	194
4.5	2	100	4.5	8.00	-	200	192
5.0	2	100	5.1	8.30	-	200	188

Table B. 2: Concentration of metals in barren solutions (mg/L).

Final pH	Cu	Co	Ni	Zn	Mn	Mg
Feed	128.96	154.40	153.20	130.76	129.52	56.32
1.5	73.69	148.20	149.60	108.04	129.56	53.68
2.0	30.47	138.20	152.60	97.54	124.78	50.92
2.5	25.64	128.80	140.80	78.41	118.58	48.84
3.0	10.67	131.60	146.40	78.66	110.66	53.60
3.5	4.96	143.40	130.40	56.87	97.68	50.74
4.1	3.61	117.20	125.60	44.91	85.00	51.44
4.5	1.86	82.60	101.80	23.65	53.46	48.36
5.1	0.85	37.60	61.00	19.28	14.10	38.36

Table B. 3: Metal concentrations in eluents corresponding to barrens at various pHs (mg/L).

pH	Cu	Co	Ni	Zn	Mn	Mg
1.5	26.40	0.51	0.82	2.61	0.87	2.92
2.0	42.12	1.85	2.07	5.20	2.39	3.42
2.5	45.50	3.16	3.15	7.34	4.85	3.40
3.0	51.50	6.29	5.86	8.53	9.37	3.50
3.5	56.20	14.50	13.18	10.20	18.84	3.80
4.1	58.80	20.50	18.2	9.69	23.1	5.13
4.5	56.00	27.90	27.10	12.29	35.1	6.69
5.1	53.40	43.20	42.90	15.18	49.62	12.05

Table B. 4: Extraction % based on adsorption.

pH	Cu	Co	Ni	Zn	Mn	Mg
1.5	42.86	4.02	2.35	17.38	-0.03	4.69
2.0	76.37	10.49	0.39	25.41	3.66	9.59
2.5	80.12	16.58	8.09	40.04	8.45	13.28
3.0	91.72	14.77	4.44	39.84	14.56	4.83
3.5	96.15	7.12	14.88	56.51	24.58	9.91
4.1	97.20	24.09	18.02	65.65	34.37	8.66
4.5	98.56	46.50	33.55	81.91	58.72	14.13
5.11	99.34	75.65	60.18	85.26	89.11	31.89

Table B. 5: Mass accountability in mass %.

pH	Cu	Co	Ni	Zn	Mn	Mg
1.5	93.99	96.57	98.61	86.22	101.24	104.63
2.0	82.74	91.67	102.05	81.79	99.68	101.39
2.5	84.98	87.20	95.70	70.31	98.46	97.86
3.0	81.36	92.69	102.56	72.10	98.67	106.53
3.5	87.52	110.91	101.64	58.47	103.35	103.05
4.1	91.26	101.66	105.03	48.72	100.23	109.01
4.5	84.81	88.19	100.41	36.14	93.31	108.67
5.1	78.51	76.95	92.46	36.57	82.91	108.33

Maximum loading tests

Table B. 6: Solution volumes and Cu concentration for Maximum loading test.

	Solution volume (mL)	Cu concentration (mg/L)	mass (mg)
Feed	1800	122.1	219.78
Barren	1782	111.6	198.8712
Barren wash	222	9.72	2.15784
Eluent	95	308	29.26
Eluent wash	100	17.4	1.74

Table B. 7: Maximum loading test results.

Mass of IEFs used (g)	0.5
maximum loading mg/g elution based	62.0
max loading mg/g adsorption based	37.5
Averaged loading mg/g	49.8
Accountability %	105.6
soln vol/fibre (g/g)	3600

Equilibrium tests

Table B. 8: Data for equilibrium tests.

solution volume (mL)	Cu feed conc (mg/L)	Cu mass in soln (mg)	mass of fibre (g)	solution to fibre ratio	filtrate (mL)	Filtrate wash (mL)	Eluent (mL)	Eluent wash (mL)
200	127	25	1.0	200	168	107	97	102
300	127	38	0.5	600	240	110	94	100
400	127	51	0.5	800	335	100	94	104
600	127	76	0.5	1200	530	99	93	102
1000	127	127	0.5	2000	930	222	95	105
1800	127	220	0.5	3600	1782	99	95	103
2000	127	254	0.5	4000	1940	98	97	104

Table B. 9: Concentration of Cu in solutions for equilibrium tests (mg/L)

ratio solution/fibre	Barren	Barren wash	Eluent	Eluent wash
200	0.36	0.20	220.80	23.20
600	37.90	4.54	250.20	13.65
800	58.20	3.46	274.50	13.80
1200	81.00	5.43	289.50	15.30
2000	95.60	7.73	294.50	15.75
3600	111.20	9.72	308.00	17.40
4000	113.40	7.29	306.00	14.25

Table B. 10: Mass Cu in various solutions and accountability for batch tests (mg).

ratio solution/fibre	Barren	Barren wash	Eluent	Eluent wash	mg Cu/g IEF	Mass % Accountability
200	0.060	0.021	21.42	2.37	23.8	97
600	9.096	0.499	23.52	1.37	49.8	90
800	19.497	0.346	25.80	1.44	54.5	93
1200	42.930	0.538	26.92	1.56	57.0	94
2000	88.908	1.716	27.98	1.65	59.3	95
3600	198.158	0.962	29.26	1.79	62.1	105
4000	219.996	0.714	29.68	1.48	62.3	99

Freundlich model fit

Equation B.1 below is the linearized Freundlich model.

$$\log q_e = \log K_F + 1/n \log C_e \quad \text{B.1}$$

1

The values of K_F and n are determined from the intercept and slope of the plot $\log q_e$ and $\log C_e$ respectively. The plot $\log q_e$ and $\log C_e$ is shown in Figure B.1 below.

$$K_F = 10^{-8.7426} = 1.81 \times 10^{-9}$$

$$n = 6.0448$$

$$R = 8.314$$

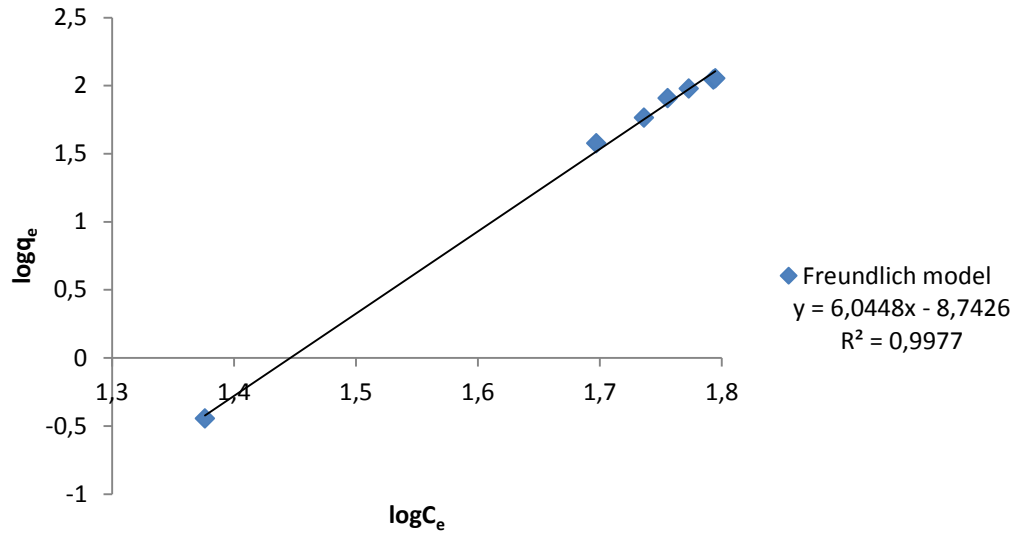


Figure B. 1: Linearized Freundlich isotherm model fit into experimental data.

Langmuir model

Equation B.2 below is the linearized Langmuir model.

$$1/q_e = 1/Q_0 + 1/(bQ_0C_e) \quad \mathbf{B. 2}$$

The values of Q_0 and b can be calculated from the slopes and intercepts of the Langmuir plots respectively. The linear plots of $1/q_e$ versus $1/C_e$ is shown in Figure B.2.

$$Q_0 = 1/0.174 = 57.47$$

$$b = 1/(0.0089 \times 57.47) = 1.955$$

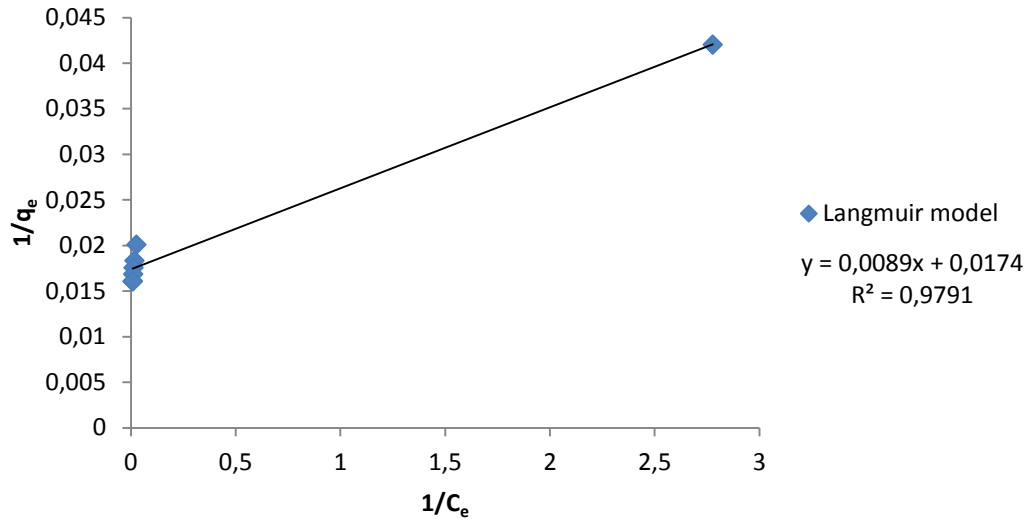


Figure B. 2: Linearized Langmuir isotherm model fit into experimental data.

Temkin

Equation B.3 is the Temkin model.

$$q_e = \frac{RT}{b \ln A} + \frac{RT}{b \ln C_e} \quad \text{B. 3}$$

The constants A and b are determined from linear plots of q_e versus $\log C_e$ shown in Figure B.3 below.

$$T = 298K$$

$$R = 8.314$$

$$b = (8.314 \times 298) / 6.4502 = 384.11$$

$$A = e^{(384.11 \times 29.565) / (8.314 \times 298)} = 97.86$$

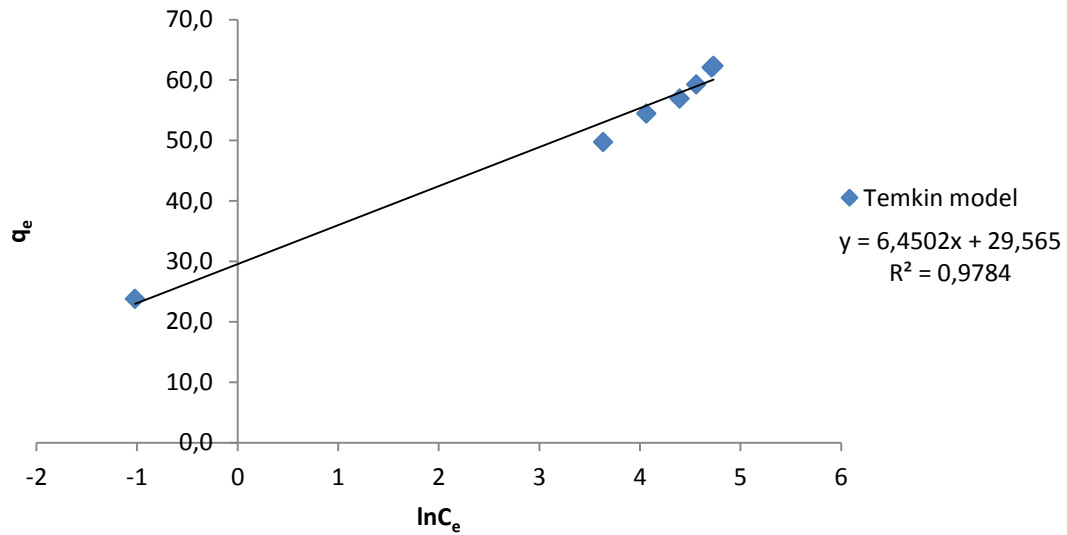


Figure B. 3: Linearized Temkin isotherm model fit into experimental data.

Dubinin & Radushkevich

Dubinin & Radushkevich model is shown in linearized form as equation B.4.

$$\ln q_e = \ln q_s - B \varepsilon^2 \quad \mathbf{B. 4}$$

The constants B and q_s were determined from the y-intercept and slope of the plot of lnq_e versus ε² (Figure B.4).

$$B = -8 \times 10^{-8}$$

$$q_s = e^{4.0486} = 57.32$$

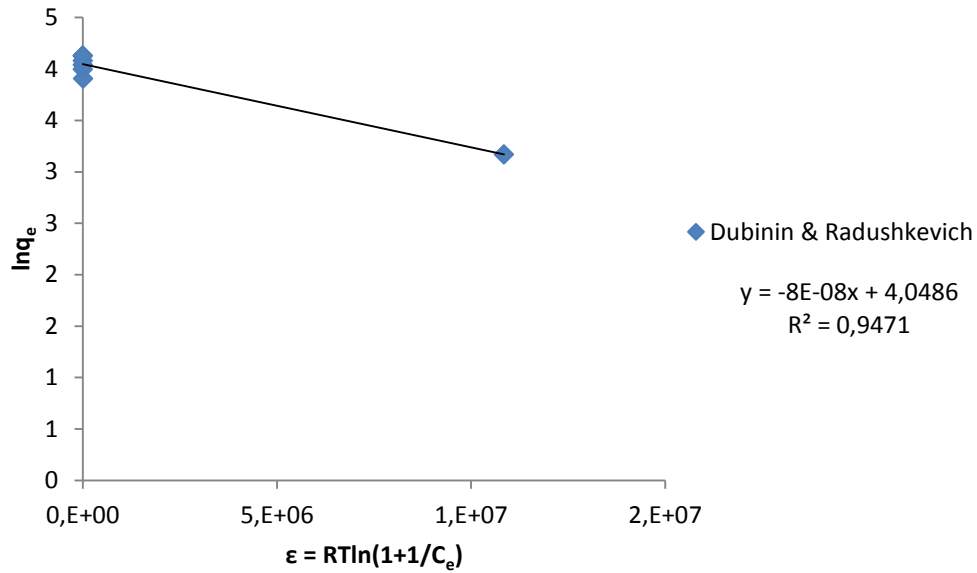


Figure B. 4: Linearized Dubinin and Radushkevich isotherm model fit into experimental data.

Redlich and Peterson

The Redlich-Peterson model is shown below as equation B.5.

$$C_e/q_e = 1/(KR) + aR/(KR)C_e^\beta \quad \text{B. 5}$$

$$\beta = 0.5$$

$$K_R = 3.54 \times 10^{10}$$

$$a_R = 5.46 \times 10^9$$

Plotting the C_e/q_e of Equation 2-3 against C_e^β to obtain the isotherm constants is impossible due to the three unknowns, aR , KR and β . A minimization procedure is therefore adopted to solve the above equation by maximizing the correlation coefficient between the theoretical data for q_e predicted from the above equation and the experimental data (Rengaraj et al., 2007).

Equation B.6 below was used to determine the values for KR and aR by minimising the error between the experimental equilibrium loading and that calculated using equation B.6.

$(q_e, \text{calculated} - q_e, \text{measured})$

B. 6

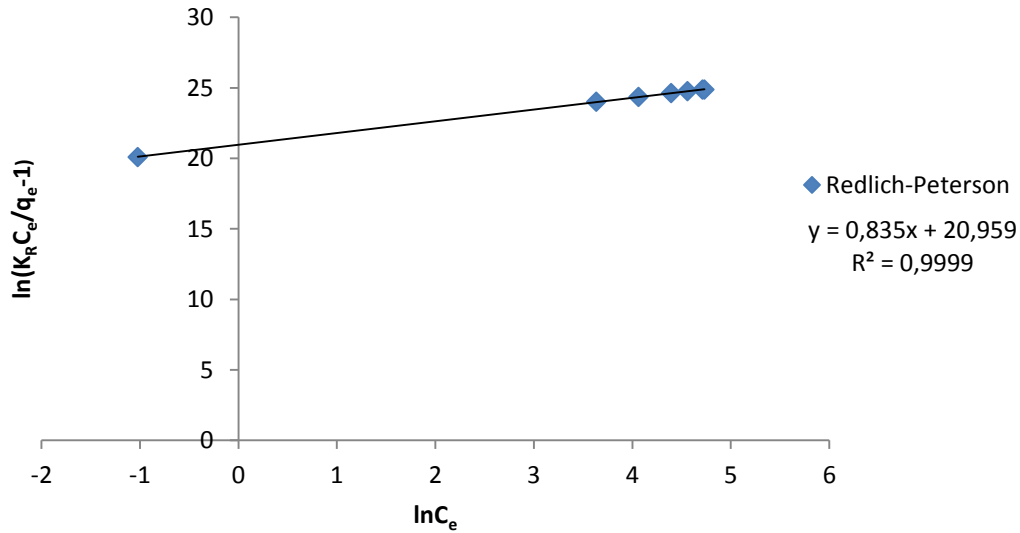


Figure B. 5: Linearised Redlich-Peterson isotherm fit into experimental data.

Table B. 11: Experimental and predicted equilibrium loading by equilibrium models.

Experimental	Redlich-Peterson	Freundlich	Langmuir	Dubinin & Radushkevich	Temkin
23.78	3.89	0.00	23.74	136.47	22.98
49.77	39.93	6.31	56.71	57.34	53.01
54.48	49.48	84.33	56.97	57.33	55.78
56.97	58.37	622.03	57.11	57.32	57.91
59.26	63.41	1693.84	57.17	57.32	58.98
62.10	68.39	4223.71	57.21	57.32	59.95
62.33	69.06	4754.72	57.21	57.32	60.08

Elution tests

Table B. 12: Data for elution tests.

feed (mL)	Barren volume (mL)	Barren wash volume (mL)	Eluent volume (mL)	Eluent Wash volume (mL)
200	165	102	93	100
200	167	106	95	105
200	168	100	95	102
200	170	102	94	103
200	168	107	97	102

Table B. 13: Cu analysis concentration (mg/L) results for various solutions during strip tests.

Barren	Barren wash	Eluent	Eluent wash
0.32	0	145.8	32.8
0.29	0.04	151.6	27.7
0.2	0.04	193.8	23.4
0.11	0.03	192.3	26.8
0.36	0.2	220.8	23.2

Table B. 14: Elution % with different HCL concentration.

HCl (M)	mass loaded (mg/g)	mass eluted (mg)	% mass eluted
0.1	19.5	6.2	31.7
0.5	19.3	6.5	33.8
1.0	19.1	7.9	41.4
1.5	19.0	7.9	41.5
2.0	18.6	9.3	50.1

Kinetics tests

A mass of 2 g IEFs was used for kinetics tests. The IEFs were contacted with synthetic Cu solution (800mL) at 127 mg/L in batch system. Samples were taken for Cu analysis at various time intervals.

Table B. 15: Data and Cu analysis for kinetics tests.

	vol (mL)	Cu conc (mg/L)	mass (mg)
0.08	5	52.2	0.26
0.17	5	51.8	0.26
0.25	5	43	0.22
0.33	5	33.4	0.17
0.50	5	31	0.16
0.67	5	25.5	0.13
0.83	5	24.4	0.12
1.00	5	25.2	0.13
2.00	5	17.1	0.09
3.00	5	18	0.09
4.00	5	14	0.07
8.00	5	12	0.06
10.00	5	1.09	0.01
24.00	700	0.35	0.25
Barren wash	315	0	0.00
Eluent	190	435	82.65
Eluent wash	95	9.81	0.93

Equation B.7 was used to calculate loading percentage. The results obtained are contained in Table B.14.

$$loading\% = \frac{C_{feed} - C_t}{C_{feed} - C_e} \times 100 \quad \mathbf{B. 7}$$

Table B. 16: Loading percentage at various time intervals.

Time (hrs)	Concentration (mg/L)	loading %
0	127	0
0.08	52.2	59
0.17	51.8	59
0.25	43	66
0.33	33.4	74
0.50	31	76
0.67	25.5	80
0.83	24.4	81
1.00	25.2	80
2.00	17.1	87
3.00	18	86
4.00	14	89
8.00	9	93
10.00	1.09	99
24.00	0.19	100

Pseudo-first-order

The linearized pseudo-first-order model is shown as equation B.8.

$$\log(q_e - q_t) = \log(q_e) - k_1 t / 2.303 \quad \text{B. 8}$$

The values of k_1 and q_e were obtained from slope and y-intercept of the plot of $\log(q_e - q_t)$ versus time shown in Figure B.6.

$$k_1 = 2.303 \times 0.0722 = 0.167$$

$$q_e = 10^{2.95} = 896.40$$

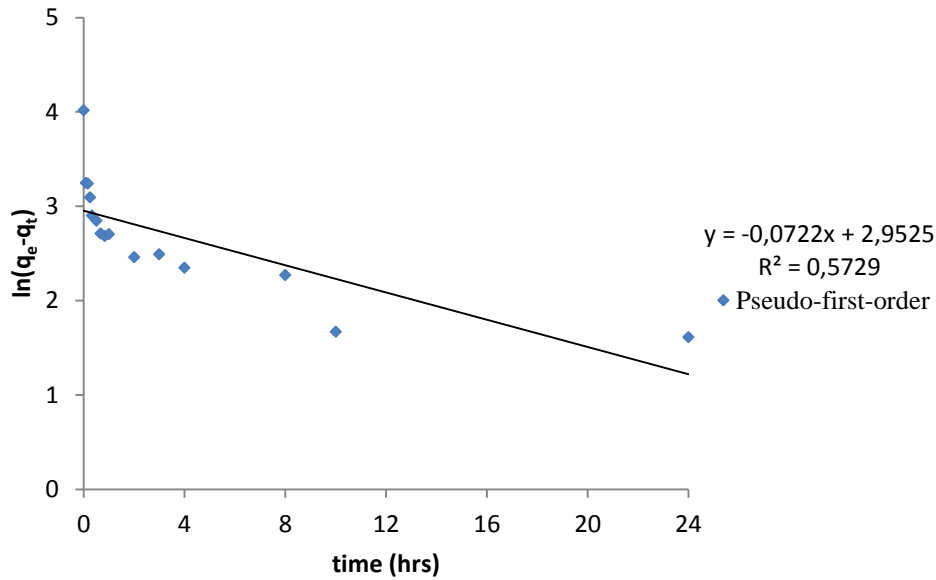


Figure B. 6: Pseudo-first-order model fit on the kinetics experimental results.

Pseudo-second-order

The linearized pseudo-second-order model is shown as equation B.9.

$$t/q_t = 1/(k_2 q_e^2) + t/q_e \quad \text{B. 9}$$

The values of k_2 and q_e were obtained from slope and y-intercept of the plot of t/q_t versus time shown in Figure B.7.

$$q_e = 1/0.02 = 50.8$$

$$k_2 = 1/(0.049 \times 50.8^2) = 0.0792$$

$$rate = k_2 q_e^2 \quad \text{B. 10}$$

$$rate = 0.0792 \times 50.8^2 = 204$$

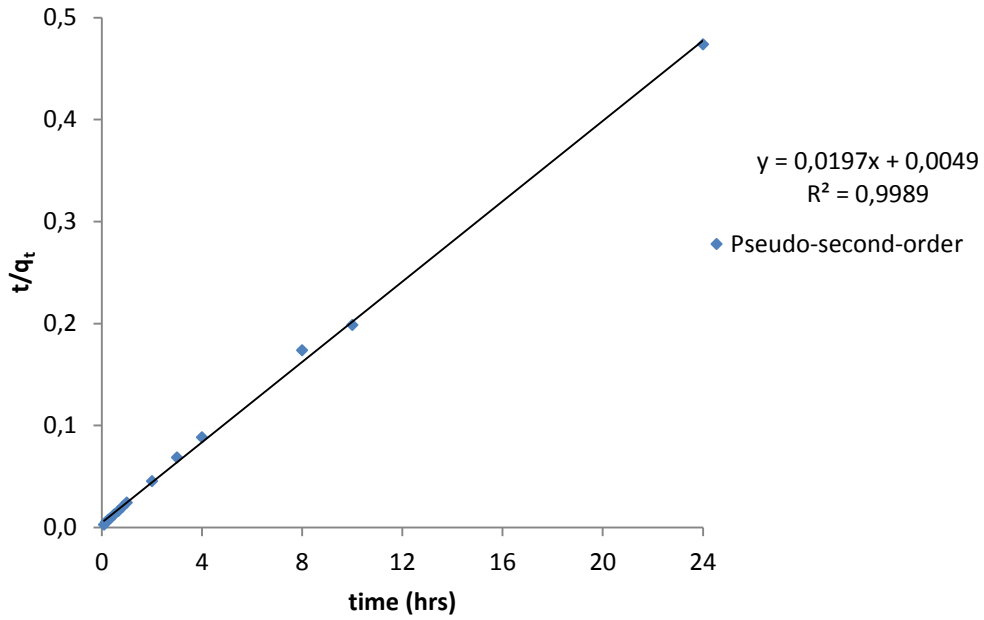


Figure B. 7: Pseudo-second-order model fit on the kinetics experimental results.

Elovich model

Elovich model is represented as equation B.11 below.

$$q_t = 1/\beta \ln(\alpha\beta) + 1/\beta \ln t \quad \mathbf{B. 11}$$

The values of α and β were obtained from y-intercept and slope of the plot of q_t versus $\ln t$ shown in Figure B.8.

$$\beta = 1/3.807 = 0.263$$

$$\alpha = 1/0.263e^{0.263 \times 40.094} = 1.43 \times 10^5$$

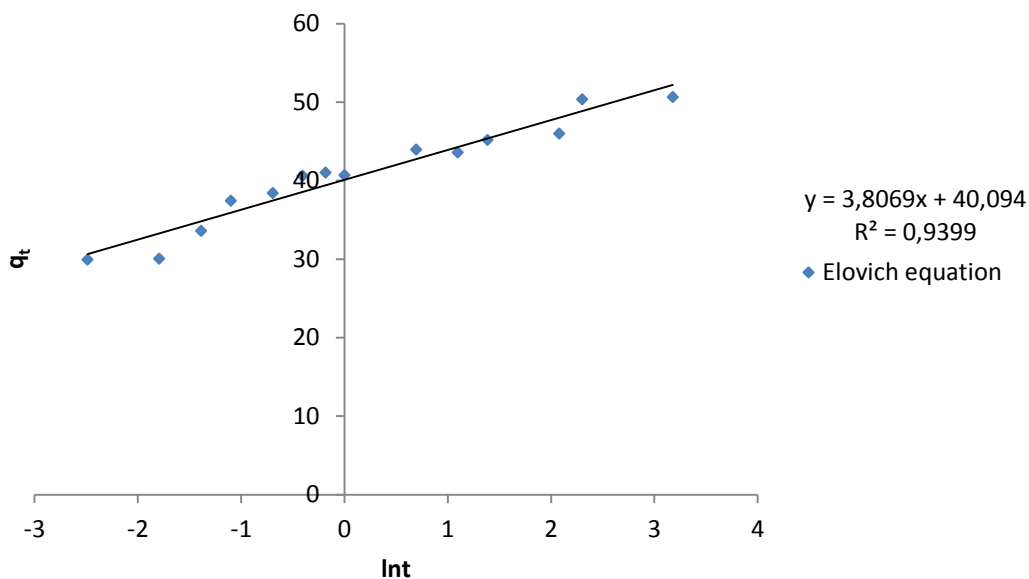


Figure B. 8: Elovich model fit on the kinetics experimental results.

The data that was used to plot the linearized pseudo-first-order, pseudo-second-order and the Elovich models is provided in Table B.15.

Table B. 17: Calculated data used for plots.

t	qt	ln(qe-qt)	t/qt	ln t	t ^{0.5}
0.0	0	4.020	0.005	Ln(0)	0.00
0.1	29.92	3.249	0.003	-2.48491	0.29
0.2	30.08	3.243	0.006	-1.79176	0.41
0.3	33.6	3.095	0.007	-1.38629	0.50
0.3	37.44	2.904	0.009	-1.09861	0.58
0.5	38.4	2.850	0.013	-0.69315	0.71
0.7	40.6	2.714	0.016	-0.40547	0.82
0.8	41.04	2.684	0.020	-0.18232	0.91
1.0	40.72	2.706	0.025	0	1.00
2.0	43.96	2.462	0.045	0.693147	1.41
3.0	43.6	2.492	0.069	1.098612	1.73
4.0	45.2	2.350	0.088	1.386294	2.00
8.0	46	2.271	0.174	2.079442	2.83
10.0	50.364	1.673	0.199	2.302585	3.16
24.0	50.66	1.615	0.474	3.178054	4.90

The loading % predicted by the kinetic models namely the pseudo-first-order, pseudo-second-order and the Elovich models are provided below in Table B.16 together with the loading % obtained experimentally.

Table B. 18: Comparison of experimental loading % with the predicted loading % from kinetic models.

experimental	Pseudo-first-order	Pseudo-second-order	Elovich
0	0	0	0
59	1	25	59
59	3	40	64
66	4	50	67
74	5	57	69
76	8	67	72
80	10	73	74
81	13	77	75
80	15	80	77
87	28	89	82
86	39	92	85
89	49	94	87
93	74	97	92
99	81	98	94
100	98	99	100

Appendix C

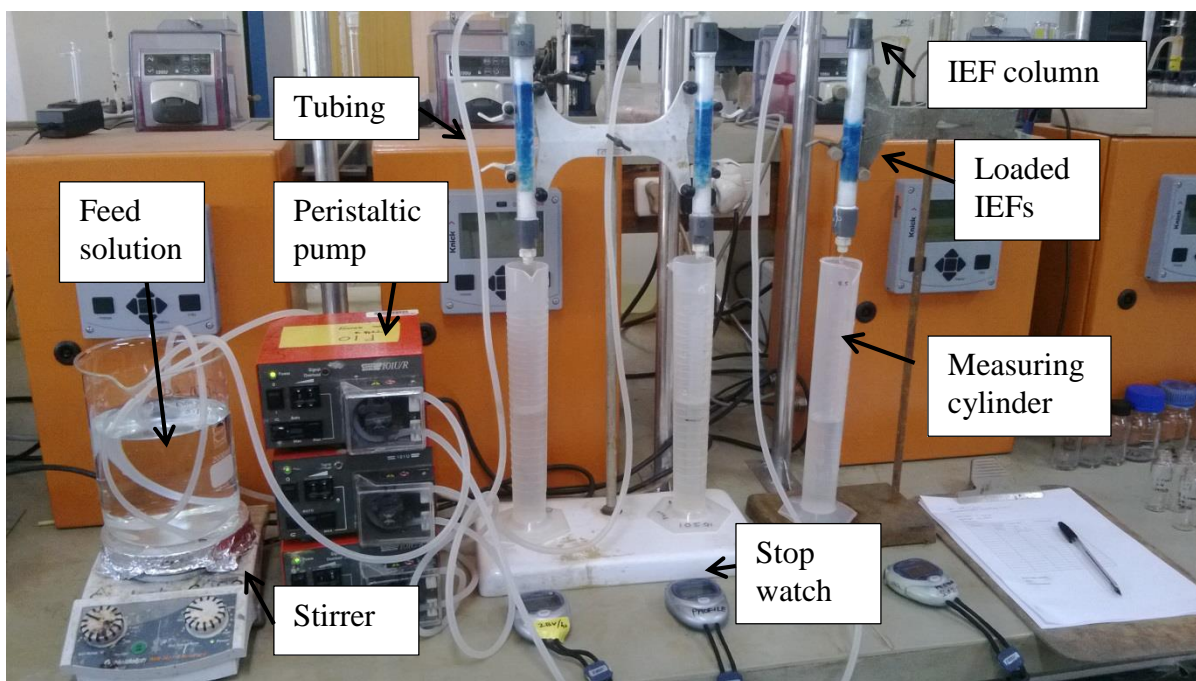


Figure C. 1: Experimental set up.

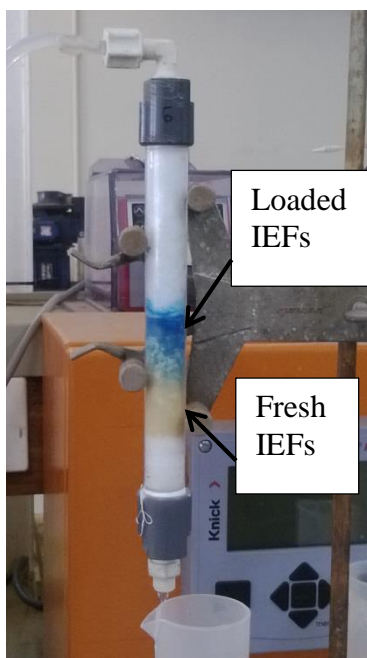


Figure C. 2: Column with fibres loaded with Cu as indicated the blue colour.

Table C. 1: Loading Run 1 data for bed packing density and flow rate of 0.16 g/cm³ and 8 mL/min.

Volume collected (mL)	Cum Vol collected (mL)	time (min)	cum time (min)	Cu conc (mg/L)
252	252	31.00	31.00	0.00
250	502	32.33	63.33	0.00
250	752	31.87	95.20	0.00
250	1002	31.80	127.00	7.52
250	1252	32.68	159.68	24.9
250	1502	33.08	192.77	52.1
250	1752	30.22	222.98	77.6
250	2002	31.92	254.90	92.6

Table C. 2: Loading Run 2 data for bed packing density and flow rate of 0.16 g/cm³ and 8 mL/min.

Volume collected (mL)	Cum Vol collected (mL)	time(min)	cum time (min)	Cu conc (mg/L)
250	250	31.67	31.67	0.00
250	500	31.90	63.57	0.00
250	750	32.57	96.13	0.00
250	1000	32.38	128.52	4.73
250	1250	33.03	161.55	22.60
250	1500	32.85	194.40	47.00
250	1750	32.00	226.40	73.80
250	2000	31.23	257.63	98.00

Table C. 3: Loading Run 3 data for bed packing density and flow rate of 0.16 g/cm³ and 8 mL/min.

Volume collected (mL)	Cum Vol collected (mL)	time(min)	cum time (min)	Cu conc (mg/L)
250	250	30.58	30.58	0.00
250	500	31.63	62.22	0.00
250	750	31.47	93.68	0.05
250	1000	32.22	125.90	7.43
250	1250	31.38	157.28	24.40
250	1500	32.65	189.93	55.40
250	1750	31.65	221.58	76.40
250	2000	30.55	252.13	95.40

Table C. 4: Averaged raw data for bed packing density and flow rate of 0.16 g/cm³ and 8 mL/min.

Volume (mL)	time (min)	Cu conc (mg/L)
250.67	31.08	0.00
500.67	63.04	0.00
750.67	95.01	0.02
1000.67	127.14	6.56
1250.67	159.51	23.97
1500.67	192.37	51.50
1750.67	223.66	75.93
2000.67	254.89	95.33

Table C. 5: Loading Run 1 data for bed packing density and flow rate of 0.20 g/cm³ and 8 mL/min.

Volume collected (mL)	Cum Vol collected (mL)	time(min)	cum time (min)	Cu conc (mg/L)
250	250	29.25	29.25	0.00
250	500	31.78	61.03	0.00
250	750	31.32	92.35	0.05
250	1000	31.80	124.15	8.20
250	1250	31.32	155.47	27.90
250	1500	31.75	187.22	58.40
250	1750	30.92	218.13	80.20
250	2000	31.00	249.13	97.20

Table C. 6: Loading Run 2 data for bed packing density and flow rate of 0.20 g/cm³ and 8 mL/min.

Volume collected (mL)	Cum Vol collected (mL)	time(min)	cum time (min)	Cu conc (mg/L)
250	250	32.02	32.02	0.00
250	500	31.67	63.68	0.00
250	750	32.13	95.82	0.90
250	1000	31.75	127.57	7.80
250	1250	32.23	159.80	25.60
250	1500	31.88	191.68	54.80
250	1750	31.67	223.35	77.40
250	2000	30.98	254.33	96.80

Table C. 7: Loading Run 3 data for bed packing density and flow rate of 0.20 g/cm³ and 8 mL/min.

Volume collected (mL)	Cum Vol collected (mL)	time(min)	cum time (min)	Cu conc (mg/L)
250	250	31.72	31.72	0.00
250	500	32.13	63.85	0.00
250	750	32.70	96.55	0.50
252	1002	31.90	128.45	9.10
250	1252	31.38	159.83	27.20
250	1502	31.60	191.43	57.00
250	1752	30.72	222.15	77.20
250	2002	32.08	254.23	95.80

Table C. 8: Averaged raw data for bed packing density and flow rate of 0.20 g/cm³ and 8 mL/min.

Volume (mL)	time (min)	Cu conc (mg/L)
250.00	30.99	0.00
500.00	62.86	0.00
750.00	94.91	0.48
1000.67	126.72	8.37
1250.67	158.37	26.90
1500.67	190.11	56.73
1750.67	221.21	78.27
2000.67	252.57	96.60

Table C. 9: Loading Run 1 data for bed packing density and flow rate of 0.28 g/cm³ and 8 mL/min.

Volume collected (mL)	Cum Vol collected (mL)	time(min)	cum time (min)	Cu conc (mg/L)
250	250	32.00	32.00	0.00
250	500	32.00	64.00	0.00
250	750	31.73	95.73	8.05
250	1000	31.15	126.88	25.00
250	1250	32.15	159.03	54.60
250	1500	31.10	190.13	79.20
250	1750	32.67	222.80	97.40
250	2000	30.72	253.52	113.40

Table C. 10: Loading Run 2 data for bed packing density and flow rate of 0.28 g/cm³ and 8 mL/min.

Volume collected (mL)	Cum Vol collected (mL)	time(min)	cum time (min)	Cu conc (mg/L)
250	250	32.27	32.27	0.00
250	500	31.87	64.13	0.00
250	750	32.35	96.48	4.74
250	1000	32.13	128.62	23.90
250	1250	32.53	161.15	55.90
250	1500	32.00	193.15	79.70
250	1750	31.00	224.15	96.60
250	2000	31.33	255.48	114.80

Table C. 11: Loading Run 3 data for bed packing density and flow rate of 0.28 g/cm³ and 8 mL/min.

Volume collected (mL)	Cum Vol collected (mL)	time(min)	cum time (min)	Cu conc (mg/L)
250	250	31.77	31.77	0.00
250	500	31.67	63.43	0.00
250	750	32.10	95.53	9.58
250	1000	32.38	127.92	27.80
250	1250	31.50	159.42	47.90
250	1500	32.23	191.65	77.20
250	1750	31.90	223.55	95.40
250	2000	31.92	255.47	113.80

Table C. 12: Averaged raw data for bed packing density and flow rate of 0.28 g/cm³ and 8 mL/min.

Volume (mL)	time (min)	Cu conc (mg/L)
250.00	32.01	0.00
500.00	63.86	0.00
750.00	95.92	7.46
1000.00	127.81	25.57
1250.00	159.87	52.80
1500.00	191.64	78.70
1750.00	223.50	96.47
2000.00	254.82	114.00

Table C. 13: Loading Run 1 data for bed packing density and flow rate of 0.37 g/cm³ and 8 mL/min.

Volume collected (mL)	Cum Vol collected (mL)	time(min)	cum time (min)	Cu conc (mg/L)
250	250	35.47	35.47	0.00
250	500	30.70	66.17	0.00
250	750	30.42	96.58	4.03
250	1000	27.27	123.85	29.20
250	1250	31.55	155.40	60.80
250	1500	33.65	189.05	80.40
250	1750	32.53	221.58	108.00
250	2000	31.40	252.98	122.00

Table C. 14: Loading Run 2 data for bed packing density and flow rate of 0.37 g/cm³ and 8 mL/min.

Volume collected (mL)	Cum Vol collected (mL)	time(min)	cum time (min)	Cu conc (mg/L)
250	250	32.78	32.78	0.00
250	500	32.03	64.82	0.00
250	750	31.32	96.13	6.46
250	1000	31.45	127.58	28.30
250	1250	32.02	159.60	62.40
250	1500	31.52	191.12	82.00
250	1750	30.93	222.05	105.80
250	2000	31.80	253.85	121.60

Table C. 15: Loading Run 3 data for bed packing density and flow rate of 0.37 g/cm³ and 8 mL/min.

Volume collected (mL)	Cum Vol collected (mL)	time(min)	cum time (min)	Cu conc (mg/L)
250	250	36.68	36.68	0.00
250	500	32.07	68.75	0.31
250	750	29.08	97.83	9.34
250	1000	30.95	128.78	26.20
250	1250	33.02	161.80	60.40
250	1500	33.23	195.03	79.60
250	1750	31.25	226.28	103.60
250	2000	31.70	257.98	120.40

Table C. 16: Averaged raw data for bed packing density and flow rate of 0.37 g/cm³ and 8 mL/min.

Volume (mL)	time (min)	Cu conc (mg/L)
250.00	34.98	0.00
500.00	66.58	0.10
750.00	96.85	6.61
1000.00	126.74	27.90
1250.00	158.93	61.20
1500.00	191.73	80.67
1750.00	223.31	105.80
2000.00	254.94	121.33

Table C. 17: Loading Run 1 data for bed packing density and flow rate of 0.16 g/cm³ and 12 mL/min.

Volume collected (mL)	Cum Vol collected (mL)	time(min)	cum time (min)	Cu conc (mg/L)
250	250	22.37	22.37	0.00
250	500	22.47	44.83	0.03
250	750	21.98	66.82	3.71
250	1000	21.48	88.30	24.70
250	1250	21.70	110.00	49.20
250	1500	21.62	131.62	68.60
250	1750	20.50	152.12	81.60
250	2000	22.05	174.17	104.00

Table C. 18: Loading Run 2 data bed packing density and flow rate of 0.16 g/cm³ and 12 mL/min.

Volume collected (mL)	Cum Vol collected (mL)	time(min)	cum time (min)	Cu conc (mg/L)
250	250	20.92	20.92	0.00
250	500	21.30	42.22	0.13
250	750	21.43	63.65	7.03
250	1000	21.23	84.88	34.60
250	1250	21.62	106.50	60.40
250	1500	21.48	127.98	67.00
250	1750	20.83	148.82	80.40
250	2000	21.53	170.35	102.00

Table C. 19: Loading Run 3 data for bed packing density and flow rate of 0.16 g/cm³ and 12 mL/min.

Volume collected (mL)	Cum Vol collected (mL)	time(min)	cum time (min)	Cu conc (mg/L)
250	250	21.45	21.45	0.03
250	500	20.67	42.12	0.04
250	750	20.07	62.18	26.70
250	1000	19.63	81.82	31.10
250	1250	19.62	101.43	55.40
250	1500	19.23	120.67	70.00
250	1750	20.33	141.00	85.00
250	2000	20.42	161.42	103.00

Table C. 20: Averaged raw data for bed packing density and flow rate of 0.16 g/cm³ and 12 mL/min.

Volume (mL)	time (min)	Cu conc (mg/L)
250.00	21.58	0.01
500.00	43.06	0.07
750.00	64.22	12.48
1000.00	85.00	30.13
1250.00	105.98	55.00
1500.00	126.76	68.53
1750.00	147.31	82.33
2000.00	168.64	103.00

Table C. 21: Loading Run 1 data for bed packing density and flow rate of 0.16 g/cm³ and 17 mL/min.

Volume collected (mL)	Cum Vol collected (mL)	time(min)	cum time (min)	Cu conc (mg/L)
252	252	14.65	14.65	0.00
250	502	14.45	29.10	3.53
250	752	14.52	43.62	23.50
250	1002	14.40	58.02	46.00
250	1252	15.03	73.05	58.00
250	1502	14.42	87.47	72.80
250	1752	15.00	102.47	86.00
250	2002	14.58	117.05	104.40

Table C. 22: Loading Run 2 data for bed packing density and flow rate of 0.16 g/cm³ and 17 mL/min.

Volume collected (mL)	Cum Vol collected (mL)	time(min)	cum time (min)	Cu conc (mg/L)
250	250	14.62	14.62	0.00
250	500	14.57	29.18	2.03
250	750	14.58	43.77	18.40
250	1000	14.52	58.28	40.40
250	1250	14.55	72.83	58.80
250	1500	14.62	87.45	72.80
250	1750	14.70	102.15	88.00
250	2000	14.42	116.57	106.40

Table C. 23: Loading Run 3 data for bed packing density and flow rate of 0.16 g/cm³ and 17 mL/min.

Volume collected (mL)	Cum Vol collected (mL)	time(min)	cum time (min)	Cu conc (mg/L)
250	250	14.42	14.42	0.00
250	500	14.60	29.02	2.57
250	750	15.07	44.08	20.60
250	1000	14.35	58.43	43.00
250	1250	14.40	72.83	62.00
250	1500	14.52	87.35	71.40
250	1750	14.75	102.10	84.00
250	2000	14.38	116.48	104.00

Table C. 24: Averaged raw data for bed packing density and flow rate of 0.16 g/cm³ and 17 mL/min.

Volume (mL)	time (min)	Cu conc (mg/L)
250.67	14.56	0.00
500.67	29.10	2.71
750.67	43.82	20.83
1000.67	58.24	43.13
1250.67	72.91	59.60
1500.67	87.42	72.33
1750.67	102.24	86.00
2000.67	116.70	104.93

Table C. 25: Loading Run 1 data for bed packing density and flow rate of 0.16 g/cm³ and 28 mL/min.

Volume collected (mL)	Cum Vol collected (mL)	time(min)	cum time (min)	Cu conc (mg/L)
250	250	9.02	9.02	0.31
250	500	9.08	18.10	11.10
250	750	9.17	27.27	33.10
250	1000	9.08	36.35	53.40
250	1250	9.05	45.40	63.20
250	1500	9.12	54.52	78.20
250	1750	9.58	64.10	88.00
250	2000	9.10	73.20	110.00

Table C. 26: Table D. 26: Loading Run 2 data for bed packing density and flow rate of 0.16 g/cm³ and 28 mL/min.

Volume collected (mL)	Cum Vol collected (mL)	time(min)	cum time (min)	Cu conc (mg/L)
260	260	9.33	9.33	0.13
250	510	8.67	18.00	10.40
250	760	8.60	26.60	30.90
250	1010	9.03	35.63	47.40
254	1264	9.78	45.42	67.60
250	1514	9.50	54.92	78.00
250	1764	9.07	63.98	93.00
250	2014	9.75	73.73	112.00

Table C. 27: Loading Run 3 data for bed packing density and flow rate of 0.16 g/cm³ and 28 mL/min.

Volume collected (mL)	Cum Vol collected (mL)	time(min)	cum time (min)	Cu conc (mg/L)
250	250	9.83	9.83	0.08
260	510	9.97	19.80	6.43
250	760	9.38	29.18	26.60
250	1010	9.15	38.33	46.40
250	1260	9.17	47.50	59.40
250	1510	9.15	56.65	72.40
250	1760	9.20	65.85	90.00
250	2010	9.17	75.02	111.00

Table C. 28: Averaged raw data for bed packing density and flow rate of 0.16 g/cm³ and 12 mL/min.

Volume (mL)	time (min)	Cu conc (mg/L)
253.33	9.39	0.17
506.67	18.63	9.31
756.67	27.68	30.20
1006.67	36.77	49.07
1258.00	46.11	63.40
1508.00	55.36	76.20
1758.00	64.64	90.33
2008.00	73.98	111.00

Table C. 29: Calculated data for equilibrium loading at bed packing density and flow rate of 0.16 g/cm³ and 8 mL/min.

Volume (mL)	Volume collected (mL)	q _e (mg)	Accumulative q _e (mg)	Accumulative q _e (mg/g)
250.67	250.67	31.83	31.83	12.43
500.67	250.00	31.75	63.58	24.83
750.67	250.00	31.75	95.33	37.23
1000.67	250.00	30.11	125.44	49.00
1250.67	250.00	25.76	151.20	59.06
1500.67	250.00	18.88	170.07	66.43
1750.67	250.00	12.77	182.84	71.41
2000.67	250.00	7.92	190.76	74.51

Table C. 30: Calculated data for equilibrium loading at bed packing density and flow rate of 0.20 g/cm³ and 8 mL/min.

Volume (mL)	Volume collected (mL)	q _e (mg)	Accumulative q _e (mg)	Accumulative q _e (mg/g)
250.00	250.00	31.75	31.75	12.40
500.00	250.00	31.75	63.5	24.80
750.00	250.00	31.62	95.12	37.15
1000.67	250.67	29.73	124.86	48.77
1250.67	250.00	25.03	149.89	58.55
1500.67	250.00	17.56	167.45	65.41
1750.67	250.00	12.18	179.64	70.16
2000.67	250.00	7.60	187.24	73.14

Table C. 31: Calculated data for equilibrium loading at bed packing density and flow rate of 0.28 g/cm³ and 8 mL/min.

Volume (mL)	Volume collected (mL)	q _e (mg)	Accumulative q _e , (mg)	Accumulative q _e (mg/g)
250.00	250.00	31.75	31.75	12.40
500.00	250.00	31.75	63.5	24.80
750.00	250.00	29.88	93.38	36.47
1000.00	250.00	25.35	118.74	46.38
1250.00	250.00	18.55	137.29	53.63
1500.00	250.00	12.07	149.36	58.34
1750.00	250.00	7.63	157.00	61.32
2000.00	250.00	3.25	160.25	62.59

Table C. 32: Calculated data for equilibrium loading at bed packing density and flow rate of 0.37 g/cm³ and 8 mL/min.

Volume (mL)	Volume collected (mL)	q _e (mg)	Accumulative q _e , (mg)	Accumulative q _e (mg/g)
250.00	250.00	31.75	31.75	12.40
500.00	250.00	31.72	63.47	24.79
750.00	250.00	30.09	93.57	36.55
1000.00	250.00	24.77	118.34	46.22
1250.00	250.00	16.45	134.79	52.65
1500.00	250.00	11.58	146.38	57.17
1750.00	250.00	5.30	151.68	59.25
2000.00	250.00	1.416	153.09	59.80

Table C. 33: Calculated data for equilibrium loading at bed packing density and flow rate of 0.16 g/cm³ and 12 mL/min.

Volume (mL)	Volume collected (mL)	q _e (mg)	Accumulative q _e , (mg)	Accumulative q _e (mg/g)
250.00	250.00	31.74	31.74	12.40
500.00	250.00	31.73	63.48	24.79
750.00	250.00	28.63	92.11	35.98
1000.00	250.00	24.21	116.32	45.44
1250.00	250.00	18.00	134.32	52.47
1500.00	250.00	14.61	148.94	58.18
1750.00	250.00	11.16	160.11	62.54
2000.00	250.00	6.00	166.11	64.88

Table C. 34: Calculated data for equilibrium loading at bed packing density and flow rate of 0.16 g/cm³ and 17 mL/min.

Volume (mL)	Volume collected (mL)	q _e (mg)	Accumulative q _e , (mg)	Accumulative q _e (mg/g)
250.67	250.67	31.83	31.83	12.43
500.67	250.00	31.07	62.90	24.57
750.67	250.00	26.54	89.44	34.94
1000.67	250.00	20.96	110.41	43.13
1250.67	250.00	16.85	127.26	49.71
1500.67	250.00	13.66	140.93	55.05
1750.67	250.00	10.25	151.18	59.05
2000.67	250.00	5.51	156.69	61.21

Table C. 35: Calculated data for equilibrium loading at bed packing density and flow rate of 0.16 g/cm³ and 28 mL/min.

Volume (mL)	Volume collected (mL)	q _e (mg)	Accumulative q _e , (mg)	Accumulative q _e (mg/g)
253.33	253.33	32.12	32.12	12.55
506.67	253.33	29.81	61.94	24.19
756.67	250.00	24.20	86.14	33.65
1006.67	250.00	19.48	105.62	41.26
1258.00	251.33	15.98	121.61	47.50
1508.00	250.00	12.70	134.31	52.46
1758.00	250.00	9.16	143.47	56.04
2008.00	250.00	4.00	147.47	57.60

Table C. 36: Elution Run 1 data for bed packing density and flow rate of 0.16 g/cm³ and 8 ml/L.

Volume collected (mL)	Cum Vol collected (mL)	time(min)	cum time (min)	Cu conc (mg/L)
14	14	1.83	1.83	5.88
16	30	2.05	3.88	3.93
16	46	2.02	5.90	8398
16	62	1.95	7.85	195
15	77	1.85	9.70	6.6
15	92	1.85	11.55	2.07
16	108	1.78	13.33	1.01

Table C. 37: Elution Run 2 data for bed packing density and flow rate of 0.16 g/cm³ and 8 ml/L.

Volume collected (mL)	Cum Vol collected (mL)	time(min)	cum time (min)	Cu conc (mg/L)
15	15	2.00	2.00	5.21
15.5	30.5	1.90	3.90	3.36
15	45.5	1.90	5.80	8738
15.5	61	1.93	7.73	572
15.5	76.5	1.95	9.68	4.40
16	92.5	1.95	11.63	1.71
15.5	108	2.00	13.63	0.81

Table C. 38: Elution Run 3 data for bed packing density and flow rate of 0.16 g/cm³ and 8 ml/L.

Volume collected (mL)	Cum Vol collected (mL)	time(min)	cum time (min)	Cu conc (mg/L)
16	16	1.95	1.95	5.94
16	32	1.95	3.90	4.07
16	48	2.03	5.93	8449
15.5	63.5	1.95	7.88	168
16	79.5	2.02	9.90	4.03
15.5	95	1.95	11.85	1.26
15	110	1.92	13.77	0.75

Table C. 39: Averaged elution raw data for bed packing density and flow rate of 0.16 g/cm³ and 8 mL/min.

Volume (mL)	time (min)	Cu conc (mg/L)
15.00	1.93	5.68
30.83	3.89	3.79
46.50	5.88	8528.33
62.17	7.82	311.67
77.67	9.76	5.01
93.17	11.68	1.68
108.67	13.58	0.86

Table C. 40: Elution Run 1 data for bed packing density and flow rate of 0.20 g/cm³ and 8 ml/L.

Volume collected (mL)	Cum Vol collected (mL)	time(min)	cum time (min)	Cu conc (mg/L)
16	16	2.03	2.03	6.42
16	32	1.98	4.02	4.45
16	48	2.07	6.08	8500
16	64	1.92	8.00	397
15	79	1.82	9.82	7.55
16	95	1.93	11.75	2.17
16	111	1.85	13.60	1.05

Table C. 41: Elution Run 2 data for bed packing density and flow rate of 0.20 g/cm³ and 8 ml/L.

Volume collected (mL)	Cum Vol collected (mL)	time(min)	cum time (min)	Cu conc (mg/L)
16	16	1.88	1.88	5.53
15	31	1.82	3.70	3.74
16	47	1.73	5.43	1337.5
16	63	1.90	7.33	7616
16	79	1.95	9.28	16.08
16	95	1.93	11.22	3.83
16	111	1.93	13.15	1.55

Table C. 42: Elution Run 3 data for bed packing density and flow rate of 0.20 g/cm³ and 8 ml/L.

Volume collected (mL)	Cum Vol collected (mL)	time(min)	cum time (min)	Cu conc (mg/L)
16	16	1.92	1.92	6.1
15.5	31.5	1.88	3.80	4.11
16	47.5	1.95	5.75	5457
16	63.5	1.93	7.68	4131
16	79.5	1.93	9.62	16
15.5	95	1.90	11.52	4.08
15	110	1.92	13.43	2

Table C. 43: Averaged elution raw data for bed packing density and flow rate of 0.20 g/cm³ and 8 mL/min.

Volume (mL)	time (min)	Cu conc (mg/L)
16.00	1.94	6.02
31.50	3.84	4.10
47.50	5.76	5098.17
63.50	7.67	4048.00
79.17	9.57	13.21
95.00	11.49	3.36
110.67	13.39	1.53

Table C. 44: Elution Run 1 data for bed packing density and flow rate of 0.28 g/cm³ and 8 ml/L.

Volume collected (mL)	Cum Vol collected (mL)	time(min)	cum time (min)	Cu conc (mg/L)
16.5	16.5	1.98	1.98	6.3
16	32.5	1.88	3.87	4.36
16	48.5	1.90	5.77	7378
15	63.5	1.87	7.63	435
16	79.5	1.95	9.58	7.29
17	96.5	2.00	11.58	1.71
16	112.5	1.95	13.53	0.76

Table C. 45: Elution Run 2 data for bed packing density and flow rate of 0.28 g/cm³ and 8 ml/L.

Volume collected (mL)	Cum Vol collected (mL)	time(min)	cum time (min)	Cu conc (mg/L)
16.5	16.5	2.00	2.00	5.4
15.5	32	2.00	4.00	3.54
15.5	47.5	1.83	5.83	7242
16	63.5	2.02	7.85	569
16	79.5	1.90	9.75	23.5
15.5	95	1.93	11.68	8.75
16	111	1.88	13.57	4.92

Table C. 46: Elution Run 3 data for bed packing density and flow rate of 0.28 g/cm³ and 8 ml/L.

Volume collected (mL)	Cum Vol collected (mL)	time(min)	cum time (min)	Cu conc (mg/L)
16	16	1.88	1.88	5.96
16	32	2.02	3.90	3.75
16.5	48.5	2.03	5.93	6664
16	64.5	2.03	7.97	274
16.5	81	2.00	9.97	12.75
15.5	96.5	2.02	11.98	4.73
15.5	112	1.92	13.90	3.19

Table C. 47: Averaged elution raw data for bed packing density and flow rate of 0.28 g/cm³ and 8 mL/min.

Volume (mL)	time (min)	Cu conc (mg/L)
16.33	1.96	5.89
32.17	3.92	3.88
48.17	5.84	7094.67
63.83	7.82	426.00
80.00	9.77	14.51
96.00	11.75	5.06
111.83	13.67	2.96

Table C. 48: Elution Run 1 data for bed packing density and flow rate of 0.37 g/cm³ and 8 ml/L.

Volume collected (mL)	Cum Vol collected (mL)	time(min)	cum time (min)	Cu conc (mg/L)
15.5	15.5	2.03	2.03	6.66
17	32.5	2.33	4.37	4.3
16	48.5	2.00	6.37	8160
15.5	64	2.03	8.40	121.9
16	80	1.93	10.33	5.83
17	97	2.15	12.48	1.37
17.5	114.5	2.28	14.77	0.77

Table C. 49: Elution Run 2 data for bed packing density and flow rate of 0.37 g/cm³ and 8 ml/L.

Volume collected (mL)	Cum Vol collected (mL)	time(min)	cum time (min)	Cu conc (mg/L)
16	16	2.02	2.02	9.85
17	33	2.25	4.27	7
16	49	1.88	6.15	8364
16	65	1.92	8.07	73.8
16.5	81.5	1.90	9.97	4.58
17	98.5	2.08	12.05	1.44
18.5	117	2.23	14.28	0.64

Table C. 50: Elution Run 3 data for bed packing density and flow rate of 0.37 g/cm³ and 8 ml/L.

Volume collected (mL)	Cum Vol collected (mL)	time(min)	cum time (min)	Cu conc (mg/L)
16	16	1.98	1.98	8.82
17.5	33.5	2.22	4.20	19.3
16	49.5	2.02	6.22	7837
16	65.5	2.10	8.32	270
16	81.5	1.95	10.27	16.9
16.5	98	2.00	12.27	7.55
17	115	2.12	14.38	3.93

Table C. 51: Averaged elution raw data for bed packing density and flow rate of 0.37 g/cm³ and 8 mL/min.

Volume (mL)	time (min)	Cu conc (mg/L)
15.83	2.01	8.44
33.00	4.28	10.20
49.00	6.24	8120.33
64.83	8.26	155.23
81.00	10.19	9.10
97.83	12.27	3.45
115.50	14.48	1.78

Table C. 52: Elution Run 1 data for bed packing density and flow rate of 0.16 g/cm³ and 12 ml/L.

Volume collected (mL)	Cum Vol collected (mL)	time(min)	cum time (min)	Cu conc (mg/L)
15	15	1.25	1.25	12.4
15.5	30.5	1.32	2.57	7.9
15	45.5	1.42	3.98	5185
15.5	61	1.35	5.33	2682
16.5	77.5	1.35	6.68	16.2
16	93.5	1.32	8.00	3.3
15.5	109	1.33	9.33	1.73

Table C. 53: Elution Run 2 data for bed packing density and flow rate of 0.16 g/cm³ and 12 ml/L.

Volume collected (mL)	Cum Vol collected (mL)	time(min)	cum time (min)	Cu conc (mg/L)
16	16	1.38	1.38	10.2
16	32	1.38	2.77	8.4
16	48	1.33	4.10	7565
15.5	63.5	1.30	5.40	48.4
15.5	79	1.30	6.70	5.48
15.5	94.5	1.35	8.05	1.77
16	110.5	1.33	9.38	1.07

Table C. 54: Elution Run 3 data for bed packing density and flow rate of 0.16 g/cm³ and 12 ml/L.

Volume collected (mL)	Cum Vol collected (mL)	time(min)	cum time (min)	Cu conc (mg/L)
16	16	1.15	1.15	10.3
16	32	1.28	2.43	7.15
16	48	1.30	3.73	6868
15.5	63.5	1.20	4.93	899
15.5	79	1.23	6.17	11.2
16	95	1.22	7.38	2.94
16.5	111.5	1.27	8.65	1.14

Table C. 55: Averaged elution raw data for bed packing density and flow rate of 0.16 g/cm³ and 12 mL/min.

Volume (mL)	time (min)	Cu conc (mg/L)
15.67	1.26	10.97
31.50	2.59	7.82
47.17	3.94	6539.33
62.67	5.22	1209.80
78.50	6.52	10.96
94.33	7.81	2.67
110.33	9.12	1.31

Table C. 56: Elution Run 1 data for bed packing density and flow rate of 0.16 g/cm³ and 17 ml/L.

Volume collected (mL)	Cum Vol collected (mL)	time(min)	cum time (min)	Cu conc (mg/L)
16	16	0.83	0.83	38.7
16	32	0.92	1.75	41.7
15.5	47.5	0.88	2.63	6307
16	63.5	0.83	3.47	767
23	86.5	1.05	4.52	8.39
16	102.5	0.90	5.42	2.22
16.5	119	0.90	6.32	1.15

Table C. 57: Elution Run 2 data for bed packing density and flow rate of 0.16 g/cm³ and 17 ml/L.

Volume collected (mL)	Cum Vol collected (mL)	time(min)	cum time (min)	Cu conc (mg/L)
15.5	15.5	0.87	0.87	15.9
15.5	31	0.87	1.73	19.7
16	47	0.92	2.65	6018
15.5	62.5	0.83	3.48	1013
22	84.5	1.13	4.62	6.62
16	100.5	0.95	5.57	1.99
16.5	117	0.93	6.50	0.76

Table C. 58: Elution Run 3 data for bed packing density and flow rate of 0.16 g/cm³ and 17 ml/L.

Volume collected (mL)	Cum Vol collected (mL)	time(min)	cum time (min)	Cu conc (mg/L)
15.5	15.5	0.83	0.83	10.67
15	30.5	0.80	1.63	24.7
16	46.5	0.87	2.50	3859
16	62.5	0.87	3.37	4080
16	78.5	0.90	4.27	12.7
16	94.5	0.88	5.15	2.87
16	110.5	0.90	6.05	1.45

Table C. 59: Averaged elution raw data for bed packing density and flow rate of 0.16 g/cm³ and 17 mL/min.

Volume (mL)	time (min)	Cu conc (mg/L)
15.67	0.84	21.76
31.17	1.71	28.70
47.00	2.59	5394.67
62.83	3.44	1953.33
83.17	4.47	9.24
99.17	5.38	2.36
115.50	6.29	1.12

Table C. 60: Elution Run 1 data for bed packing density and flow rate of 0.16 g/cm³ and 28 ml/L.

Volume collected (mL)	Cum Vol collected (mL)	time(min)	cum time (min)	Cu conc (mg/L)
16.5	16.5	0.58	0.58	5.03
16	32.5	0.58	1.17	35.7
16	48.5	0.58	1.75	7140
17	65.5	0.60	2.35	15.7
16	81.5	0.57	2.92	7.43
17	98.5	0.62	3.53	6.01
16	114.5	0.58	4.12	3.58

Table C. 61: Elution Run 2 data for bed packing density and flow rate of 0.16 g/cm³ and 28 ml/L.

Volume collected (mL)	Cum Vol collected (mL)	time(min)	cum time (min)	Cu conc (mg/L)
17	17	0.60	0.60	15.28
16	33	0.58	1.18	3.35
16	49	0.58	1.77	6800
16	65	0.58	2.35	156
16.5	81.5	0.60	2.95	7.77
18.5	100	0.65	3.60	3.86
16.5	116.5	0.63	4.23	2.95

Table C. 62: Elution Run 3 data for bed packing density and flow rate of 0.16 g/cm³ and 28 ml/L.

Volume collected (mL)	Cum Vol collected (mL)	time(min)	cum time (min)	Cu conc (mg/L)
16	16	0.58	0.58	5.69
15.5	31.5	0.53	1.12	4
16.5	48	0.62	1.73	6035
16	64	0.58	2.32	106.8
17	81	0.62	2.93	6.09
16	97	0.58	3.52	3.26
16.5	113.5	0.58	4.10	1.12

Table C. 63: Averaged elution raw data for bed packing density and flow rate of 0.16 g/cm³ and 28 mL/min.

Volume (mL)	time (min)	Cu conc (mg/L)
16.50	0.59	8.67
32.33	1.16	14.35
48.50	1.75	6658.33
64.83	2.34	92.83
81.33	2.93	7.10
98.50	3.55	4.38
114.83	4.15	2.55

Table C. 64: Data for plotting linearised Thomas, Yoon-Nelson and Adam's Bohart model at bed packing density and flow rate of 0.16 g/cm³ and 8 mL/min.

time (min)	$\text{Ln}(C_o/C_t-1)$	$\text{Ln}(C_t/(C_o-C_t))$	$\text{Ln}(C_t/C_o)$
31.08	-	-	-
63.04	-	-	-
95.01	8.94	-8.94	-8.94
127.14	2.91	-2.91	-2.96
159.51	1.46	-1.46	-1.67
192.37	0.38	-0.38	-0.90
223.66	-0.40	0.40	-0.51
254.89	-1.10	1.10	-0.29

Table C. 65: Data for plotting linearised Thomas, Yoon-Nelson and Adam's Bohart model at bed packing density and flow rate of 0.20 g/cm³ cm and 8 mL/min.

time (min)	$\text{Ln}(C_o/C_t-1)$	$\text{Ln}(C_t/(C_o-C_t))$	$\text{Ln}(C_t/C_o)$
30.99	-	-	-
62.86	-	-	-
94.91	5.57	-5.57	-5.57
126.72	2.65	-2.65	-2.72
158.37	1.31	-1.31	-1.55
190.11	0.21	-0.21	-0.81
221.21	-0.47	0.47	-0.48
252.57	-1.16	1.16	-0.27

Table C. 66: Data for plotting linearised Thomas, Yoon-Nelson and Adam's Bohart model at bed packing density and flow rate of 0.28 g/cm³ and 8 mL/min.

time (min)	$\text{Ln}(C_o/C_t-1)$	$\text{Ln}(C_t/(C_o-C_t))$	$\text{Ln}(C_t/C_o)$
32.01	-	-	-
63.86	-	-	-
95.92	2.77	-2.77	-2.84
127.81	1.38	-1.38	-1.60
159.87	0.34	-0.34	-0.88
191.64	-0.49	0.49	-0.48
223.50	-1.15	1.15	-0.27
254.82	-2.17	2.17	-0.11

Table C. 67: Data for plotting linearised Thomas, Yoon-Nelson and Adam's Bohart model at bed packing density and flow rate of 0.37 g/cm³ cm and 8 mL/min.

time (min)	$\text{Ln}(C_o/C_t-1)$	$\text{Ln}(C_t/(C_o-C_t))$	$\text{Ln}(C_t/C_o)$
34.98	-	-	-
66.58	7.11	-7.11	-7.11
96.85	2.90	-2.90	-2.96
126.74	1.27	-1.27	-1.52
158.93	0.07	-0.07	-0.73
191.73	-0.55	0.55	-0.45
223.31	-1.61	1.61	-0.18
254.94	-3.06	3.06	-0.05

Table C. 68: Data for plotting linearised Thomas, Yoon-Nelson and Adam's Bohart model at bed packing density and flow rate of 0.16 g/cm³ and 12 mL/min.

time (min)	$\text{Ln}(C_o/C_t-1)$	$\text{Ln}(C_t/(C_o-C_t))$	$\text{Ln}(C_t/C_o)$
21.58	9.45	-9.45	-9.45
43.06	7.55	-7.55	-7.55
64.22	2.22	-2.22	-2.32
85.00	1.17	-1.17	-1.44
105.98	0.27	-0.27	-0.84
126.76	-0.16	0.16	-0.62
147.31	-0.61	0.61	-0.43
168.64	-1.46	1.46	-0.21

Table C. 69: Data for plotting linearised Thomas, Yoon-Nelson and Adam's Bohart model at bed packing density and flow rate of 0.16 g/cm³ and 17 mL/min.

time (min)	$\text{Ln}(C_o/C_t-1)$	$\text{Ln}(C_t/(C_o-C_t))$	$\text{Ln}(C_t/C_o)$
14.56	-	-	-
29.10	3.83	-3.83	-3.85
43.82	1.63	-1.63	-1.81
58.24	0.66	-0.66	-1.08
72.91	0.12	-0.12	-0.76
87.42	-0.28	0.28	-0.56
102.24	-0.74	0.74	-0.39
116.70	-1.56	1.56	-0.19

Table C. 70: Data for plotting linearised Thomas, Yoon-Nelson and Adam's Bohart model at bed packing density and flow rate of 0.16 g/cm³ and 0.28 mL/min.

time (min)	Ln(C _o /C _t -1)	Ln(C _t /(C _o -C _t))	Ln(C _t /C _o)
9.39	6.60	-6.60	-6.60
18.63	2.54	-2.54	-2.61
27.68	1.16	-1.16	-1.44
36.77	0.46	-0.46	-0.95
46.11	0.00	0.00	-0.69
55.36	-0.41	0.41	-0.51
64.64	-0.90	0.90	-0.34
73.98	-1.94	1.94	-0.13

Thomas

The Thomas model employs Langmuir isotherm for equilibrium and second order reversible reaction kinetics as it assumes plug flow behaviour in the bed (Ahmad and Hameed, 2010; Kalavathy et al., 2010). The Thomas model neglects the intraparticle diffusion as well as the external resistance during the ion exchange process (Kalavathy et al., 2010). The linearized Thomas model is expressed as follows (Equation C.1):

$$\ln\left(\frac{C_o}{C_t} - 1\right) = \frac{k_{Th}q_o w}{Q} - k_{Th}C_o t \quad \text{C. 1}$$

Where: - k_{Th} : Thomas rate constant (mL/min mg)
 q_o : equilibrium Cu uptake (mg/g)
 C_o : feed concentration of Cu (mg/L)
 C_t : effluent Cu concentration (mg/L)
 w : mass of IEFs (g)
 Q : flow rate (mL/min).

The values of k_{Th} and q_o were determined from the slope and intercepts of linear plots of $\ln(C_o/C_t-1)$ versus t (Figure C.3-C9). The least squares fit method was used to determine the slope and intercepts of the best fit line. The Thomas model parameters (k_{Th} and q_o) are listed in Table C.71.

Table C. 71: Thomas model parameters at various conditions using the least squares fit method.

packing density (g/cm ³)	Flow rate (mL/min)	k _{TH} (mL/min mg)	q ₀ (mg/g)	R ²
0.16	8	4.31E-04	8.43E+04	0.80
0.20	8	3.17E-04	8.16E+04	0.92
0.28	8	2.35E-04	6.96E+04	0.99
0.37	8	2.76E-04	6.52E+04	0.98
0.16	12	2.61E-04	7.41E+04	0.98
0.16	17	3.17E-04	6.78E+04	0.98
0.16	28	4.86E-04	6.26E+04	0.98

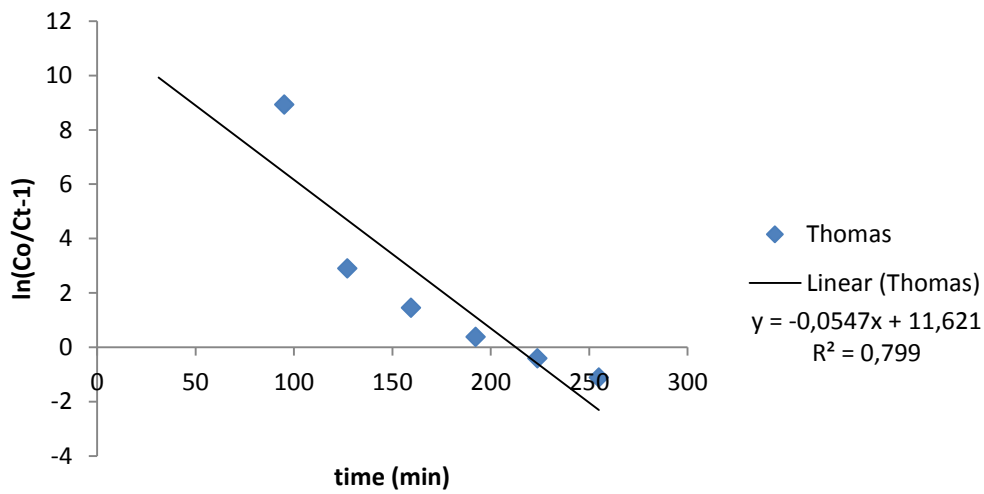


Figure C. 3: Linearised Thomas plot at bed packing density and flow rate of 0.16 g/cm³ and 8 mL/min.

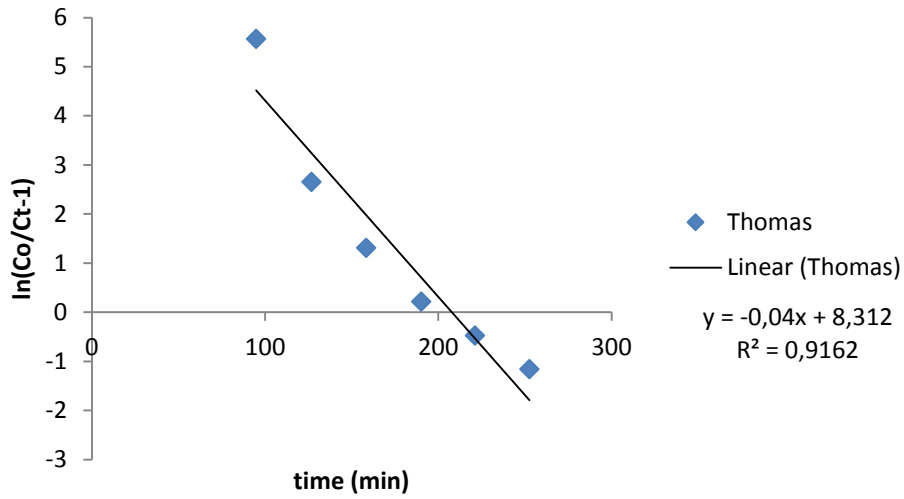


Figure C. 4: Linearised Thomas plot at bed packing density and flow rate of 0.20 g/cm³ and 8 mL/min.

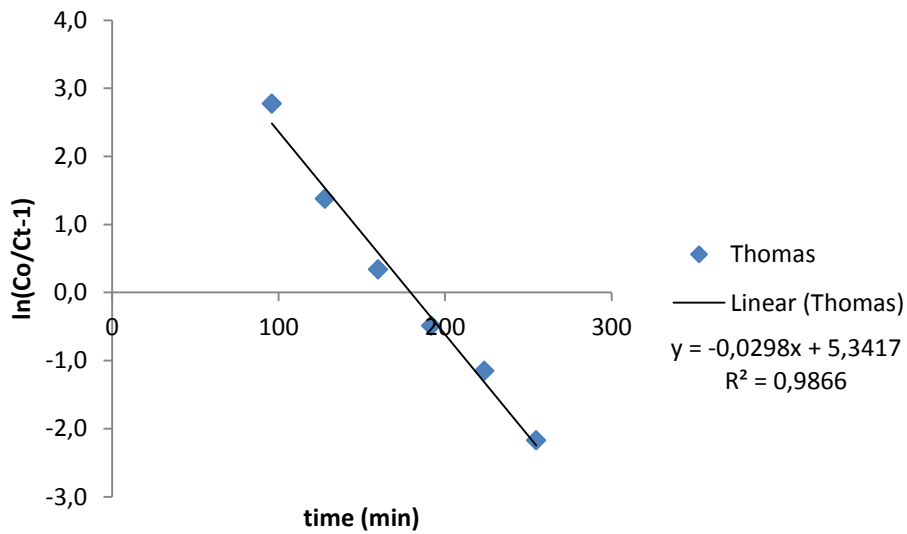


Figure C. 5: Linearised Thomas plot at bed packing density and flow rate of 0.28 g/cm³ cm and 8 mL/min.

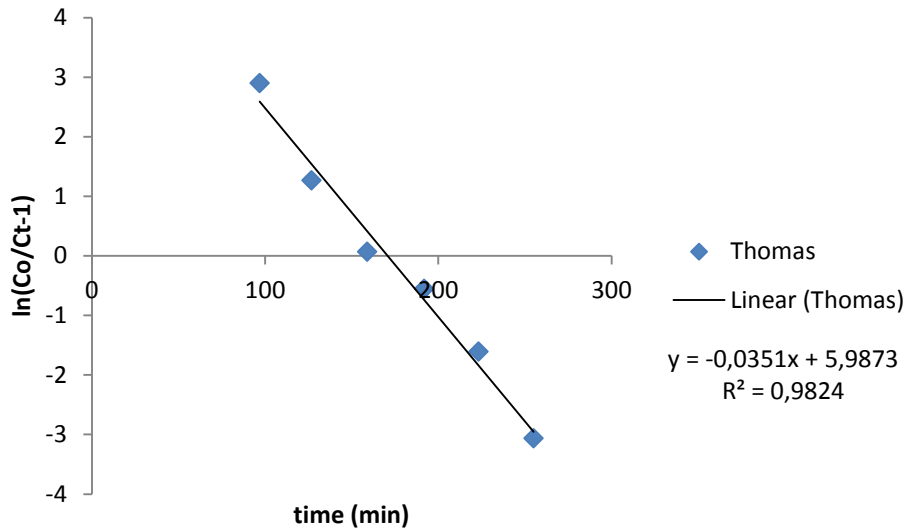


Figure C. 6: Linearised Thomas plot at bed packing density and flow rate of 0.37 g/cm³ and 8 mL/min.

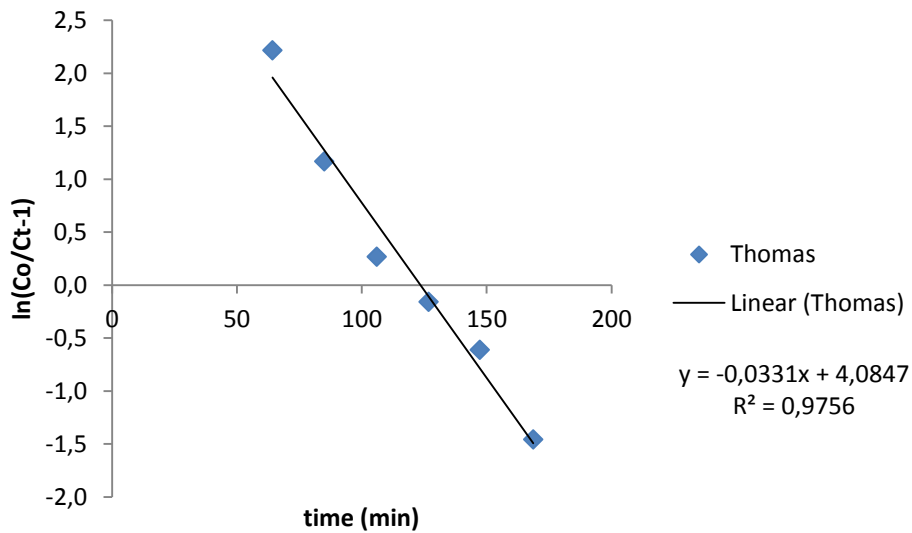


Figure C. 7: Linearised Thomas plot at bed packing density and flow rate of 0.16 g/cm³ and 12 mL/min.

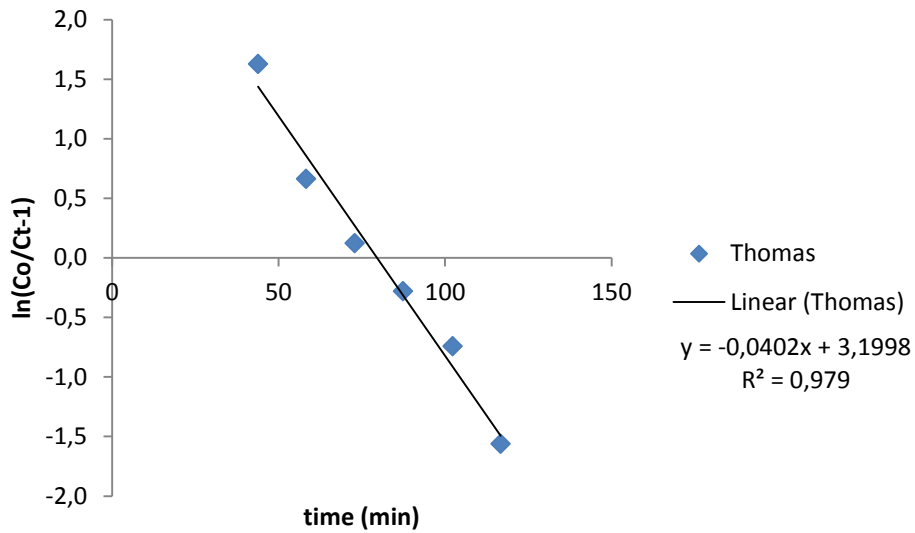


Figure C. 8: Linearised Thomas plot at b bed packing density and flow rate of 0.16 g/cm³ and 17 mL/min.

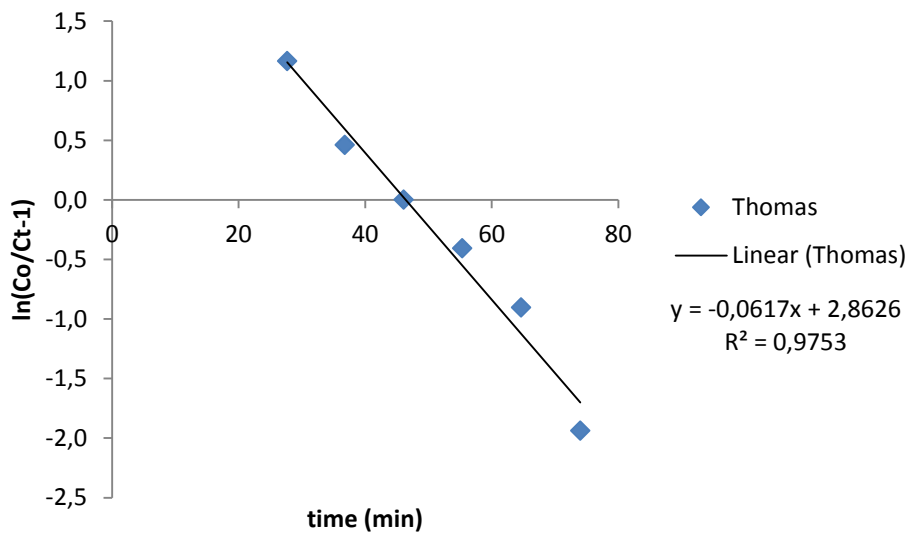


Figure C. 9: Linearised Thomas plot at bed packing density and flow rate of 0.16 g/cm³ and 28 mL/min.

Yoon-Nelson model

The Yoon-Nelson model assumes that the rate of decrease in the probability of loading of each ion is proportional to the probability of ion loading and the probability of ion breakthrough on IEFs (Aksu and Gonen, 2004). The linearised form of the Yoon-Nelson model is expressed as Equation C.2 provided below (Nwabanne and Igbokwe, 2012; Kalavathy et al, 2010; Trgo et al., 2011; Aksu and Gonen, 2004).

$$\ln\left(\frac{C_t}{C_o - C_t}\right) = k_{YN}t - \tau k_{YN} \quad \text{C. 2}$$

- Where: -
- C_t: effluent Cu concentration (mg/L)
 - C_o: feed concentration of Cu (mg/L)
 - k_{YN}: Yoon-Nelson rate constant (1/min)
 - t: time (min)
 - τ: time required for 50% adsorbate breakthrough (min).

The Yoon-Nelson rate constant generally increases with bed height as listed in Table C.72 below. The values of k_{YN} and τ were obtained from slope and y-intercept of the plots in Figure C.10-C.16.

Table C. 72: Yoon-Nelson model parameters at various conditions using the least squares fit method.

Packing density (g/cm ³)	Flow rate (mL/min)	k _{YN} (1/min)	Yoon-Nelson τ (min)	experimental range of τ (min)	R ²
0.16	8	5.47E-02	212	192-223	0.80
0.20	8	4.02E-02	207	190-221	0.92
0.28	8	2.98E-02	179	159-191	0.99
0.37	8	3.51E-02	171	158-191	0.98
0.16	12	3.31E-02	123	105-126	0.98
0.16	17	4.02E-02	80	72-87	0.98
0.16	28	6.17E-02	46	36-46	0.98

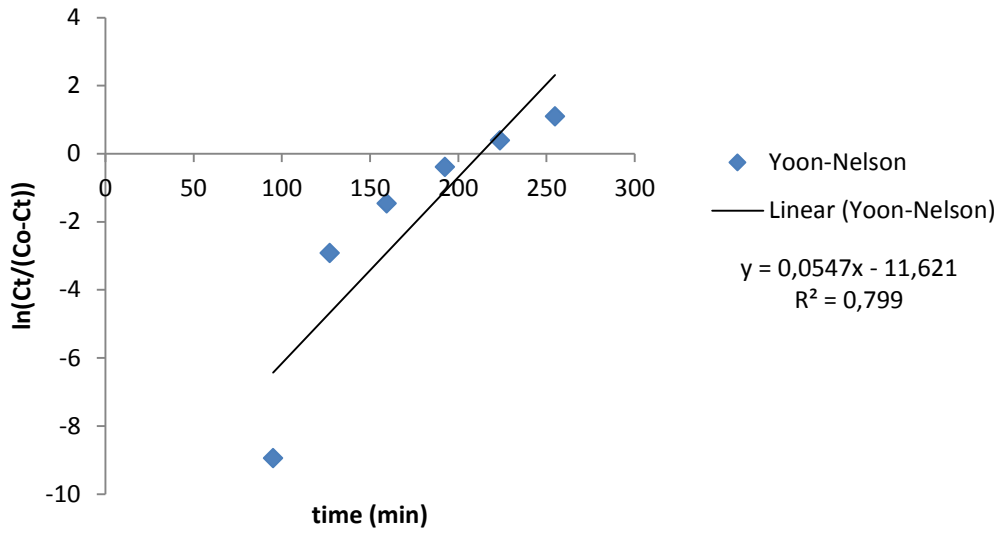


Figure C. 10: Linearised Yoon-Nelson plot at bed packing density and flow rate 0.16 g/cm³ and 8 mL/min.

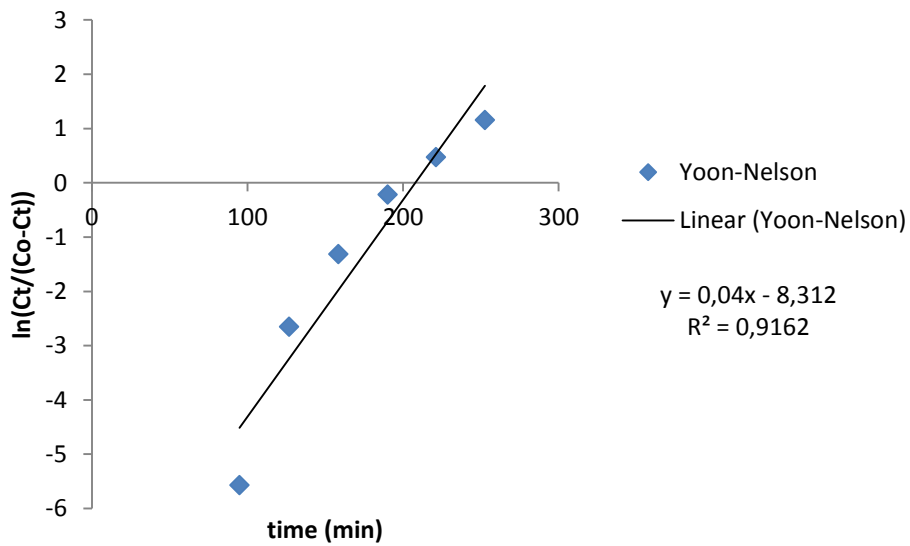


Figure C. 11: Linearised Yoon-Nelson plot at bed packing density and flow rate 0.20 g/cm³ and 8 mL/min.

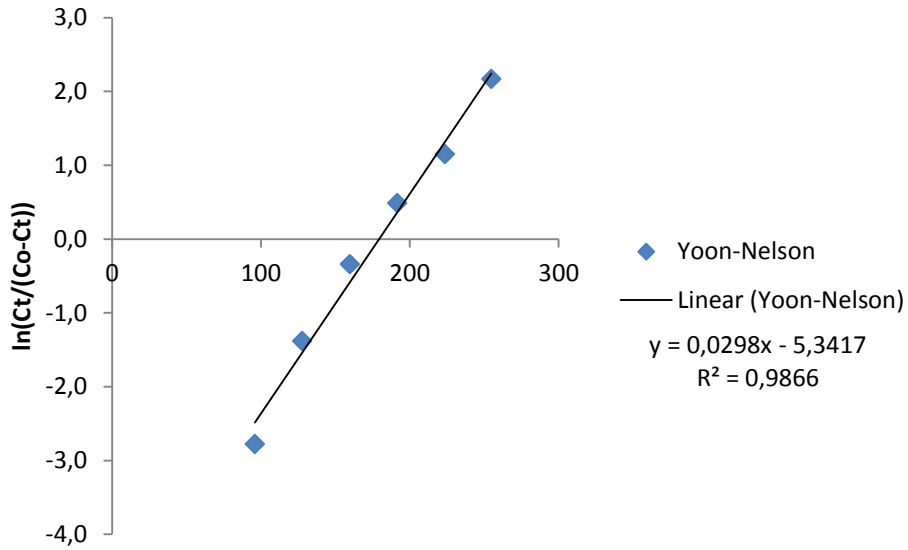


Figure C. 12: Linearised Yoon-Nelson plot at bed packing density and flow rate 0.28 g/cm³ and 8 mL/min.

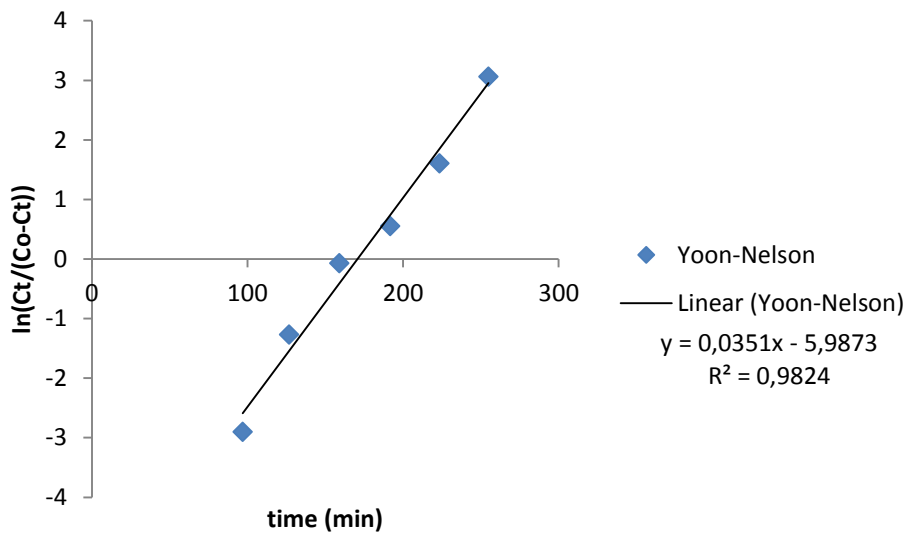


Figure C. 13: Linearised Yoon-Nelson plot at bed packing density and flow rate 0.37 g/cm³ and 8 mL/min.

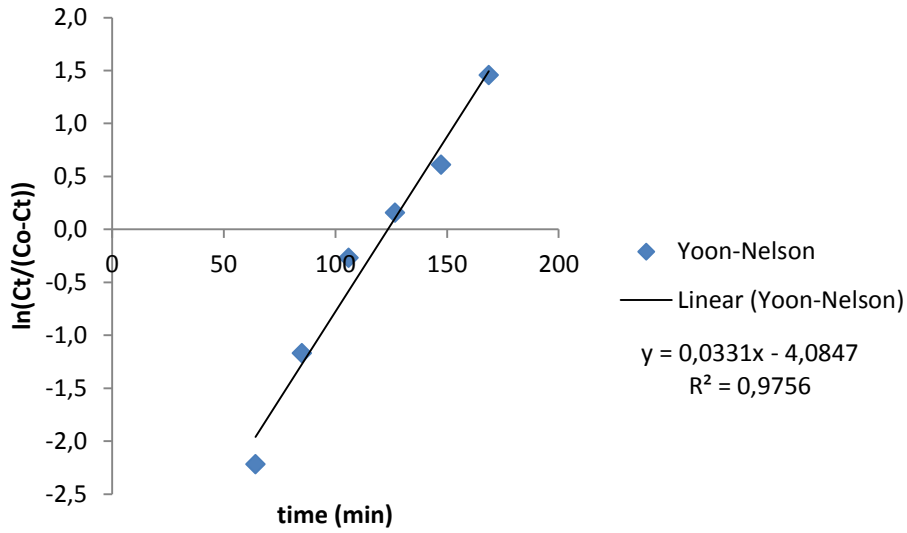


Figure C. 14: Linearised Yoon-Nelson plot at bed packing density and flow rate 0.16 g/cm³ and 12 mL/min.

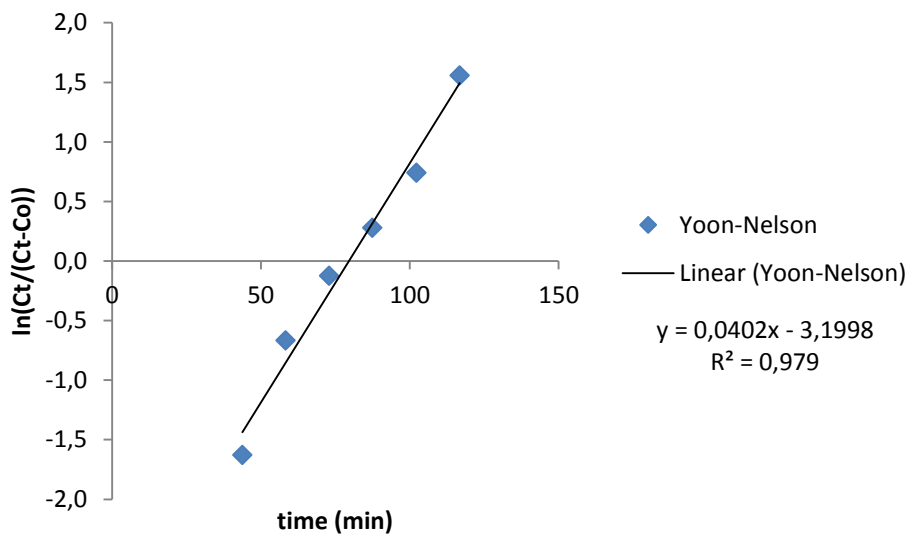


Figure C. 15: Linearised Yoon-Nelson plot at bed packing density and flow rate 0.16 g/cm³ and 17 mL/min.

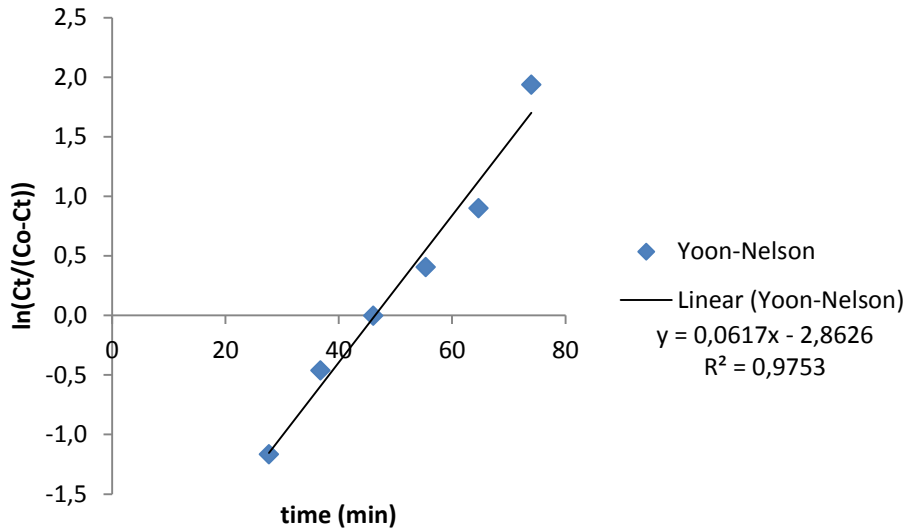


Figure C. 16: Linearised Yoon-Nelson plot at bed packing density and flow rate 0.16 g/cm³ and 28 mL/min.

Adam's Bohart model

The Adam's-Bohart model describes the relationship between C_t/C_o and t during continuous operation (Kalavathy et al., 2010). The Adam's-Bohart model is normally used to describe the initial part of the breakthrough curve (Kalavathy et al., 2010). The Adam's-Bohart model equation is provided below (Equation C.3).

$$\ln \frac{C_t}{C_o} = k_{AB} C_o t - k_{AB} N_o \frac{Z}{F} \quad \text{C. 3}$$

- Where : -
- C_t : effluent Cu concentration (mg/L)
 - C_o : feed concentration of Cu (mg/L)
 - t : time (min)
 - k_{AB} : Adam's-Bohart kinetic constant (L/mg min)
 - N_o : saturation concentration (mg/L)
 - Z : bed height (cm)
 - F : linear velocity (cm/min)

The values of K_{AB} and N_o listed in Table C.73 were determined from intercepts and slopes of the plot of $\ln C_t/C_o$ against t shown in Figure C.17-C.23. The correlation coefficients (R^2)

between the plots of $\ln C_t/C_0$ against t ranged between 0.71 and 0.95 as listed in Table C.73 below.

Table C. 73: Adam's-Bohart model parameters at various conditions using the least squares fit method.

packing density (g/cm ³)	Flow rate (mL/min)	k _{AB}	N ₀ (mg/L)	R ²
0.16	8	3.61E-04	1.44E+04	0.71
0.20	8	2.43E-04	1.82E+04	0.82
0.28	8	1.28E-04	2.70E+04	0.87
0.37	8	1.33E-04	3.42E+04	0.83
0.16	12	1.49E-04	1.57E+04	0.89
0.16	17	1.59E-04	1.62E+04	0.90
0.16	28	2.07E-04	1.63E+04	0.95

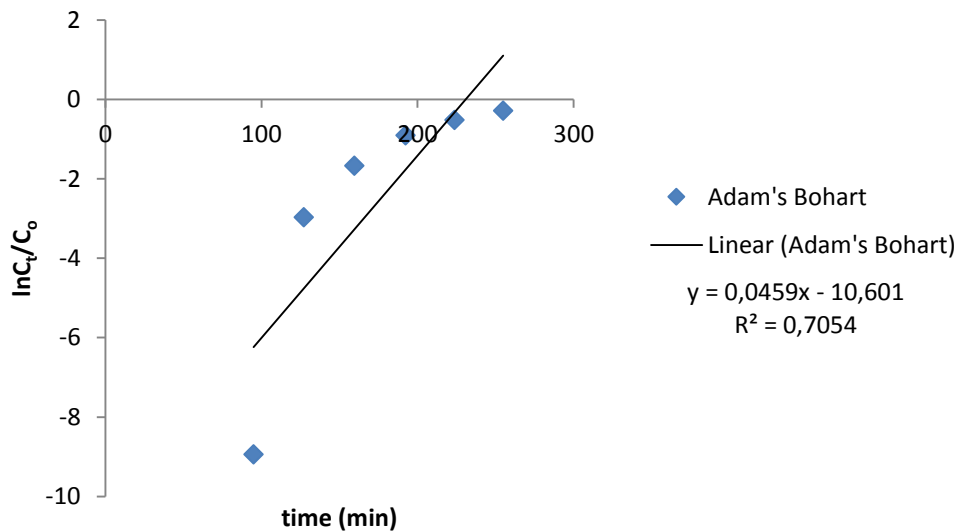


Figure C. 17: Linearised Adams's Bohart plot at bed packing density and flow rate 0.16 g/cm³ and 8 mL/min.

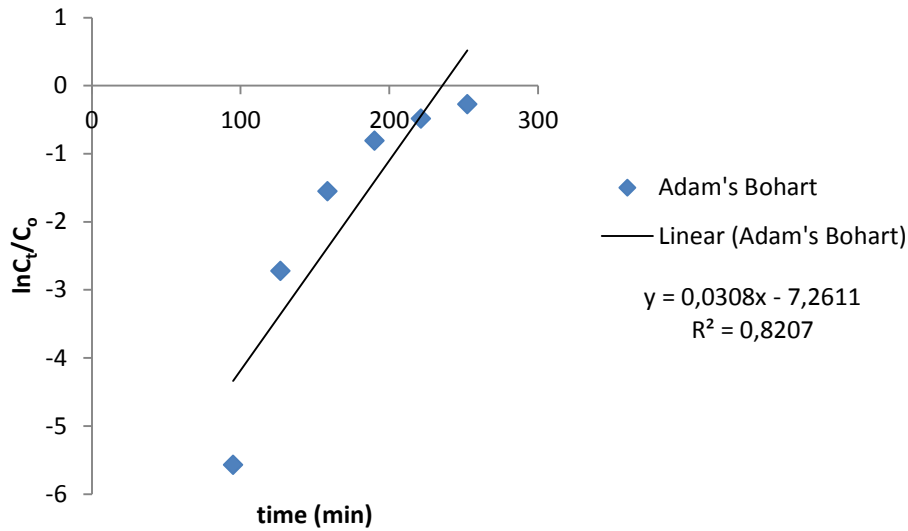


Figure C. 18: Linearised Adams's Bohart plot at bed packing density and flow rate 0.20 g/cm³ and 8 mL/min.

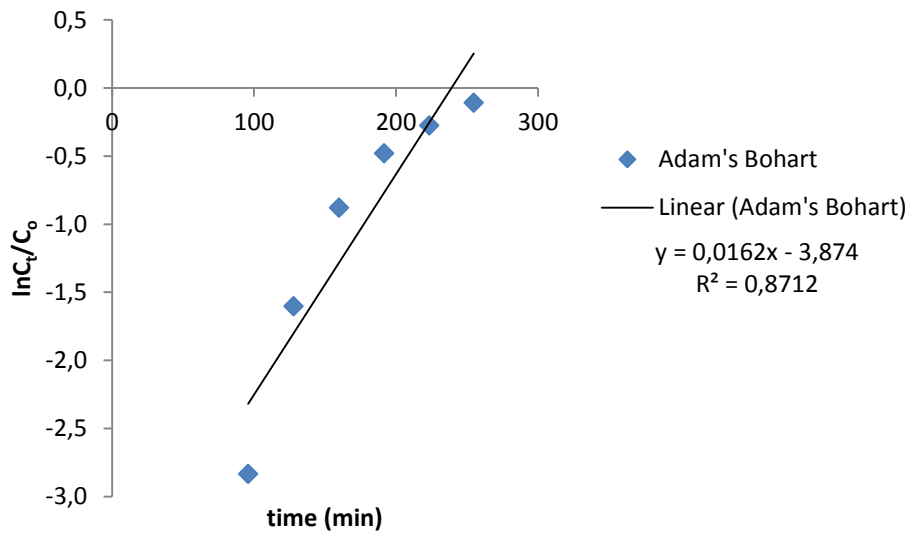


Figure C. 19: Linearised Adams's Bohart plot at bed packing density and flow rate 0.28 g/cm³ and 8 mL/min.

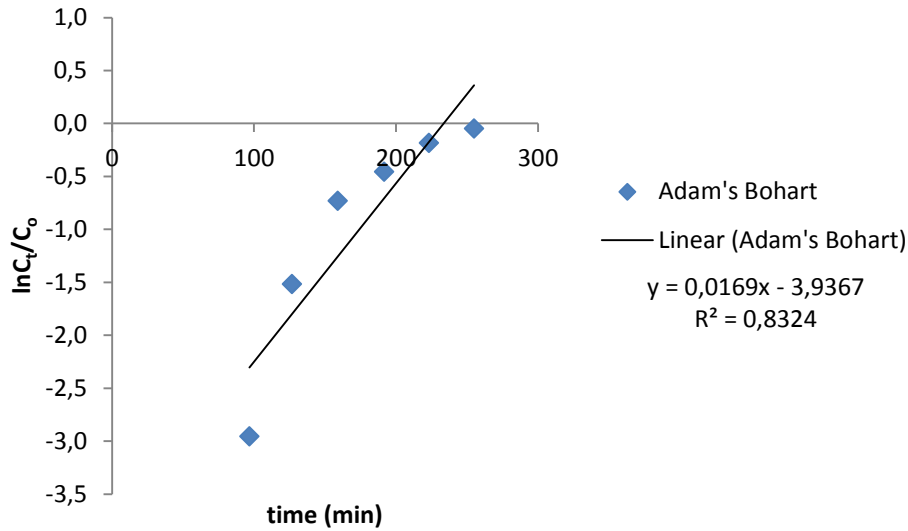


Figure C. 20: Linearised Adams's Bohart plot at bed packing density and flow rate 0.37 g/cm³ and 8 mL/min.

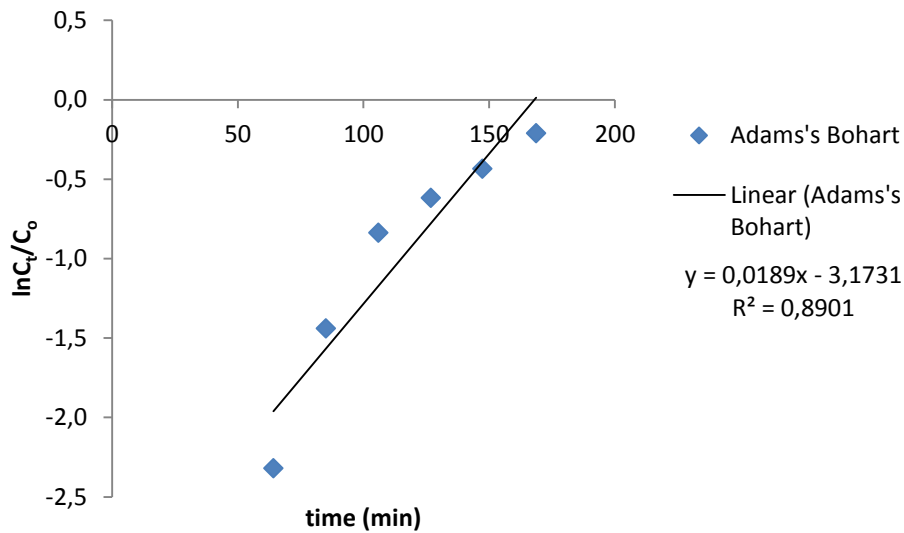


Figure C. 21: Linearised Adams's Bohart plot at bed packing density and flow rate 0.16 g/cm³ and 12 mL/min.

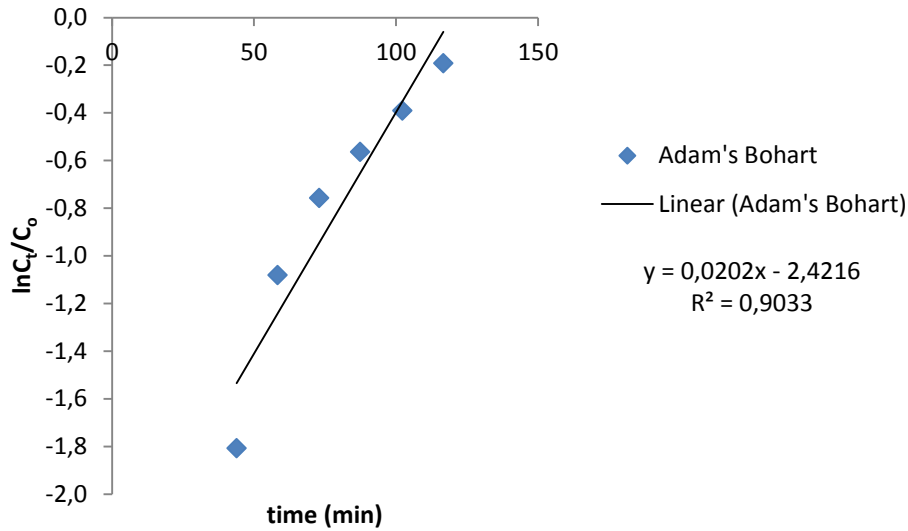


Figure C. 22: Linearised Adams's Bohart plot at bed packing density and flow rate 0.16 g/cm³ and 17 mL/min.

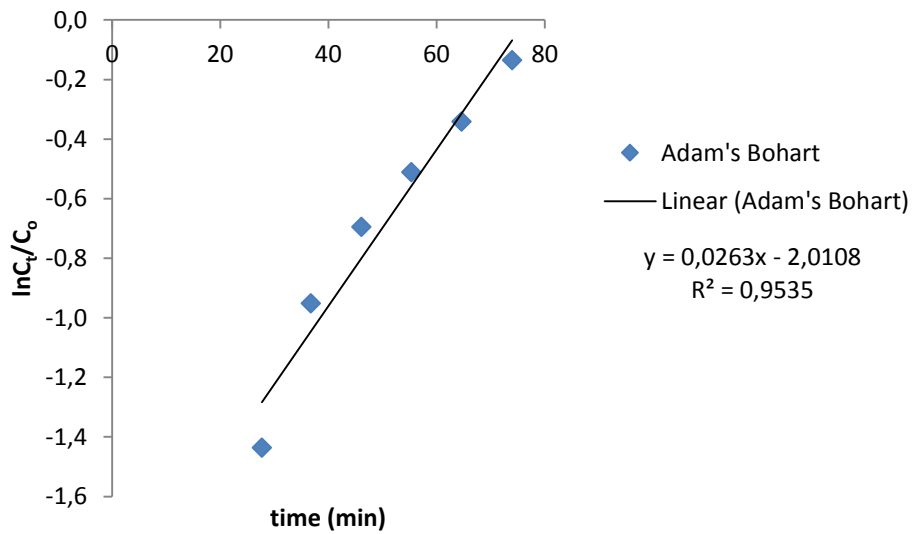


Figure C. 23: Linearised Adams's Bohart plot at bed packing density and flow rate 0.16 g/cm³ and 28 mL/min.

Table C. 74: Concentrations (mg/L) of Cu predicted by the Thomas, Yoon-Nelson and Adam's Bohart at various times at bed packing density and flow rate 0.16 g/cm³ and 8 mL/min.

time (min)	C _t (experimental)	C _t (Thomas)	C _t (Yoon-Nelson)	C _t (Adam's Bohart)
31.08	0.00	0.01	0.01	0.01
63.04	0.00	0.03	0.04	0.06
95.01	0.02	0.17	0.21	0.25
127.14	6.56	1.00	1.18	1.08
159.51	23.97	5.68	6.65	4.78
192.37	51.50	27.96	31.75	21.60
223.66	75.93	77.45	82.37	90.83
254.89	95.33	113.81	115.65	380.92

Table C. 75: Concentrations (mg/L) of Cu predicted by the Thomas, Yoon-Nelson and Adam's Bohart at various times at bed packing density and flow rate 0.20 g/cm³ and 8 mL/min.

time (min)	C _t (experimental)	C _t (Thomas)	C _t (Yoon-Nelson)	C _t (Adam's Bohart)
30.99	0.00	0.11	0.11	0.23
62.86	0.00	0.38	0.38	0.61
94.91	0.48	1.37	1.37	1.65
126.72	8.37	4.78	4.78	4.40
158.37	26.90	15.55	15.55	11.65
190.11	56.73	42.34	42.34	30.97
221.21	78.27	80.75	80.75	80.71
252.57	96.60	109.26	109.26	212.01

Table C. 76: Concentrations (mg/L) of Cu predicted by the Thomas, Yoon-Nelson and Adam's Bohart at various times at bed packing density and flow rate 0.28 g/cm³ and 8 mL/min.

time (min)	C _t (experimental)	C _t (Thomas)	C _t (Yoon-Nelson)	C _t (Adam's Bohart)
32.01	0.00	1.56	1.56	4.43
63.86	0.00	3.95	3.95	7.42
95.92	7.46	9.78	9.78	12.48
127.81	25.57	22.55	22.55	20.92
159.87	52.80	45.65	45.65	35.16
191.64	78.70	75.09	75.09	58.84
223.50	96.47	100.20	100.20	98.58
254.82	114.00	114.91	114.91	163.74

Table C. 77: Concentrations (mg/L) of Cu predicted by the Thomas, Yoon-Nelson and Adam's Bohart at various times at bed packing density and flow rate 0.37 g/cm³ and 8 mL/min.

time (min)	C _t (experimental)	C _t (Thomas)	C _t (Yoon-Nelson)	C _t (Adam's Bohart)
34.98	0.00	1.08	1.08	4.48
66.58	0.10	3.22	3.22	7.63
96.85	6.61	8.88	8.88	12.73
126.74	27.90	22.44	22.44	21.10
158.93	61.20	50.70	50.70	36.36
191.73	80.67	86.05	86.05	63.29
223.31	105.80	109.75	109.75	107.92
254.94	121.33	120.75	120.75	184.19

Table C. 78: Concentrations (mg/L) of Cu predicted by the Thomas, Yoon-Nelson and Adam's Bohart at various times at bed packing density and flow rate 0.16 g/cm³ and 12 mL/min.

time (min)	C _t (experimental)	C _t (Thomas)	C _t (Yoon-Nelson)	C _t (Adam's Bohart)
21.58	0.01	4.22	4.22	8.41
43.06	0.07	8.31	8.31	12.61
64.22	12.48	15.69	15.69	18.82
85.00	30.13	27.82	27.82	27.87
105.98	55.00	45.68	45.68	41.43
126.76	68.53	67.02	67.02	61.36
147.31	82.33	87.39	87.39	90.49
168.64	103.00	103.79	103.78	135.43

Table C. 79: Concentrations (mg/L) of Cu predicted by the Thomas, Yoon-Nelson and Adam's Bohart at various times at bed packing density and flow rate 0.16 g/cm³ and 17 mL/min.

time (min)	C _t (experimental)	C _t (Thomas)	C _t (Yoon-Nelson)	C _t (Adam's Bohart)
14.56	0.00	8.66	8.66	15.13
29.10	2.71	14.74	14.74	20.30
43.82	20.83	24.36	24.36	27.32
58.24	43.13	37.81	37.81	36.57
72.91	59.60	55.01	55.01	49.17
87.42	72.33	73.41	73.41	65.92
102.24	86.00	90.56	90.56	88.93
116.70	104.93	103.67	103.67	119.10

Table C. 80: Concentrations (mg/L) of Cu predicted by the Thomas, Yoon-Nelson and Adam's Bohart at various times at bed packing density and flow rate 0.16 g/cm³ and 0.28 mL/min.

time (min)	C _t (experimental)	C _t (Thomas)	C _t (Yoon-Nelson)	C _t (Adam's Bohart)
9.39	0.17	11.75	11.75	21.77
18.63	9.31	19.40	19.40	27.76
27.68	30.20	30.44	30.44	35.21
36.77	49.07	45.18	45.18	44.72
46.11	63.40	62.93	62.93	57.17
55.36	76.20	80.63	80.63	72.92
64.64	90.33	95.90	95.90	93.09
73.98	111.00	107.42	107.42	119.00

The plots of barren concntrations predicted by the Thomas, Yoon-Nelson and Adam's Bohart models versut time are shown in Figure D.22-D.28 together with the barren concentrations obtained experimentally. The plots are for the various bed heights and flow rates investigated in this study.

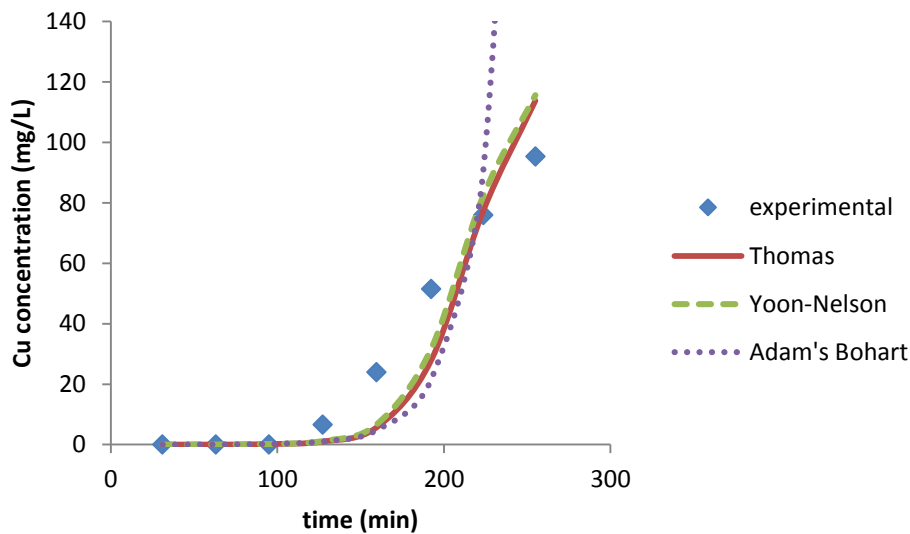


Figure C. 24: PLOT of Cu concentration from experiments and those predicted by the Thomas, Yoon-Nelson and Adam's Bohart model versus time at bed packing density and flow rate 0.16 g/cm³ and 8 mL/min.

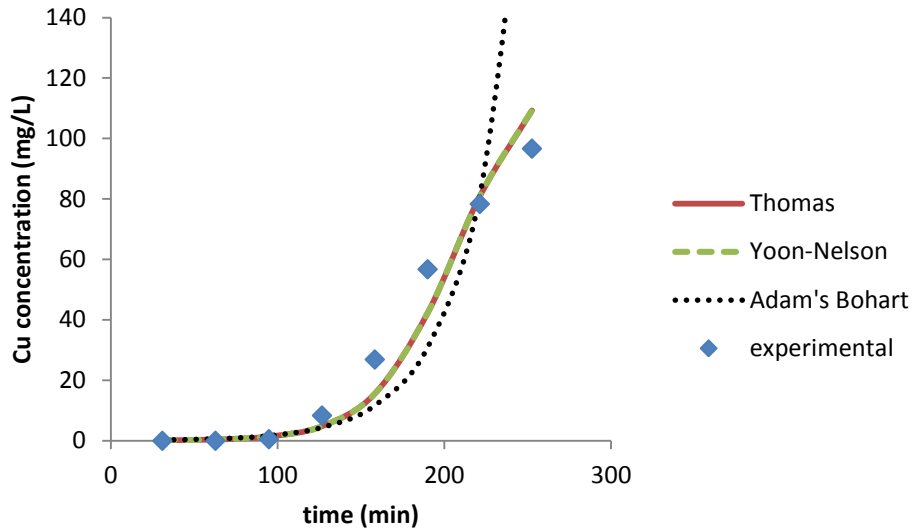


Figure C. 25: Plot of Cu concentration from experiments and those predicted by the Thomas, Yoon-Nelson and Adam's Bohart model versus time at bed packing density and flow rate 0.20 g/cm^3 and 8 mL/min .

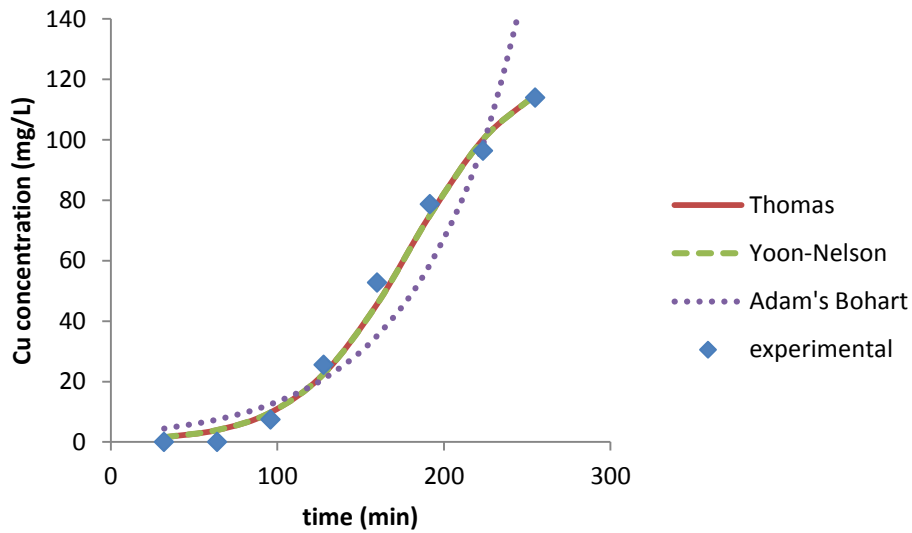


Figure C. 26: Plot of Cu concentration from experiments and those predicted by the Thomas, Yoon-Nelson and Adam's Bohart model versus time at bed packing density and flow rate 0.28 g/cm^3 and 8 mL/min .

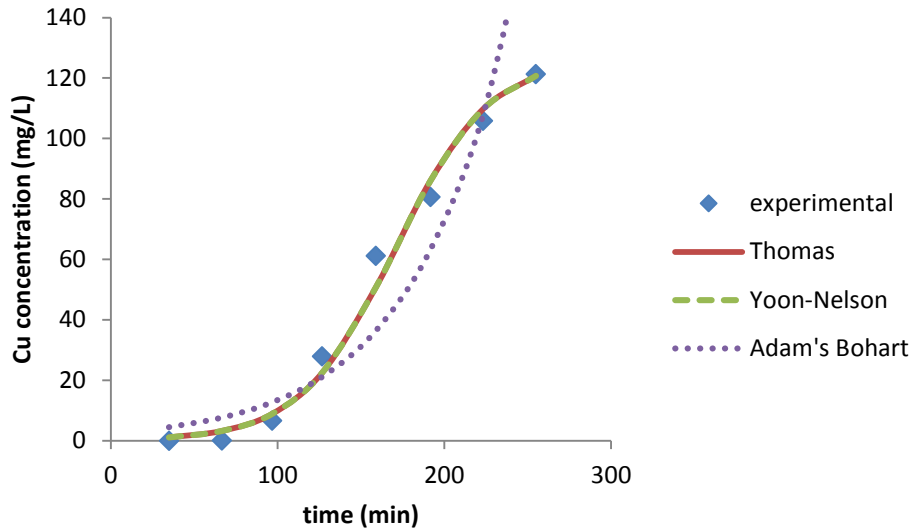


Figure C. 27: Plot of Cu concentration from experiments and those predicted by the Thomas, Yoon-Nelson and Adam's Bohart model versus time at bed packing density and flow rate 0.37 g/cm^3 and 8 mL/min .

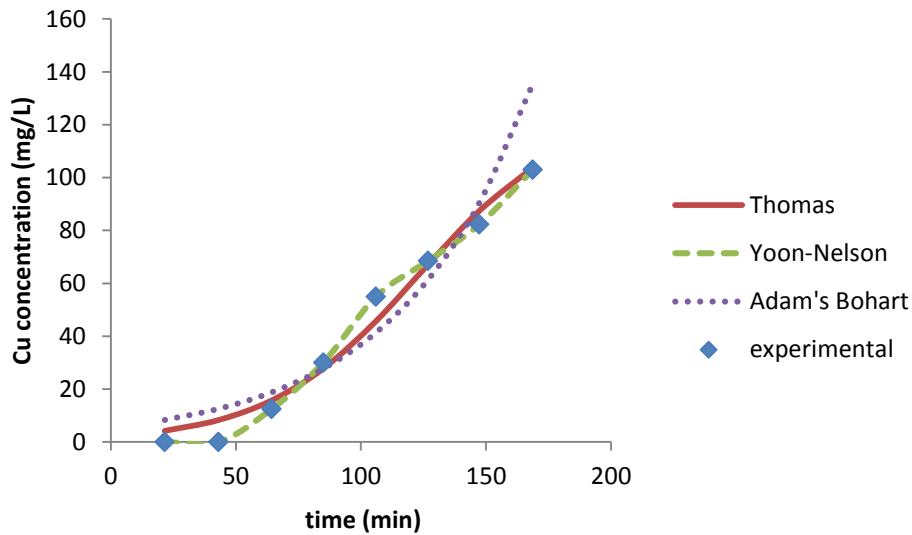


Figure C. 28: Plot of Cu concentration from experiments and those predicted by the Thomas, Yoon-Nelson and Adam's Bohart model versus time at bed packing density and flow rate 0.16 g/cm^3 and 12 mL/min .

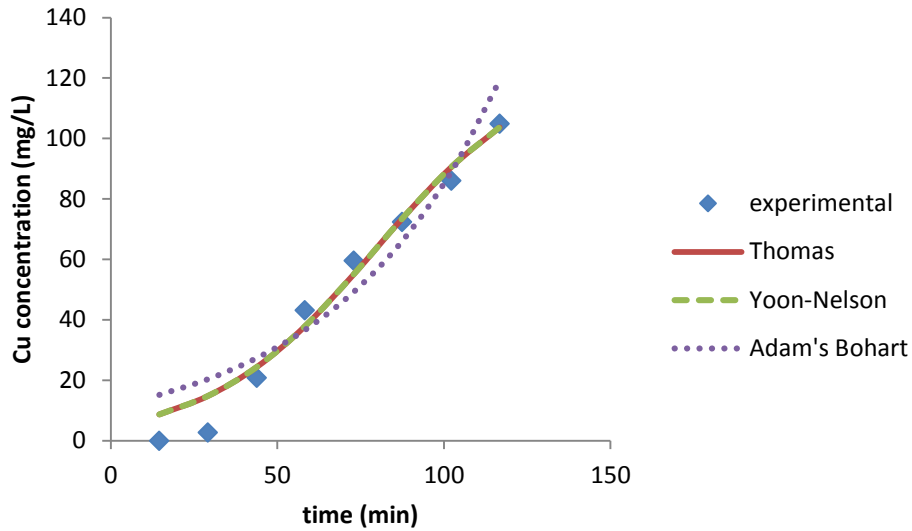


Figure C. 29: Plot of Cu concentration from experiments and those predicted by the Thomas, Yoon-Nelson and Adam's Bohart model versus time at bed packing density and flow rate 0.16 g/cm^3 and 17 mL/min .

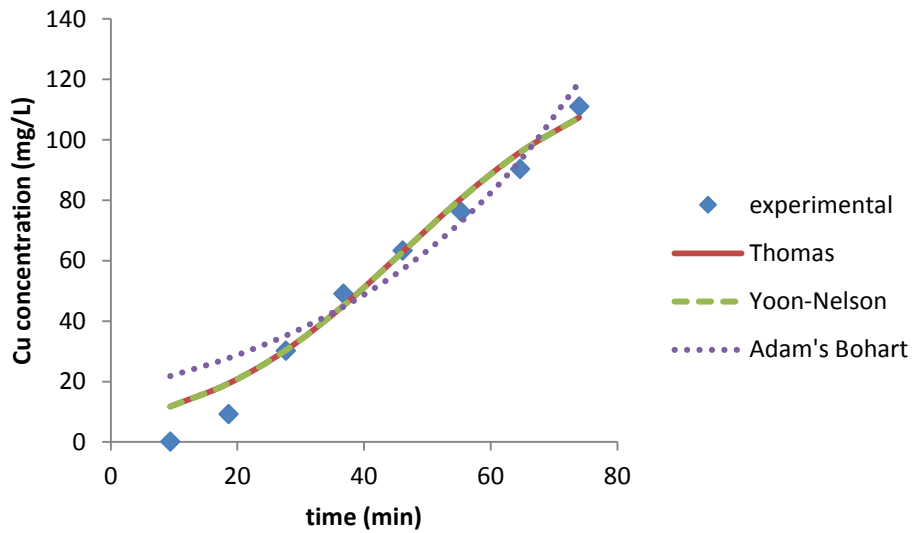


Figure C. 30: Plot of Cu concentration from experiments and those predicted by the Thomas, Yoon-Nelson and Adam's Bohart model versus time at bed packing density and flow rate 0.16 g/cm^3 and 28 mL/min .

Table C. 81: Absolute error between experimental concentrations and those predicted by the Thomas, Yoon-Nelson and Adam's Bohart model at bed packing density and flow rate 0.16 g/cm³ and 8 mL/min.

Thomas	Yoon-Nelson	Adam's Bohart
0.01	0.01	0.01
0.03	0.04	0.06
0.16	0.19	0.23
5.56	5.38	5.48
18.29	17.32	19.19
23.54	19.75	29.90
1.52	6.44	14.90
18.48	20.32	285.59
$\Sigma=67.58$	$\Sigma=69.43$	$\Sigma=355.34$

Table C. 82: Absolute error between experimental concentrations and those predicted by the Thomas, Yoon-Nelson and Adam's Bohart model at bed packing density and flow rate 0.20 g/cm³ and 8 mL/min.

Thomas	Yoon-Nelson	Adam's Bohart
0.11	0.11	0.23
0.38	0.38	0.61
0.88	0.88	1.17
3.59	3.59	3.97
11.35	11.35	15.25
14.40	14.40	25.76
2.48	2.48	2.45
12.66	12.66	115.41
$\Sigma=45.83$	$\Sigma=45.83$	$\Sigma=164.85$

Table C. 83: Absolute error between experimental concentrations and those predicted by the Thomas, Yoon-Nelson and Adam's Bohart model at bed packing density and flow rate 0.28 g/cm³ and 8 mL/min.

Thomas	Yoon-Nelson	Adam's Bohart
1.56	1.56	4.43
3.95	3.95	7.42
2.33	2.33	5.02
3.02	3.02	4.65
7.15	7.15	17.64
3.61	3.61	19.86
3.73	3.73	2.12
0.91	0.91	49.74
$\Sigma=26.25$	$\Sigma=26.25$	$\Sigma=110.88$

Table C. 84: Absolute error between experimental concentrations and those predicted by the Thomas, Yoon-Nelson and Adam's Bohart model at bed packing density and flow rate 0.37 g/cm³ and 8 mL/min.

Thomas	Yoon-Nelson	Adam's Bohart
1.08	1.08	4.48
3.11	3.11	7.53
2.27	2.27	6.12
5.46	5.46	6.80
10.50	10.50	24.84
5.38	5.38	17.37
3.95	3.95	2.12
0.58	0.58	62.85
$\Sigma=32.34$	$\Sigma=32.34$	$\Sigma=132.11$

Table C. 85: Absolute error between experimental concentrations and those predicted by the Thomas, Yoon-Nelson and Adam's Bohart model at bed packing density and flow rate 0.16 g/cm³ and 12 mL/min.

Thomas	Yoon-Nelson	Adam's Bohart
4.21	4.21	8.40
8.24	8.24	12.55
3.21	3.21	6.34
2.31	2.31	2.26
9.32	9.32	13.57
1.51	1.52	7.17
5.06	5.06	8.16
0.79	0.78	32.43
$\Sigma=34.65$	$\Sigma=34.65$	$\Sigma=90.87$

Table C. 86: Absolute error between experimental concentrations and those predicted by the Thomas, Yoon-Nelson and Adam's Bohart model at bed packing density and flow rate 0.16 g/cm³ and 17 mL/min.

Thomas	Yoon-Nelson	Adam's Bohart
8.66	8.66	15.13
12.03	12.03	17.59
3.53	3.53	6.49
5.33	5.33	6.57
4.59	4.59	10.43
1.07	1.07	6.41
4.56	4.56	2.93
1.26	1.26	14.16
$\Sigma=41.03$	$\Sigma=41.03$	$\Sigma=79.70$

Table C. 87: Absolute error between experimental concentrations and those predicted by the Thomas, Yoon-Nelson and Adam's Bohart model at bed packing density and flow rate 0.16 g/cm³ and 28 mL/min.

Thomas	Yoon-Nelson	Adam's Bohart
11.58	11.58	21.60
10.09	10.09	18.45
0.24	0.24	5.01
3.88	3.88	4.34
0.47	0.47	6.23
4.43	4.43	3.28
5.56	5.56	2.75
3.58	3.58	8.00
$\Sigma=39.84$	$\Sigma=39.84$	$\Sigma=69.67$

Appendix D

Adsorption stages

Operating line

$$\text{Maximum Cu loading} = 62 \text{ mg / g}$$

$$[Cu]_{\text{feed}} (\text{meq / L}) = 127 / 63.5 \times 2 = 4 \text{ meq / L}$$

$$\text{Theoretical maximum Cu loading} = 3.74 \text{ meq / g}$$

$$\text{maximum permissible [Cu]} = 2 \text{ mg / L}$$

$$m_{\text{IEF}, \text{required}} = \frac{C_{\text{Cu}, \text{feed}} - C_{\text{Cu}, \text{effluent}}}{\text{maximum Cu loading}} = \frac{127 - 2}{62 \times 0.28} = 2.56 \text{ g}$$

A mass safety factor of 28% for IEFs was allowed to ensure that Cu loading is always maximised. The feed concentration was allowed to be 16% than the desired concentration for design purposes. This will account for the variations in feed concentrations that may occur.

$$\text{operating line slope} = 4 \times 1.16 / (2.56 \times 3.74) = 0.486$$

The maximum Cu loading corresponding to 127 mg/L barren solution is 60 mg Cu/g IEFs and it will be the point whereby the operating line passes through. Therefore, the y-intercept of the operating is calculated as follows:-

$$y - \text{intercept} = 60 - (0.486 \times 127) = -1.740$$

Therefore, the operating line is presented below as equation D.1:-

$$q_e = 0.486C_e - 1.740 \quad \text{D. 1}$$

The equilibrium curve was defined by the Temkin model and it is presented as equation D.2:-

$$q_e = RT / b \ln (AC_e) \quad \text{D. 2}$$

$$\text{Where: } R = 8.314 \text{ Pa m}^3 \text{ mol}^{-1} \text{ K}^{-1}$$

$$T = 298 \text{ K}$$

$$b = 384.11 \text{ Pa m}^3 \text{ mol}^{-1} \text{ mg}^{-1} \text{ g}$$

$$A = 97.864 \text{ L/mg}$$

The theoretical number of stages required to produce a barren solution is shown in Figure D.1. The required stages were determined by the number of right angled triangles formed between the operating line and equilibrium curve as shown in Figure D.1 below. As shown in the figure below, 3 adsorption stages are needed to reduce feed concentration to below 1.5 mg/L.

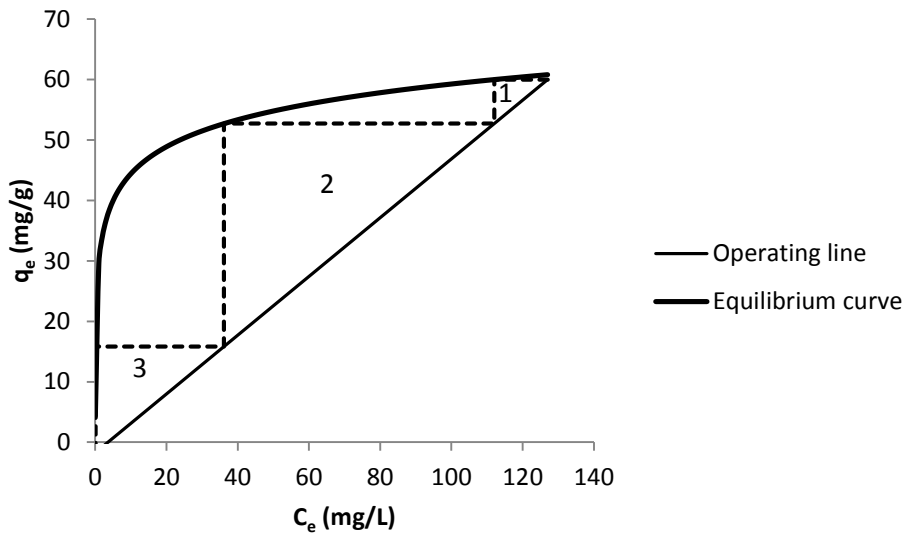


Figure D. 1: Number of theoretical adsorption stages required to produce a barren solution

Table D. 1: Data used to plot equilibrium curve and operating line.

C_e	$q_{e,\text{equilibrium}}$	$q_{e,\text{operating}}$	C_e	$q_{e,\text{equilibrium}}$	$q_{e,\text{operating}}$	C_e	$q_{e,\text{equilibrium}}$	$q_{e,\text{operating}}$
0.02	4.33	-1.73	22	49.50	8.95	44	53.97	19.65
1	29.56	-1.25	23	49.79	9.44	45	54.12	20.14
2	34.04	-0.77	24	50.06	9.93	46	54.26	20.62
3	36.65	-0.28	25	50.33	10.41	47	54.40	21.11
4	38.51	0.20	26	50.58	10.90	48	54.53	21.59
5	39.95	0.69	27	50.82	11.39	49	54.67	22.08
6	41.12	1.18	28	51.06	11.87	50	54.80	22.57
7	42.12	1.66	29	51.28	12.36	51	54.93	23.05
8	42.98	2.15	30	51.50	12.84	52	55.05	23.54
9	43.74	2.63	31	51.71	13.33	53	55.17	24.03
10	44.42	3.12	32	51.92	13.82	54	55.29	24.51
11	45.03	3.61	33	52.12	14.30	55	55.41	25.00
12	45.59	4.09	34	52.31	14.79	56	55.53	25.48
13	46.11	4.58	35	52.50	15.27	57	55.64	25.97
14	46.59	5.07	36	52.68	15.76	58	55.76	26.46
15	47.03	5.55	37	52.86	16.25	59	55.87	26.94
16	47.45	6.04	38	53.03	16.73	60	55.97	27.43
17	47.84	6.52	39	53.20	17.22	61	56.08	27.91
18	48.21	7.01	40	53.36	17.71	62	56.19	28.40
19	48.56	7.50	41	53.52	18.19	63	56.29	28.89
20	48.89	7.98	42	53.67	18.68	64	56.39	29.37
21	49.20	8.47	43	53.83	19.16	65	56.49	29.86

Table C.1 (cont.)

C_e	$q_{e,\text{equilibrium}}$	$q_{e,\text{operating}}$	C_e	$q_{e,\text{equilibrium}}$	$q_{e,\text{operating}}$	C_e	$q_{e,\text{equilibrium}}$	$q_{e,\text{operating}}$
66	56.59	30.35	88	58.44	41.04	108	59.77	50.76
67	56.69	30.83	89	58.52	41.53	109	59.82	51.25
68	56.78	31.32	90	58.59	42.01	110	59.88	51.74
69	56.88	31.80	91	58.66	42.50	111	59.94	52.22
70	56.97	32.29	92	58.73	42.98	112	60.00	52.71
71	57.06	32.78	93	58.80	43.47	113	60.06	53.19
72	57.15	33.26	94	58.87	43.96	114	60.11	53.68
73	57.24	33.75	95	58.94	44.44	115	60.17	54.17
74	57.33	34.23	96	59.01	44.93	116	60.23	54.65
75	57.41	34.72	97	59.07	45.42	117	60.28	55.14
76	57.50	35.21	98	59.14	45.90	118	60.34	55.62
77	57.58	35.69	99	59.20	46.39	119	60.39	56.11
78	57.67	36.18	100	59.27	46.87	120	60.44	56.60
79	57.75	36.67	101	59.33	47.36	121	60.50	57.08
80	57.83	37.15	102	59.40	47.85	122	60.55	57.57
81	57.91	37.64	103	59.46	48.33	123	60.60	58.06
82	57.99	38.12	104	59.52	48.82	124	60.66	58.54
83	58.07	38.61	105	59.58	49.30	125	60.71	59.03
84	58.14	39.10	106	59.64	49.79	126	60.76	59.51
85	58.22	39.58	107	59.71	50.28	127	60.81	60.00
86	58.30	40.07						
87	58.37	40.55						

Design of IEF sorption pan

Table D. 2: Lab column data

Q (mL/min)	8
d_{pc} (cm)	1.4
h_b (cm)	10.5
ρ_b (g/cm ³)	0.16
$V_{\text{breakthrough}}$ (mL)	1000
$Q_{\text{experimental}}$ (mg/g)	74.5

Optimal superficial velocity (u) of the packed column

$$u = Q_{feed}/A_{column} = (8\text{mL}/\text{min})/(\pi(1.4\text{cm})^2/4) = 5.20\text{cm}/\text{min}$$

The u computed above is used to design the sorption pan of the proposed contactor.

Cross sectional area of the sorption pan

$$A_{column} = Q_{feed}/u = (80\text{mL}/\text{min})/(5.2\text{cm}/\text{min}) = 15.39\text{cm}^2$$

The sorption pan was designed to operate at a feed flow rate of 80mL/min to get tangible dimensions of the sorption pan so that it can be easily constructed. Bigger dimensions will also allow easy packing of IEFs into the sorption pan. The cross sectional area of the sorption pan is determined using the equation below. The cross section of the sorption pan is shown in the Figure D.2 below.

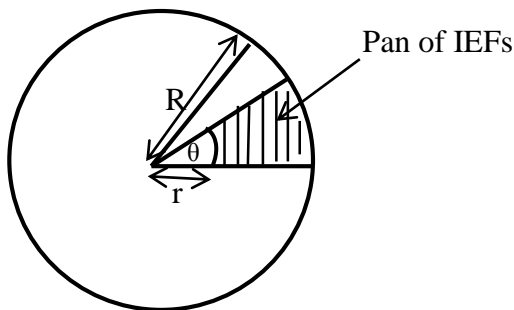


Figure D. 2: Schematic representation of the pan showing the angle between the outer walls of the pan from the centre as well as the inner (r) and inner (R) radius.

$$A_{contactor} = \theta / 360\pi(R^2 - r^2)$$

The inner radius was selected to be 4 cm as a basis for determination of the outer radius. The outer radius (R) was determined by rearranging the equation above and substitution the know variables as show below.

$$R = \sqrt{15.39 \times 360 / (45\pi) + 4^2} = 8.65 \text{ cm}$$

Contact time of the IEF column

$$\tau = V_{bed} / Q_{feed} = ((\Pi(1.4cm)^2 / 4) \times 10.5cm) / (8mL / min) = 2.02 \text{ min}$$

To obtain similar mass transfer characteristics as stated above, the IEF sorption pan should have the same empty bed contact time as the column.

$$H_{contactor} = \tau \times Q_{feed} / A_{contactor} = (2.02 \text{ min}) \times (98 \text{ mL} / \text{min}) / (18.86 \text{ cm}^2) = 10.5 \text{ cm}$$

The height of the sorption pan is the same as that of the column due its dependence on filtration rate and empty bed contact time which should be the same for both the column and sorption pan.

Mass of IEF required in the sorption pan

$$V_{bed} = A_{bed} \times H_{bed} = (18.86 \text{ cm}^2)(10.5 \text{ cm}) = 198 \text{ cm}^3$$

$$V_{contactor} = A_{contactor} \times H_{contactor} = (18.86 \text{ cm}^2)(12.5 \text{ cm}) = 235.72 \text{ cm}^3$$

$$m_{IEF} = V_{bed} \times \rho_c = 198 \text{ cm}^3 \times 0.16 \text{ g} / \text{cm}^3 = 31.36 \text{ g}$$

The packing density of the IEFs was used for the calculations so that the same void of the IEF packing that allows the same filtration as in the column is obtained.

Estimation of feed volume to be treated before breakthrough

$$V_{breakthrough} = (m_{IEF} \times q_e) / (C_f \times Q_{feed}) = (31.36 \text{ g} \times 74.5 \text{ mg} / \text{g}) / (127 \text{ mg} / \text{L}) = 18396.22 \text{ mL}$$

Estimation of cycle duration/breakthrough time of the sorption pan.

$$t_{breakthrough} = (m_{IEF} \cdot q_e) / (C_f \cdot Q_f) = (31.36 \text{ g} \times 74.5 \text{ mg} / \text{g}) / (127 \text{ mg} / \text{L} \times 98 \text{ mL} / \text{min}) = 188 \text{ min}$$

The breakthrough time of the sorption pan is estimated to be about 3 hours and 8 minutes.

Determine eluent requirements

$$m_{IEF,contactor} / m_{IEF,column} = 31.36g / 2.56g = 12.25$$

The volume of acid required to elute the fully loaded IEFs in the proposed sorption pan will be 12.25 times that used in column tests as it is the ratio by which the mass of IEFs changed by. The filtration rate and contact time should be kept constant during elution in the sorption pan to achieve the same extent of elution. Therefore, the acid flow rate will be 98 mL/min.

$$V_{acid_required} = 12.25 \times 105mL = 1286.25mL$$

$$Q_{acid} = Q_{feed} = 98mL / \text{min}$$

Determine the volume of rinsing water required

$$V_{water} = 12.25 \times 120mL = 1470mL$$

$$Q_{water} = Q_{feed} = 98mL / \text{min}$$

The volume of water required to rinse the eluted IEFs in the proposed sorption pan will be 15 times that used in column tests as it is the ratio by which the mass of IEFs changed by. The filtration rate and contact time should be kept constant during rinsing in the sorption pan to remove any entrained acid or feed in the IEFs. Therefore, the rinse water flow rate will be 98 mL/min.

The contactor design results are summarized in Table D.3 below.

Table D. 3: IEF contactor specifications.

Parameters	
$\rho_{b,\text{packing}}$ (g/cm ³)	0.16
$A_{\text{contactor}}$ (cm ²)	18.86
θ	45
r (cm)	4
R (cm)	8.00
$R-r$ (cm)	4.00
V_{bed} (cm ³)	198.00
h_{bed} (cm)	10.5
$H_{\text{contactor}}$ (cm)	12.5
$V_{\text{contactor}}$ (cm ³)	235.72
m_{IEFs} (g)	31.36
q_e (mg Cu/g IEF)	74.51
$t_{\text{breakthrough}}$ (min)	188
$V_{\text{breakthrough}}$ (mL)	18400
V_{eluent} (mL)	1286
$V_{\text{rinse water}}$ (mL)	1470

Appendix E

The image of the fabricated IEF contactor is provided in Figure E.1 below. The picture labelled a) shows the designed pan with IEFs in H^+ form, b) show prototype of fibre pan after loading of Cu^{2+} ions which is indicated by the blue colour. The top and bottom sections of the fabricated pan are shown in c) and d).

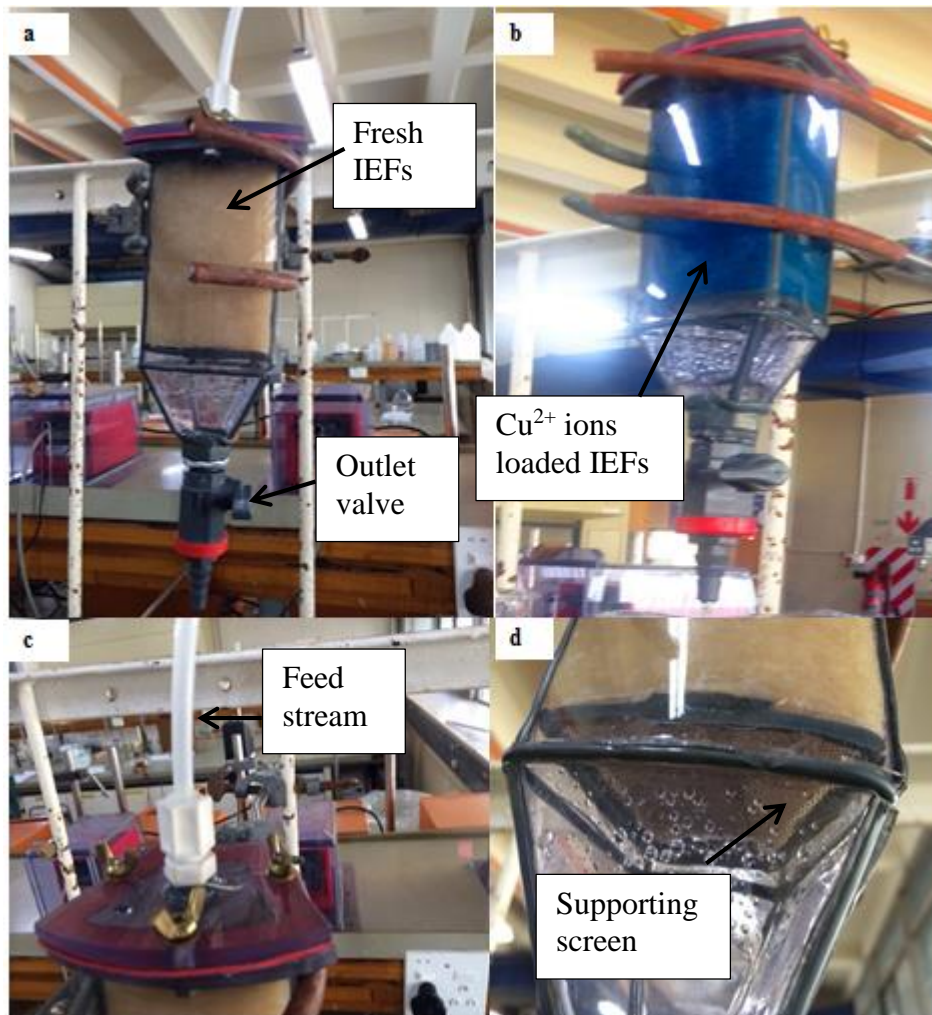


Figure E. 1: Image of the lab scale constructed IEFs contactor pan: a) Contactor packed with IEFs in H^+ form; b) contactor after loading of Cu^{2+} ions onto IEFs; c) Top part of the contactor pan; d) bottom part of the contactor.

Table E. 1: Loading Run 1 data for the IEFs contactor pan (packing density = 0.16 g/cm³).

Volume collected (mL)	Cumulative Volume collected (mL)	time (min)	cumulative time (min)	Cu concentration (mg/L)
2000	2000	21.70	21.70	0.00
2000	4000	21.67	43.37	0.26
2000	6000	21.67	65.03	0.41
2000	8000	21.55	86.58	16.70
2000	10000	21.58	108.17	30.20
2260	12260	24.13	132.30	45.40
2000	14260	21.53	153.83	55.00
2000	16260	21.52	175.35	69.20
2000	18260	21.50	196.85	73.80
2000	20260	21.60	218.45	84.20
2000	22260	21.55	240.00	86.80
2000	24260	21.50	261.50	87.00
2000	26260	21.63	283.13	91.20
2000	28260	21.55	304.68	94.40
2000	30260	21.57	326.25	101.20

Table E. 2: Loading Run 2 data for the IEFs contactor pan (packing density = 0.16 g/cm³).

Volume collected (mL)	Cumulative Volume collected (mL)	time(min)	cumulative time (min)	Cu concentration (mg/L)
2000	2000	21.52	21.52	0.00
2000	4000	21.58	43.10	1.30
2000	6000	21.50	64.60	9.20
2200	8200	22.72	87.32	27.40
2000	10200	21.50	108.82	46.20
2200	12400	21.80	130.62	64.80
2000	14400	21.50	152.12	79.80
2000	16400	21.45	173.57	90.60
2000	18400	21.45	195.02	99.20
2000	20400	21.33	216.35	107.20
2000	22400	21.45	237.80	112.40
2000	24400	21.33	259.13	114.40
2000	26400	21.42	280.55	121.00
2000	28400	21.33	301.88	123.40
2000	30400	21.33	323.22	118.60

Table E. 3: Loading Run 3 data for the IEFs contactor pan (packing density = 0.16 g/cm³).

Volume collected (mL)	Cumulative Volume collected (mL)	time(min)	cumulative time (min)	Cu concentration (mg/L)
2000	2000	21.55	21.55	0.03
2000	4000	21.60	43.15	4.11
2000	6000	21.60	64.75	15.10
2000	8000	21.58	86.33	34.30
2000	10000	21.47	107.80	48.40
2000	12000	21.60	129.40	67.20
2000	14000	21.57	150.97	78.40
2000	16000	21.55	172.52	86.20
2000	18000	21.53	194.05	92.20
2000	20000	21.60	215.65	101.00
2000	22000	21.57	237.22	109.80
2000	24000	21.60	258.82	115.40
2000	26000	21.60	280.42	114.80
2000	28000	21.62	302.03	116.40
2000	30000	21.52	323.55	116.20

Table E. 4: Averaged loading data for the IEFs contactor pan (packing density = 0.16 g/cm³).

Volume collected (mL)	Cumulative Volume collected (mL)	time(min)	cumulative time (min)	Cu concentration (mg/L)	C_t/C_f
2000.00	2.00	21.59	21.59	0.01	0.00
2000.00	4.00	21.62	43.21	1.89	0.02
2000.00	6.00	21.59	64.79	8.24	0.07
2066.67	8.07	21.95	86.74	26.13	0.21
2000.00	10.07	21.52	108.26	41.60	0.33
2153.33	12.22	22.51	130.77	59.13	0.47
2000.00	14.22	21.53	152.31	71.07	0.56
2000.00	16.22	21.51	173.81	82.00	0.65
2000.00	18.22	21.49	195.31	88.40	0.70
2000.00	20.22	21.51	216.82	97.47	0.77
2000.00	22.22	21.52	238.34	103.00	0.82
2000.00	24.22	21.48	259.82	105.60	0.84
2000.00	26.22	21.55	281.37	109.00	0.87
2000.00	28.22	21.50	302.87	111.40	0.88
2000.00	30.22	21.47	324.34	112.00	0.89

Table E. 5: Loading Run 1 data for the IEFs contactor pan (packing density = 0.28 g/cm³).

Volume collected (mL)	Cumulative Volume collected (mL)	time(min)	cumulative time (min)	Cu concentration (mg/L)
2000	2000	21.70	21.70	2.02
2000	4000	21.67	43.37	3.76
2000	6000	21.67	65.03	9.90
2000	8000	21.55	86.58	25.80
2000	10000	21.58	108.17	47.00
2000	12000	24.13	132.30	67.40
2000	14000	21.53	153.83	87.00
2000	16000	21.52	175.35	95.20
2000	18000	21.50	196.85	100.00
2000	20000	21.60	218.45	106.20
2000	22000	21.55	240.00	111.00
2000	24000	21.50	261.50	115.20
2000	26000	21.63	283.13	118.40
2000	28000	21.55	304.68	120.80
2000	30000	21.57	326.25	122.40

Table E. 6: Loading Run 2 data for the IEFs contactor pan (packing density = 0.28 g/cm³).

Volume collected (mL)	Cumulative Volume collected (mL)	time(min)	cumulative time (min)	Cu concentration (mg/L)
2000	2000	21.70	21.70	1.89
2000	4000	21.67	43.37	4.60
2000	6000	21.67	65.03	9.00
2000	8000	21.55	86.58	25.80
2000	10000	21.58	108.17	46.20
2000	12000	24.13	132.30	61.00
2000	14000	21.53	153.83	82.60
2000	16000	21.52	175.35	95.20
2000	18000	21.50	196.85	101.60
2000	20000	21.60	218.45	108.00
2000	22000	21.55	240.00	111.40
2000	24000	21.50	261.50	115.20
2000	26000	21.63	283.13	115.80
2000	28000	21.55	304.68	120.20
2000	30000	21.57	326.25	122.20

Table E. 7: Loading Run 3 data for the IEFs contactor pan (packing density = 0.28 g/cm³).

Volume collected (mL)	Cumulative Volume collected (mL)	time(min)	cumulative time (min)	Cu concentration (mg/L)
2000	2000	21.70	21.70	1.56
2000	4000	21.67	43.37	3.89
2000	6000	21.67	65.03	9.78
2000	8000	21.55	86.58	25.50
2000	10000	21.58	108.17	45.20
2000	12000	24.13	132.30	69.60
2000	14000	21.53	153.83	82.80
2000	16000	21.52	175.35	93.20
2000	18000	21.50	196.85	99.80
2000	20000	21.60	218.45	105.60
2000	22000	21.55	240.00	111.60
2000	24000	21.50	261.50	112.00
2000	26000	21.63	283.13	117.60
2000	28000	21.55	304.68	119.40
2000	30000	21.57	326.25	121.80

Table E. 8: Averaged loading data for the IEFs contactor pan (packing density = 0.28 g/ cm³).

Volume collected (mL)	Cumulative Volume collected (L)	time(min)	cumulative time (min)	Cu concentration (mg/L)	C_t/C_f
2000.00	2.00	21.70	21.70	1.82	0.01
2000.00	4.00	21.67	43.37	4.08	0.03
2000.00	6.00	21.67	65.03	9.56	0.08
2000.00	8.00	21.55	86.58	25.70	0.20
2000.00	10.00	21.58	108.17	46.13	0.36
2000.00	12.00	24.13	132.30	66.00	0.52
2000.00	14.00	21.53	153.83	84.13	0.66
2000.00	16.00	21.52	175.35	94.53	0.74
2000.00	18.00	21.50	196.85	100.47	0.79
2000.00	20.00	21.60	218.45	106.60	0.84
2000.00	22.00	21.55	240.00	111.33	0.88
2000.00	24.00	21.50	261.50	114.13	0.90
2000.00	26.00	21.63	283.13	117.27	0.92
2000.00	28.00	21.55	304.68	120.13	0.95
2000.00	30.00	21.57	326.25	122.13	0.96

Table E. 9: Loading Run 1 data for the IEFs contactor pan (packing density = 0.37 g/cm³).

Volume collected (mL)	Cum Vol collected (mL)	time(min)	cum time (min)	Cu conc (mg/L)
2000	2000	21.52	21.52	1.91
2000	4000	21.58	43.10	3.50
2000	6000	21.50	64.60	13.00
2000	8000	22.72	87.32	28.95
2000	10000	21.50	108.82	52.90
2000	12000	21.80	130.62	76.00
2000	14000	21.50	152.12	96.80
2000	16000	21.45	173.57	106.20
2000	18000	21.45	195.02	110.00
2000	20000	21.33	216.35	119.60
2000	22000	21.45	237.80	121.00
2000	24000	21.33	259.13	126.20
2000	26000	21.42	280.55	126.80
2000	28000	21.33	301.88	127.60
2000	30000	21.33	323.22	127.00

Table E. 10: Loading Run 2 data for the IEFs contactor pan (packing density = 0.37 g/cm³).

Volume collected (mL)	Cumulative Volume collected (mL)	time(min)	cumulative time (min)	Cu concentration (mg/L)
2000	2000	21.52	21.52	2.00
2000	4000	21.58	43.10	2.90
2000	6000	21.50	64.60	13.12
2000	8000	22.72	87.32	28.85
2000	10000	21.50	108.82	50.90
2000	12000	21.80	130.62	74.70
2000	14000	21.50	152.12	97.00
2000	16000	21.45	173.57	105.80
2000	18000	21.45	195.02	112.80
2000	20000	21.33	216.35	117.80
2000	22000	21.45	237.80	121.80
2000	24000	21.33	259.13	127.60
2000	26000	21.42	280.55	126.20
2000	28000	21.33	301.88	126.00
2000	30000	21.33	323.22	127.00

Table E. 11: Loading Run 3 data for the IEFs contactor pan (packing density = 0.37 g/cm³).

Volume collected (mL)	Cumulative Volume collected (mL)	time(min)	cumulative time (min)	Cu conc (mg/L)
2000	2000	21.52	21.52	1.80
2000	4000	21.58	43.10	3.77
2000	6000	21.50	64.60	13.04
2000	8000	22.72	87.32	29.20
2000	10000	21.50	108.82	52.90
2000	12000	21.80	130.62	75.40
2000	14000	21.50	152.12	98.40
2000	16000	21.45	173.57	104.00
2000	18000	21.45	195.02	109.60
2000	20000	21.33	216.35	116.00
2000	22000	21.45	237.80	122.40
2000	24000	21.33	259.13	123.20
2000	26000	21.42	280.55	126.80
2000	28000	21.33	301.88	126.80
2000	30000	21.33	323.22	127.00

Table E. 12: Averaged loading data for the IEFs contactor pan (packing density = 0.37 g/ cm³).

Volume collected (mL)	Cumulative Volume collected (L)	time(min)	cumulative time (min)	Cu concentration (mg/L)	C_t/C_f
2000.00	2.00	21.52	21.52	1.90	0.01
2000.00	4.00	21.58	43.10	3.39	0.03
2000.00	6.00	21.50	64.60	13.05	0.10
2000.00	8.00	22.72	87.32	29.00	0.23
2000.00	10.00	21.50	108.82	52.23	0.41
2000.00	12.00	21.80	130.62	75.37	0.59
2000.00	14.00	21.50	152.12	97.40	0.77
2000.00	16.00	21.45	173.57	105.33	0.83
2000.00	18.00	21.45	195.02	110.80	0.87
2000.00	20.00	21.33	216.35	117.80	0.93
2000.00	22.00	21.45	237.80	121.73	0.96
2000.00	24.00	21.33	259.13	125.67	0.99
2000.00	26.00	21.42	280.55	126.60	1.00
2000.00	28.00	21.33	301.88	126.80	1.00
2000.00	30.00	21.33	323.22	127.00	1.00

Table E. 13: Loading Run 1 data for the nonwoven IEFs contactor pan (packing density = 0.16 g/ cm³).

Volume collected (mL)	Cumulative Volume collected (mL)	time(min)	cumulative time (min)	Cu concentration (mg/L)
700	700	7.03	7.03	0.68
700	1400	6.93	13.97	9.10
700	2100	6.80	20.77	21.30
700	2800	7.25	28.02	35.70
700	3500	7.13	35.15	51.10
700	4200	7.10	42.25	64.10
700	4900	7.10	49.35	79.10
700	5600	7.25	56.60	80.60
700	6300	7.63	64.23	87.80
700	7000	7.27	71.50	89.60
700	7700	7.13	78.63	92.00
700	8400	7.15	85.78	94.80
700	9100	8.15	93.93	100.40
700	9800	7.25	101.18	103.00
700	10500	7.15	108.33	107.20

Table E. 14: Loading Run 2 data for the nonwoven IEFs contactor pan (packing density = 0.16 g/ cm³).

Volume collected (mL)	Cumulative Volume collected (mL)	time(min)	cumulative time (min)	Cu concentration (mg/L)
700	700	7.03	7.03	0.76
700	1400	6.60	13.63	9.10
700	2100	6.72	20.35	21.30
700	2800	7.18	27.53	35.90
700	3500	7.30	34.83	51.40
700	4200	7.10	41.93	65.10
700	4900	7.43	49.37	79.60
700	5600	7.23	56.60	82.60
700	6300	7.80	64.40	87.20
700	7000	7.28	71.68	89.80
700	7700	7.30	78.98	92.80
700	8400	7.15	86.13	97.80
700	9100	7.15	93.28	102.40
700	9800	7.25	100.53	102.80
700	10500	7.32	107.85	105.40

Table E. 15: Loading Run 3 data for the nonwoven IEFs contactor pan (packing density = 0.16 g/ cm³).

Volume collected (mL)	Cumulative Volume collected (mL)	time(min)	cumulative time (min)	Cu concentration (mg/L)
700	700	7.37	7.37	0.70
700	1400	6.95	14.32	8.80
700	2100	6.47	20.78	21.00
700	2800	7.25	28.03	34.70
700	3500	7.13	35.17	50.10
700	4200	7.93	43.10	64.10
700	4900	7.10	50.20	78.90
700	5600	7.30	57.50	80.40
700	6300	7.63	65.13	87.60
700	7000	7.32	72.45	91.60
700	7700	7.47	79.92	92.80
700	8400	7.15	87.07	95.60
700	9100	7.32	94.38	100.60
700	9800	7.25	101.63	105.00
700	10500	7.65	109.28	106.00

Table E. 16: Averaged loading data for the nonwoven IEFs contactor pan (packing density = 0.16g/ cm³).

Volume collected (mL)	Cumulative Volume collected (L)	time(min)	cumulative time (min)	Cu concentration (mg/L)	C_t/C_f	Bed volumes
700.00	0.70	7.14	7.14	0.71	0.01	10
700.00	1.40	6.83	13.97	9.00	0.08	21
700.00	2.10	6.66	20.63	21.20	0.20	31
700.00	2.80	7.23	27.86	35.43	0.33	42
700.00	3.50	7.19	35.05	50.87	0.47	52
700.00	4.20	7.38	42.43	64.43	0.60	63
700.00	4.90	7.21	49.64	79.20	0.73	73
700.00	5.60	7.26	56.90	81.20	0.75	84
700.00	6.30	7.69	64.59	87.53	0.81	94
700.00	7.00	7.29	71.88	90.33	0.84	105
700.00	7.70	7.30	79.18	92.53	0.86	115
700.00	8.40	7.15	86.33	96.07	0.89	126
700.00	9.10	7.54	93.87	101.13	0.94	136
700.00	9.80	7.25	101.12	103.60	0.96	147
700.00	10.50	7.37	108.49	106.20	0.99	157

Table E. 17: Elution Run 1 data for the IEFs contactor pan (packing density = 0.16 g/cm³).

Volume collected (mL)	Cumulative Volume collected (mL)	time(min)	cumulative time (min)	Cu concentration (mg/L)
160	160	1.70	1.70	8.7
165	325	1.73	3.43	7088
160	485	1.70	5.13	628
162	647	1.72	6.85	12.6
160	807	1.72	8.57	3.92
160	967	1.72	10.28	1.42
160	1127	1.72	12.00	1.11
170	1297	1.83	13.83	0.76

Table E. 18: Elution Run 2 data for the IEFs contactor pan (packing density = 0.16 g/cm³).

Volume collected (mL)	Cumulative Volume collected (mL)	time(min)	cumulative time (min)	Cu concentration (mg/L)
160	160	1.68	1.68	13.2
160	320	1.72	3.40	7780
160	480	1.72	5.12	1080
160	640	1.73	6.85	9
160	800	1.70	8.55	1.69
160	960	1.72	10.27	0.9
160	1120	1.73	12.00	0.52
166	1286	1.78	13.78	0.44

Table E. 19: Elution Run 3 data for the IEFs contactor pan (packing density = 0.16 g/cm³).

Volume collected (mL)	Cumulative Volume collected (mL)	time(min)	cumulative time (min)	Cu concentration (mg/L)
163	163	1.73	1.73	14.9
160	323	1.72	3.45	6540
160	483	1.70	5.15	686
162	645	1.73	6.88	4.53
160	805	1.78	8.67	0.93
160	965	1.78	10.45	0.49
160	1125	1.80	12.25	0.49
162	1287	1.77	14.02	0.07

Table E. 20: Averaged elution data for the IEFs contactor pan (packing density = 0.16 g/cm³).

Volume collected (mL)	Cumulative Volume collected (mL)	time(min)	cumulative time (min)	Cu concentration (mg/L)	mass eluted (mg)	% mass eluted
161.00	161.00	1.71	1.71	12.27	1.97	0.15
161.67	322.67	1.72	3.43	7136.00	1153.65	89.90
160.00	482.67	1.71	5.13	798.00	127.68	99.84
161.33	644.00	1.73	6.86	8.71	1.41	99.95
160.00	804.00	1.73	8.59	2.18	0.35	99.97
160.00	964.00	1.74	10.33	0.94	0.15	99.99
160.00	1124.00	1.75	12.08	0.71	0.11	99.99
166.00	1290.00	1.79	13.88	0.42	0.07	100.00

Table E. 21: Elution Run 1 data for the IEFs contactor pan (packing density = 0.28 g/cm³).

Volume collected (mL)	Cumulative Volume collected (mL)	time(min)	cumulative time (min)	Cu concentration (mg/L)
160	160	1.73	3.90	13.2
160	320	1.72	5.62	7060
160	480	1.70	7.32	1120
160	640	1.73	9.05	8.7
160	800	1.78	10.83	1.665
160	960	1.78	12.62	0.9
160	1120	1.80	14.42	0.52
160	1280	1.77	16.18	0.44

Table E. 22: Elution Run 2 data for the IEFs contactor pan (packing density = 0.28 g/cm³).

Volume collected (mL)	Cumulative Volume collected (mL)	time(min)	cumulative time (min)	Cu concentration (mg/L)
160	160	1.73	3.90	13.2
160	320	1.72	5.62	6780
160	480	1.70	7.32	1080
160	640	1.73	9.05	6.9
160	800	1.78	10.83	1.69
160	960	1.78	12.62	0.9
160	1120	1.80	14.42	0.52
160	1280	1.77	16.18	0.44

Table E. 23: Elution Run 3 data for the IEFs contactor pan (packing density = 0.28 g/cm³).

Volume collected (mL)	Cumulative Volume collected (mL)	time(min)	cumulative time (min)	Cu concentration (mg/L)
160	160	1.73	3.90	13.2
160	320	1.72	5.62	6840
160	480	1.70	7.32	1050
160	640	1.73	9.05	8.6
160	800	1.78	10.83	1.69
160	960	1.78	12.62	0.9
160	1120	1.80	14.42	0.52
160	1280	1.77	16.18	0.44

Table E. 24: Averaged elution data for the IEFs contactor pan (packing density = 0.28 g/cm³).

Volume collected (mL)	Cumulative Volume collected (mL)	time(min)	cumulative time (min)	Cu concentration (mg/L)	mass eluted (mg)	% mass eluted
160.00	160.00	1.73	3.90	13.20	2.11	5.17
160.00	320.00	1.72	5.62	6893.33	1102.93	2701.69
160.00	480.00	1.70	7.32	1083.33	173.33	424.59
160.00	640.00	1.73	9.05	8.07	1.29	3.16
160.00	800.00	1.78	10.83	1.68	0.27	0.66
160.00	960.00	1.78	12.62	0.90	0.14	0.35
160.00	1120.00	1.80	14.42	0.52	0.08	0.20
160.00	1280.00	1.77	16.18	0.44	0.07	0.17

Table E. 25: Elution Run 1 data for the IEFs contactor pan (packing density = 0.37 g/cm³).

Volume collected (mL)	Cumulative Volume collected (mL)	time(min)	cumulative time (min)	Cu concentration (mg/L)
160	160	1.73	3.90	12.4
160	320	1.72	5.62	6920
160	480	1.70	7.32	950
160	640	1.73	9.05	30
160	800	1.78	10.83	1.34
160	960	1.78	12.62	1.55
160	1120	1.80	14.42	0.52
160	1280	1.77	16.18	0.44

Table E. 26: Elution Run 2 data for the IEFs contactor pan (packing density = 0.37 g/cm³).

Volume collected (mL)	Cumulative Volume collected (mL)	time(min)	cumulative time (min)	Cu concentration (mg/L)
160	160	1.73	3.90	13.2
160	320	1.72	5.62	6660
160	480	1.70	7.32	1010
160	640	1.73	9.05	6.9
160	800	1.78	10.83	1.69
160	960	1.78	12.62	1.3
160	1120	1.80	14.42	0.52
160	1280	1.77	16.18	0.32

Table E. 27: Elution Run 3 data for the IEFs contactor pan (packing density = 0.37 g/ cm³).

Volume collected (mL)	Cumulative Volume collected (mL)	time(min)	cumulative time (min)	Cu concentration (mg/L)
160	160	1.73	3.90	12.2
160	320	1.72	5.62	6960
160	480	1.70	7.32	1080
160	640	1.73	9.05	8.6
160	800	1.78	10.83	1.69
160	960	1.78	12.62	1
160	1120	1.80	14.42	0.5
160	1280	1.77	16.18	0.43

Table E. 28: Averaged elution data for the IEFs contactor pan (packing density = 0.37 g/ cm³).

Volume collected (mL)	Cumulative Volume collected (mL)	time(min)	cumulative time (min)	Cu concentration (mg/L)	mass eluted (mg)	% mass eluted
160.00	160.00	1.73	3.90	12.60	2.02	5.01
160.00	320.00	1.72	5.62	6846.67	1095.47	2720.78
160.00	480.00	1.70	7.32	1013.33	162.13	402.69
160.00	640.00	1.73	9.05	15.17	2.43	6.03
160.00	800.00	1.78	10.83	1.57	0.25	0.63
160.00	960.00	1.78	12.62	1.28	0.21	0.51
160.00	1120.00	1.80	14.42	0.51	0.08	0.20
160.00	1280.00	1.77	16.18	0.40	0.06	0.16

Figures E.2 - E.4 are the linearised plots of the Thomas, Yoon-Nelson and Adam's Bohart models. Plots in the respective figures were used to obtain the parameters for the three above stated models. The parameters of the models are listed in Tables E.9 - E.11 below. The parameters were obtained using method described in Appendix C.

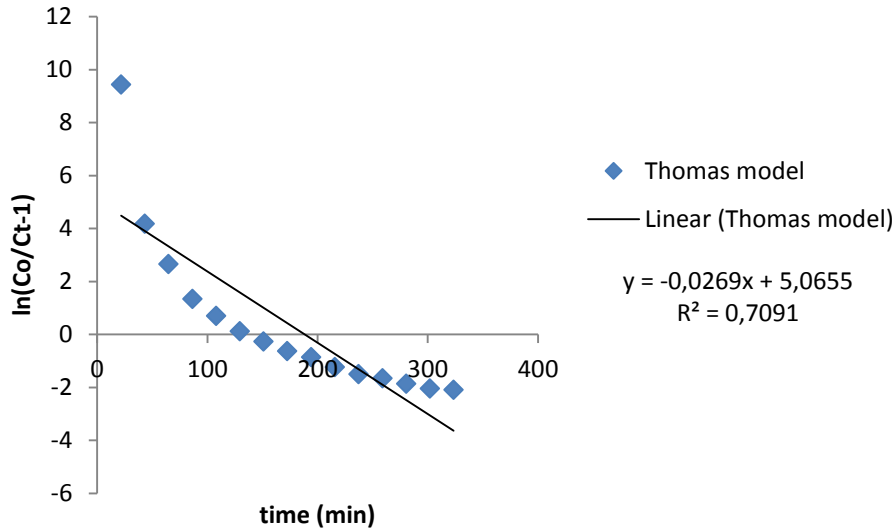


Figure E. 2: Linearised Thomas plot for the IEFs contactor pan.

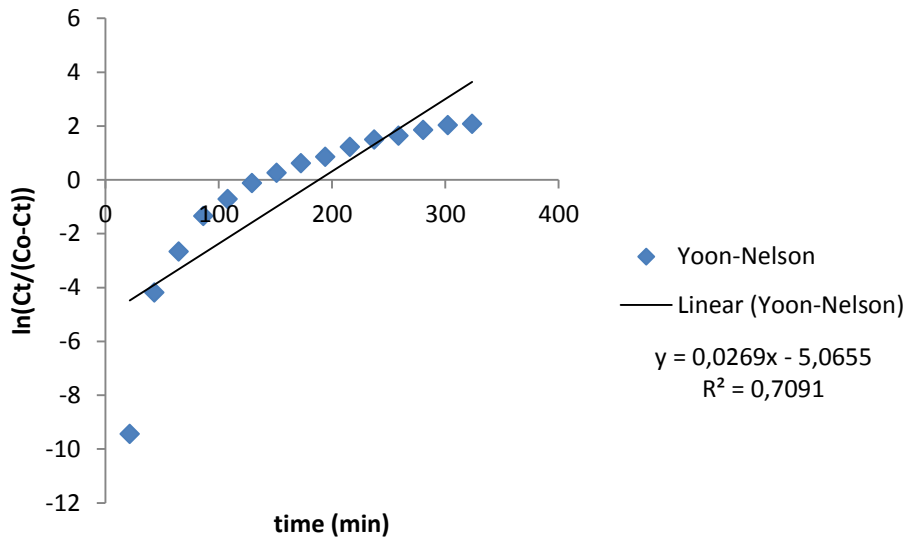


Figure E. 3: Linearised Yoon-Nelson plot for the IEFs contactor pan.

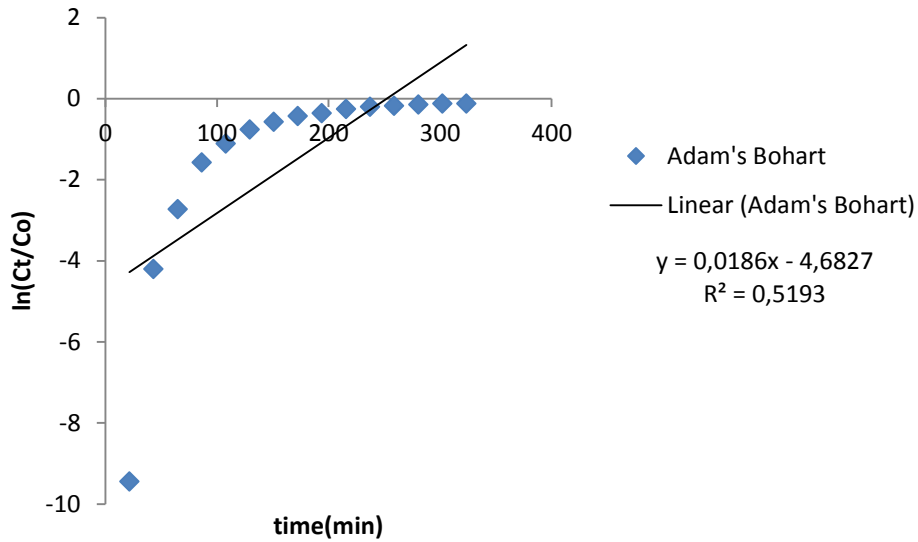


Figure E. 4: Linearised Adam's Bohart plot for the IEFs contactor pan.

Table E. 29: Thomas model parameters for the IEFs contactor pan.

k_{TH} (mL/min mg)	experimental q_0 (mg/g)	predicted q_0 (mg/g)	R^2
0.000214	69	70451.54	0.71

Table E. 30: Yoon-Nelson model parameters for the IEFs contactor pan.

k_{YN} (1/min)	τ (min)	experimental range of τ (min)	R^2
0.0269	188.31	130-152	0.71

Table E. 31: Adam's Bohart model parameters for the IEFs contactor pan.

k_{AB}	Experimental N_0 (mg/L)	N_0 (mg/L)	R^2
0.000148	127	14917.93	0.52

Table E. 32: Experimental and predicted Cu concentration by the Thomas, Yoon-Nelson and Adam's Bohart at various times for the IEF contactor pan.

time (min)	C_t (experimental)	C_t (Thomas model)	C_t (Yoon- Nelson)	C_t(Adam's Bohart)
21.55	0.01	1.40	1.40	1.74
43.15	1.89	2.49	2.49	2.60
64.75	8.24	4.38	4.38	3.89
86.33	26.13	7.62	7.62	5.81
107.80	41.60	12.96	12.96	8.65
129.40	59.13	21.43	21.43	12.93
150.97	71.07	33.76	33.76	19.32
172.52	82.00	49.79	49.79	28.84
194.05	88.40	67.82	67.82	43.05
215.65	97.47	85.13	85.13	64.34
237.22	103.00	99.29	99.29	96.09
258.82	105.60	109.50	109.50	143.60
280.42	109.00	116.18	116.18	214.61
302.03	111.40	120.29	120.29	320.82
323.55	112.00	122.71	122.71	478.70

Table E. 33: Absolute error between experimental concentrations and those predicted by the Thomas, Yoon-Nelson and Adam's Bohart model for the IEF contactor.

Thomas model	Yoon-Nelson	Adam's Bohart
1.39	1.39	1.73
0.60	0.60	0.71
3.86	3.86	4.35
18.52	18.52	20.33
28.64	28.64	32.95
37.71	37.71	46.20
37.31	37.31	51.75
32.21	32.21	53.16
20.58	20.58	45.35
12.33	12.33	33.13
3.71	3.71	6.91
3.90	3.90	38.00
7.18	7.18	105.61
8.89	8.89	209.42
10.71	10.71	366.70
227.54	227.54	1016.29